Quantification of shallow land subsidence in Groningen since the start of the gas extraction in 1963 using daily groundwater dynamics

Luuk Reudink

Partial fulfilment of the degree of Master
of Science in the Earth Sciences

Department of Physical Geography,
Faculty of Geosciences
Utrecht University

Supervisors:
C.J.E. Janssen, MSc
Dr. E. Stouthamer

Utrecht, May, 2021

Utrecht University

ABSTRACT

Land subsidence is an important environmental and societal issue in the Netherlands. Lowering of the surface-level requires additional artificial drainage to maintain the current human-designated functions of the landscape such as agriculture. Moreover, during peat oxidation greenhouse gasses are emitted to the atmosphere that contribute to global warming. The Groningen gas field area in the northern Netherlands provides a good example of a region where various subsidence mechanisms cause a differential subsidence signal. Commercial exploitation of gas since 1963 from a porous sandstone layer at 2 to 3-kilometre depth has triggered deep compression. In addition, the shallow subsurface contains fine-grained deposits in which shallow subsidence mechanisms such as compression and peat oxidation occur. Although various studies have quantified deep compression initiated by the gas extraction, no previous study has investigated shallow subsidence in the Groningen gasfield area. The main objective of this thesis was to quantify shallow subsidence in the Groningen gasfield area since 1963 using a differential subsurface saturation state based on daily modelled groundwater levels.

Several research strategies were combined to achieve this goal. For the selected study area in Nieuwolda, groundwater levels were modelled from 2016 till 2019 using the one-dimensional, process-based SWAP-model. After calibration, modelled groundwater levels were incorporated into a newly developed, empirical, shallow subsidence model. In this model, daily groundwater levels are used to compute differences in the subsurface saturation state through time, enabling the incorporation of seasonal or daily groundwater dynamics in the computation of peat oxidation using an exponential decay function. Additionally, shallow subsidence since 1963 is quantified by comparing historic and more recent measurements regarding lithology and surface-level. Finally, the shallow subsurface build-up was obtained by a field study in Nieuwolda and Appingedam.

The subsidence model with incorporated groundwater level dynamics indicated an average shallow subsidence rate of 0.5 cm/year between 2016 and 2019 due to peat oxidation and (reversible) compression, which is in the same order of magnitude as subsidence measurements in this research area. Comparing the thickness of fine-grained deposits in the shallow subsurface between 1970 and 2021 yielded an average shallow subsidence rate of 0.2 cm/year. Differences in regional surface elevation measurements over time point out that the shallow subsidence rate varies between 0 and 0.9 cm/year, determined by a local, heterogeneous shallow subsurface. Modelling groundwater levels using SWAP was proven to be valuable in mimicking groundwater level dynamics, since the trend, the extremes and the mean of modelled groundwater levels match groundwater level measurements.

Keywords: Land subsidence, shallow subsurface, Groningen, groundwater level, compression, peat oxidation, tidal inlet system, differential subsidence.

PREFACE AND ACKNOWLEDGEMENT

This thesis on shallow subsidence is part of the fulfilment to obtain my MSc degree as a physical geographer in the master programme Earth Surface & Water at Utrecht University. This MSc research is performed within the research programme DeepNL entitled *''monitoring and modelling the Groningen subsurface''*, as part of the work packages entitled *''Improvement of geophysical models at Holocene and Pleistocene depths: soils, hydrology and water management''* This thesis supported the early start of this work package and is performed in close collaboration with PhD-candidate C.J.E. Janssen, who will continue to work on the subject matter the next years. The thesis is supervised by C.J.E. Janssen MSc and Dr. E. Stouthamer.

Looking back at the final result I realize that this MSc thesis matches the courses I followed during the first year of my master programme, combining (un)saturated zone hydrology, tidal and coastal dynamics and quaternary environments. Apart from the contextual background, the skills that I obtained earlier in my studies such as programming, hand drilling and teaching were useful. I put a lot of effort into performing this MSc research and I am proud of the final result. The variation between doing research and assisting bachelor courses contributed to the fact that I remained motivated until the end.

I have learned a great deal during the process of this MSc-Thesis. First, I learned how to set up a field study, which I enjoyed most out of all my work activities. All field preparations regarding permission, planning, strategy and equipment made me aware of the intention and goals, such that I felt very grateful to be part of it. Second, I developed my programming skills by continue modelling in MATLAB and start learning a new model (SWAP) in a new modelling environment (FORTRAN). Third, I gained a lot of knowledge on shallow subsidence and water management, topics in which I am very interested and hope continue to work in the next years.

Chayenne, thank you for the months of close and pleasant collaboration. Having weekly discussions contributed to mastering the subject matter at a fast pace. Spending one week together in the field was a joyful experience. Esther, thank you for supervising this thesis as the contextual expert on shallow subsidence. I always looked forward to discuss the developments in my research with you since it governed a new perspective for the next weeks. Due to your broad social network, I could connect with different experts. Moreover, I would like to thank the following experts on different topics that offered guidance during this research:

- Rob Hendriks (WUR) and Jan van den Akker (WUR, retired) for their expertise and advice using SWAP.
- Marius Heinen (WUR) for delivering and explaining the national soil-hydraulic properties database.
- Anton Bartelds (waterschap Hunze & Aa) for delivering water level data and help to contact landowners.
- Jaap de Wit (SWECO) for his advice performing fieldwork in Groningen.
- Ebbing Kiestra (WUR, retired) for his knowledge on the Groningen subsurface.
- Ramon Hanssen (TU Delft) for providing constructive feedback on first results.
- Peter Fokker (TNO) for his advice on the quantification of shallow subsidence mechanisms.
- Manon Verberne (TNO) for fruitful discussions and advice modelling compression.
- Kim Cohen (UU) for fieldwork and GIS advice.

Landowners Hofstra, Weeke and Breedijk in Appingedam and especially Eric-Jan van Buizen in Nieuwolda are acknowledged for allowing a field campaign on their land. Friends Marleen Ketelaars, Jeroen Poortstra, Ruben Jongbloed, Harm van Oorschot, Muriël Reudink, Elbert Besaris, Wilbert Poppink, Suzanne Kappé, Bente Lexmond and Pepijn van Elderen are thanked for discussing the subject matter and/or checking parts of the final report. Iris, you were my greatest support. By listening daily to my developments you fulfilled the greatest task of all.

CONTENTS

1. INTRODUCTION

The province of Groningen in the northern Netherlands provides a good example of a region where various subsidence mechanisms cause differential subsidence (Fokker *et al.* 2019). Commercial exploitation of gas from a porous sandstone layer at approximately 2-3 kilometre depth since 1963 has triggered compression (Van Thienen-Visser *et al.* 2015, Fokker *et al.* 2018, NAM 2020). In addition, Groningen is part of the Dutch deltaic system containing fine-grained sediment and peat in the shallow subsurface [0-15m deep] (Kiestra 2000, Stouthamer *et al.* 2020). Such low lying deltas that are densely populated and intensively used as agricultural farmland are often prone to subsidence initiated in the shallow subsurface (Syvitski *et al.* 2009).

1.1 PROBLEM DEFINITION AND MSC-THESIS AIM & OBJECTIVES

Land subsidence in the northern Netherlands has already been studied either directly, by investigating one or multiple subsidence mechanisms (Van Thienen-Visser *et al.* 2015, Fokker *et al.* 2019, NAM 2020) or indirectly, by investigating relative sea-level rise that, among others, is being influenced by land subsidence (Vermeersen *et al.* 2018). Fokker et al. (2018) already highlighted the mechanisms that cause a differential subsidence signal in the Dutch Wadden Sea, focussing on anthropogenic causes such as gas extraction. Other studies have quantified deep subsidence, caused by compression within the gas reservoir (Van Thienen-Visser *et al.* 2015, NAM 2020). However, no previous scientific study has quantified shallow subsidence in the northern Netherlands yet. This is a problem because the contribution of shallow subsidence to total subsidence due to, for example, regional water management is still unknown. In addition, the relative contribution of shallow subsidence is expected to become more important, as the extraction of gas will end within the coming years (Rijksoverheid 2021). Generic understanding and quantification of shallow subsidence are required to accurately predict the impact of shallow subsidence on future land cultivation and management.

In contrast to the northern Netherlands, various studies in the western Netherlands have investigated subsidence in the shallow subsurface (J. J. H. Van den Akker *et al.* 2007, R. Hendriks *et al.* 2014, Fokker *et al.* 2015, 2019, Stouthamer & Van Asselen 2015, Koster *et al.* 2018, Van Asselen *et al.* 2018, 2020). Although the studied mechanisms are assumed to be similarly active in Groningen, the local, Holocene subsurface build-up, associated subsurface properties and water management are expected to be different compared to the western Netherlands. Differences in the subsurface build-up include the total thickness of fine-grained sediment, composition and soil-hydraulic properties (Kiestra 2000). Differences in water management include local groundwater and surface water levels that are maintained by regional water authorities. In order to properly use the principles of subsidence research from the western Netherlands, the Groningen subsurface build-up, properties and water management should be determined.

Finally, extremes in groundwater level are expected to occur more often within the coming years due to longer droughts and heavy rainfall as a consequence of global warming. Especially extremely low groundwater levels can significantly contribute to shallow subsidence (Brouns *et al.* 2014). Previous shallow subsidence research already managed to include groundwater in the computations of shallow subsidence (Hoogland *et al.* 2012, R. Hendriks *et al.* 2014, Fokker *et al.* 2015, 2019, Stouthamer & Van Asselen 2015, Koster *et al.* 2018, Van Asselen *et al.* 2018, Kooi & Erkens 2020). However, the quality and the temporal resolution of the included groundwater levels vary. Studies that modelled linear groundwater levels have neglected the natural dynamics caused by variable weather conditions or water management (Koster *et al.* 2018, Fokker *et al.* 2019). In other studies that modelled monthly or yearly averaged groundwater levels, daily extremes remained unconsidered (Kooi & Erkens 2020). Some studies managed to include daily groundwater level dynamics in shallow subsidence research but only focussed on the contribution of oxidation and did not consider compression (J. J. H. Van den Akker *et al.* 2007, R. Hendriks *et al.* 2014).

These described problems lead to the following main objective of this thesis:

To quantify shallow subsidence in the Groningen gasfield area since 1963, using a differential subsurface saturation state based on daily modelled groundwater levels.

The following subobjectives were defined that contribute to achieving this main objective:

1) *To assemble and assess historical data regarding the development of surface elevation, groundwater level, surface water level, and lithological layer characteristics in the Groningen gasfield area since 1963.*
2) *To assess the potential and reliability of modelling of daily groundwater levels using the SWAP-model.*
3) *To create and validate an empirical shallow subsidence model that incorporates daily groundwater levels to compute the differential saturation state of the unsaturated zone through time.*
4) *To (indirect) measure historic, shallow subsidence since 1963 using historical measurements*
5) *To investigate the effect of subsurface heterogeneity on shallow subsidence in the Groningen gas field area.*

1.2 RELEVANCE

Regardless of the origin of the experienced subsidence, the created accommodation space under natural conditions would be filled with new sediment by regular floods or tidal inundations. However, as sea dikes nowadays prevent the hinterland from flooding, there is no natural supply of new sediment anymore. This artificial change in the natural system makes that subsidence is not compensated for, resulting in a net lowering of the land surface.

The drop of surface level over time requires additional artificial drainage to maintain the current human-designated functions of the landscape such as agriculture and housing. The PBL (Netherlands Environmental Assessment Agency) has shown that this artificial drainage costs a lot of money for government agencies such as water authorities (Van den Born *et al.* 2016). Second, the active lowering of the phreatic groundwater level enhances peat oxidation and associated greenhouse gas emission (Van den Akker et al., 2007; Van den Born et al., 2016). Investigating historic subsidence as a consequence of local subsurface heterogeneity and/or differential groundwater level can indicate what made certain areas vulnerable for subsidence. Current land and water management can use these new insights in the establishment of future management strategies.

Another economic importance of this study specifically for the area in Groningen that experience subsidence due to the gas extraction is to clarify the contribution of shallow subsidence on the total experienced subsidence. Water authorities need to lower the groundwater level continuously in order to retain the cultivation of the land for agriculture because water levels rise relatively with respect to surface elevation due to subsidence. As subsidence in Groningen is caused by various mechanisms, questions arise who is responsible for the experienced subsidence and who will pay the costs for the additional artificial drainage. Through a better understanding of the relative contribution of shallow subsidence to the total experienced subsidence in Groningen these questions can be more effectively answered.

1.3 THESIS OUTLINE

This thesis is structured according to the steps of scientific research. First, the geological setting and the development of the research area are described (Chapter 2). Next, the mechanisms and drivers that contribute to subsidence are discussed based on a literature review (Chapter 3). This review elaborates on differential subsidence due to dynamic groundwater level. Then, the approach and the research methods will be explained (Chapter 4). Subsequently, the results of the data inventory, field study and model computations will be presented (Chapter 5). Next, these results will be compared to literature and discussed in terms of value and potential for future research (Chapter 6). Finally, the conclusion of this thesis is presented (Chapter 7).

2. GEOLOGICAL BACKGROUND

This paragraph presents the subsurface build-up of northeast Groningen. Firstly, the geographical setting of the study area is described (section 2.1). Subsequently, the depositional environments of a tidal system are presented (section 2.2). Finally, the development of these depositional environments during the Holocene are discussed(section 2.3)

2.1 GEOGRAPHICAL SETTING

The research area is located in the northeastern part of the province of Groningen, the Netherlands (Figure 1). The Ems-Dollard estuary is located on the eastern side of the research area and functions as the natural border with Germany. The Ems-Dollard estuary connects the river Ems to the Wadden Sea. The surface elevation varies for the largest part between -1.0 and -2.5 m below Dutch Ordnance Datum, the Dutch reference surface elevation level which is approximately equal to current mean sea level. Water authority Hunze & Aa is responsible for the regional water management. Land use is dominated by agriculture for crop growth or meadows for cattle breeding.

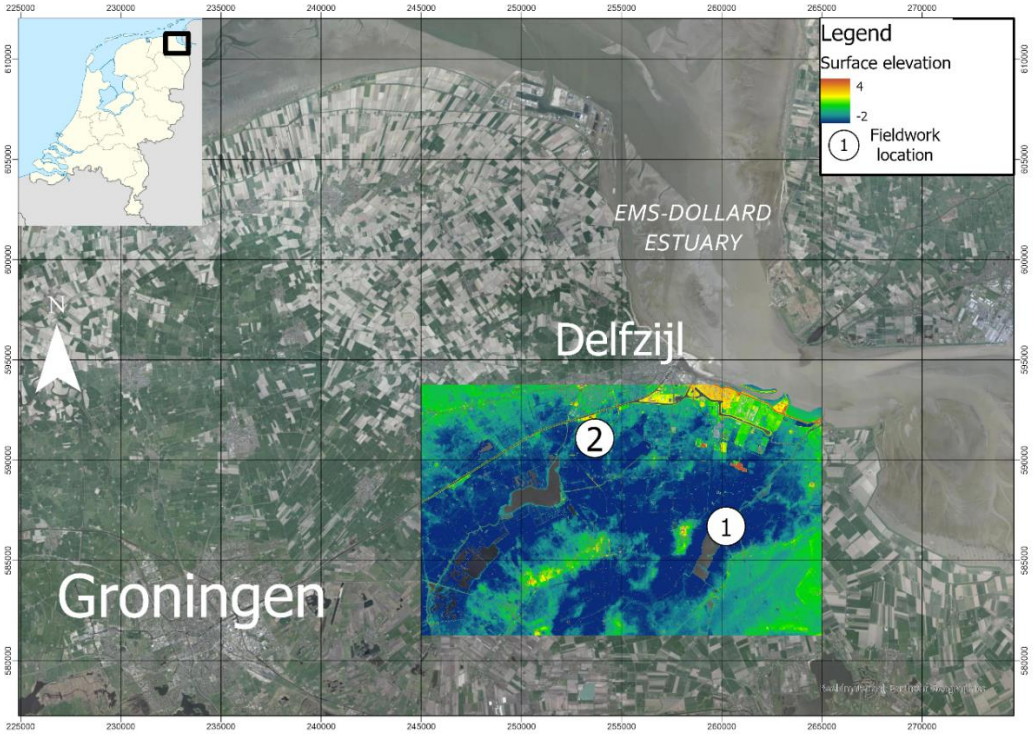

FIGURE 1: OVERVIEW OF THE RESEARCH AREA IN NORTHEAST GRONINGEN.

The current vertical surface motion of the research area varies between -5 and -10 mm/year (Bodemdalingskaart.nl, 2020; Figure 2). The region is influenced by gas extraction and is located slightly east of the centre of the subsidence bowl caused by the gas extraction (Figure 3). The total amount of subsidence in the research area caused by the gas extraction since 1963 varies between 22 and at 30 cm (NAM, 2020; Figure 3).

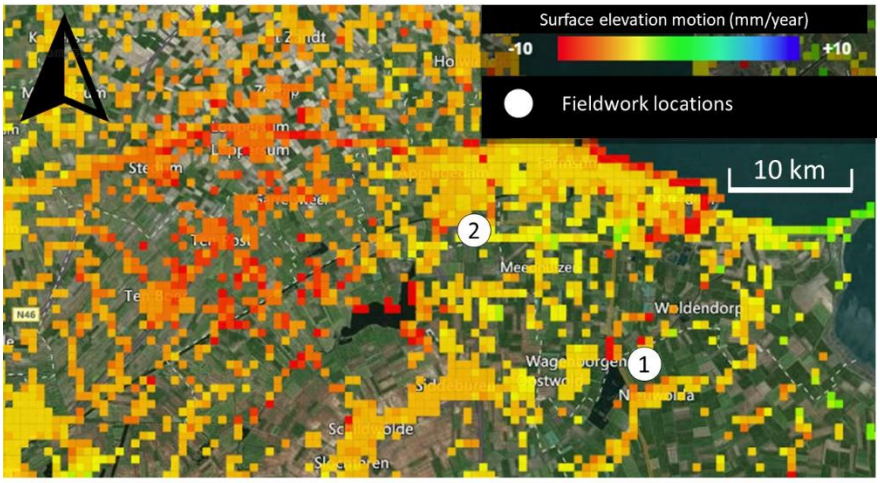

FIGURE 2: OVERVIEW CURRENT MEASURED VERTICAL MOTION IN THE RESEARCH AREA (FROM: BODEMDALINGSKAART.NL, 2020).

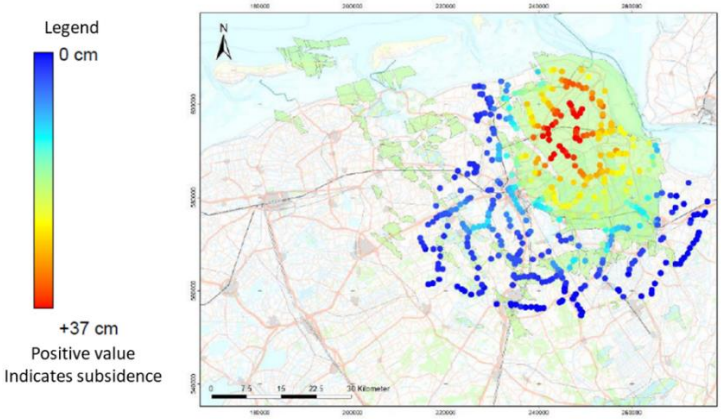

FIGURE 3: OVERVIEW OF THE (CUMULATIVE) MEASURED SUBSIDENCE SINCE 1963 DUE TO THE GAS EXTRACTION (NAM 2020).

2.2 TIDAL INLET SYSTEM

The province of Groningen was part of a tidal inlet system during the Middle and Late Holocene (Vos & Knol 2015). A tidal system is a dynamic system in which multiple depositional environments are active over the entire coastal plain. This paragraph addresses the main characteristics of a tidal inlet system and the associated depositional environments that were active in Groningen throughout the Holocene.

The Wadden Sea is considered as a mesotidal coast with a large lagoon behind the Wadden islands (Boothroyd 1978). This mesotidal coastal regime is connected to the tide-dominated Ems-Dollard estuary (G. Nichols 2009). In this dynamic coastal plain system, different landforms coexist (Pierik et al., 2016; Figure 4; Figure 5). Generally, a large tidal inlet splits into smaller tidal channels and eventually branches into a series of tidal creeks (Figure 4). The subdivision between depositional environments was based on tidal energy and will be discussed in terms of decreasing hydrodynamics.

SUBTIDAL ZONE

The subtidal zone comprises the part of the coastal plain in which channels are filled with water at average low tide. Via the primary inlet channel in between the barrier islands, sediment is brought into the basin by tidal dispersion, tidal asymmetry and estuarine circulation (Friedrichs 2011). Tidal channels are wide near the inlet channel and decrease in size protruding the inland coastal zone (Stouthamer et al., 2020; Figure 4). Therefore, tidal flow near the mouth can transport and deposit coarse- grained sand (*proximal environment*), when tidal channels narrow grain size decreases (*distal environments*) (Stouthamer *et al.* 2020).

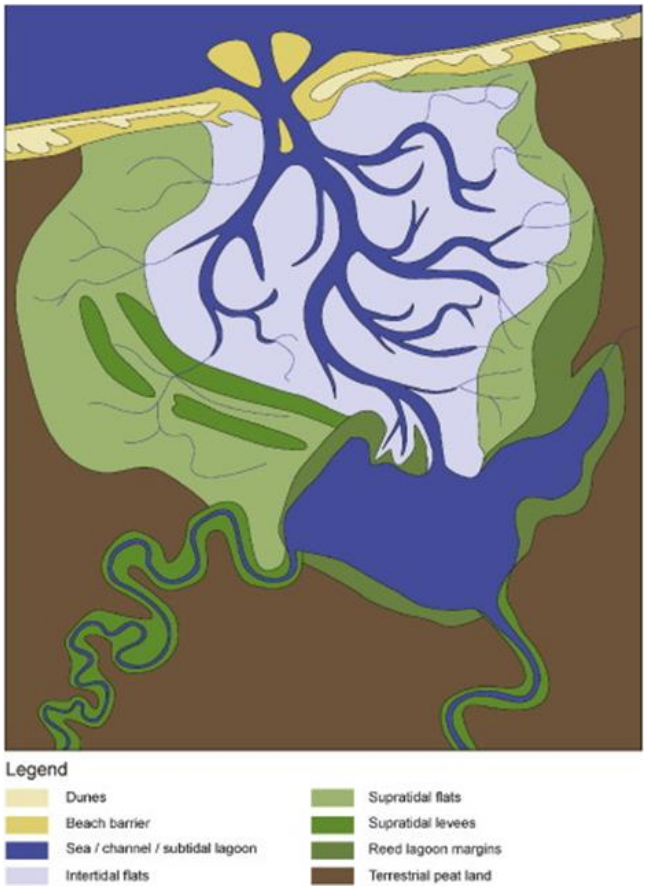

FIGURE 4: GEOMORPHOLOGICAL FEATURES OF A TIDAL INLET SYSTEM (PIERIK *ET AL.* 2016).

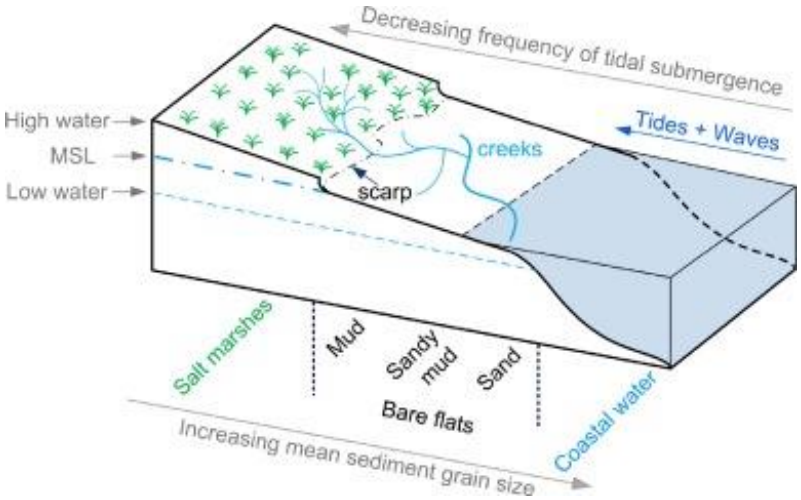

FIGURE 5: 3D-VIEW OF THE ZONATION AND DEPOSITS ON A TIDAL FLAT DURING ONE TIDAL CYCLE (ZHOU *ET AL.* 2016).

INTERTIDAL ZONE

The intertidal zone comprises the realm that is variably covered by water or exposed to air during one tidal cycle (Nichols, 2009; Stouthamer et al., 2020). These regions are considered to be the tidal bars adjacent to the larger tidal channels, and the inland located tidal flats along the margins of the coastal plain (Nichols, 2009). Deposits from the intertidal zone might differ in grain size from fine-medium sand up to clay (Stouthamer *et al.* 2020). The largest grain sizes are deposited on tidal flats that are only limited subaerially exposed during low tide. more

distal parts that are rarely inundated will contain smaller grain sizes such as clay, mostly referred to as tidal mudflats.

SUPRATIDAL ZONE

Only during extremely high tides or storm surges sediment can be transported into the supratidal zone (Stouthamer *et al.* 2020). Due to the sporadic inundations, salt-adapted vegetation can settle on the slightly sloping relief (Figure 5). This landscape in the supratidal zone is referred to as saltmarsh (Pethick 1984, G. Nichols 2009, Zhou *et al.* 2016) and the associated geomorphological landform as supratidal flat (Pierik *et al.* 2017, De Haas *et al.* 2018). Tidal creeks might reach and cut into these supratidal flats, delivering sediment further inland (G. Nichols 2009). The frequency of tidal inundations is important in the supply of sediment. During flood, coarse-grained sediment will be deposited earlier when friction with the bed forces the flow velocity to decelerate. Fine-grained sediment (fine clays) will be deposited further inland on the supratidal flat. The continuation of these extreme inundations during a transgression might contribute to the development of a supratidal levee (Pierik *et al.* 2017). Inundations are rare at the terrestrial side of the supratidal flat, such that juvenile soils start to develop.

COASTAL PLAIN PEATLANDS

In the distal regions where vegetation has stabilized, terrestrial peatlands may form under high groundwater levels (Stouthamer et al., 2020; Figure 4). The composition of the peat might shift over the aerial extent of this coastal plain peatland. Rare inundations during extreme weather conditions can sporadically deliver clay to the hinterland, resulting in a clastic admixture within the peat.

2.3 GEOLOGICAL DEVELOPMENT NORTHEAST GRONINGEN

The depositional environments discussed in the last paragraph have shifted spatially and temporarily during the Holocene. The development of this tidal inlet system, and all others, is determined by the balance between the accommodation space and sediment supply (Nichols, 1989). This paragraph chronologically discusses the development of these depositional environments throughout the Holocene in northeast Groningen. This paragraph is structured according to the dominant forcing mechanism causing changes in the depositional environment. Where relative sea-level rise determined the shift of the depositional environments during the Early and Middle Holocene, human interventions have controlled the geological development since 2500 BP (Pierik *et al.* 2017). Moreover, similarities and differences between the development of northern and western Netherlands will be addressed

PRE-, EARLY AND MIDDLE HOLOCENE

The Pleistocene surface developed during the Weichselian glacial. A periglacial environment in the Netherlands enabled local transport and large spreading of aeolian sands (Stouthamer *et al.* 2020). This layer of cover sand forms the Pleistocene substrate and is lithostratigraphically referred to as the Boxtel Formation.

Absolute sea level rise started after the Last Glacial Maximum around 20.000 BP due to the melting of icecaps. Many studies showed that the relative sea level rose fast during the Early and Middle Holocene (Vink *et al.* 2007, Hijma & Cohen 2010, De Haas *et al.* 2018), although these sea-level rise rates may vary regionally because of differential subsidence rates (Stouthamer *et al.* 2020). Vink et al. (2007) found that the relative sea level rose faster in the Wadden Sea compared to the western Netherlands, explained by differential glacio-isostatic subsidence. The forebulge collapse, triggered by the retreat of the Scandinavian glacier after the Weichselian, was more pronounced in the northern Netherlands which lead to relative high glacio-isostatic subsidence. In addition, this is one of the explanations for the fact that the Pleistocene surface has a steeper slope in the northern Netherlands (Stouthamer *et al.* 2020).

Transgressions reached the northern coastal plain around 7500 BP (Vos 2015, De Haas *et al.* 2018). The tidal basins such as the Hunze, Fivel and Ems were the first to become inundated in the north-eastern Netherlands (Meijles 2015, Vos & Knol 2015). As a consequence of the relative sea-level rise, groundwater levels grew

simultaneously such that peat formation shifted landward. This inland migration of peat formation resulted in a basal peat layer on top of the Pleistocene substrate for large parts of northern Netherlands (Vos 2015). Due to the flood-dominated tidal asymmetry of the Wadden Sea, sediment supply filled the created accommodation space such that deposition migrated land inward (De Haas *et al.* 2018). As water depth grew and more of the coastal peatlands became tide-dominated (supra-, intertidal), peat deposition shifted towards clay and even fine sands in tidal creeks. Sediments associated with this middle Holocene transgressive systems are lithostratigraphically referred to as the Naaldwijk Formation, Wormer Layer.

Around 6000 BP sea-level rise decreased, such that in the western Netherlands the barrier complexes grew together and marine sediments could fill the back-barrier basin (Bungenstock & Schäfer 2009, Vos 2015, De Haas *et al.* 2018, Stouthamer *et al.* 2020). However, the northern Netherlands coast developed differently in this period (Van der Spek 1994, Oost 1995). For example, the barrier complexes did not intertwine but kept an open connection to the back-barrier basin, which can be explained by a couple of determining mechanisms. Firstly, the northern Netherlands experienced higher glacio-isostatic subsidence which required more input of sediment to keep up with relative sea-level rise. Secondly, the dominant western wind direction resulted in a stronger alongshore drift and associated sand transport in the western Netherlands, which was absent at the parallel oriented northern coastline. Finally, the Rhine-Meuse river system functioned as an additional supply of sediment in the coast of the western Netherlands, whereas such large river systems lack in the northern Netherlands (Meijles 2015, Stouthamer *et al.* 2020) For example, the Ems river has a discharge of 90 m3/s, twenty times smaller compared to the river Rhine with a discharge of 2000 m3/s (Van Maren *et al.* 2016). As a consequence, tidal inlet systems remained in contact with the back-barrier basin and this prevented the early formation of large scale coastal peatlands such as in the western Netherlands. Nonetheless, also along the margins of the tidal basins of the Hunze, Fivel and Ems terrestrial peat was formed (Meijles 2015). The peat that formed behind the back-barrier complexes is lithostratigraphically referred to as the Nieuwkoop Formation, Holland Peat Layer (Stouthamer *et al.* 2020). As sediment supply starts to exceed the accommodation space by a decreasing relative sea-level rise in the next thousands of years, coastal progradation continues and the back-barrier basin slowly fills up the inland part of the Wadden Sea (Vos & Knol 2015)

Late Holocene

This coastal progradation continued until 3000 – 2500 BP when new tidal inlet systems intruded the coastal plain. The transgressions do not only originate from sea level rise but increasingly from human interference in the tidal system (Vos & Knol 2015, Pierik *et al.* 2017, De Haas *et al.* 2018). Some of these transgression systems were part of an old tidal basin that had not been filled during the former coastal progradation such as the Hunze and Fivel basin. On the other hand, new transgression systems originated, especially connected to the Ems-Dollard estuary, such as the Ae, Termunter en Dollard- system (Vos & Knol, 2015; Figure 6).

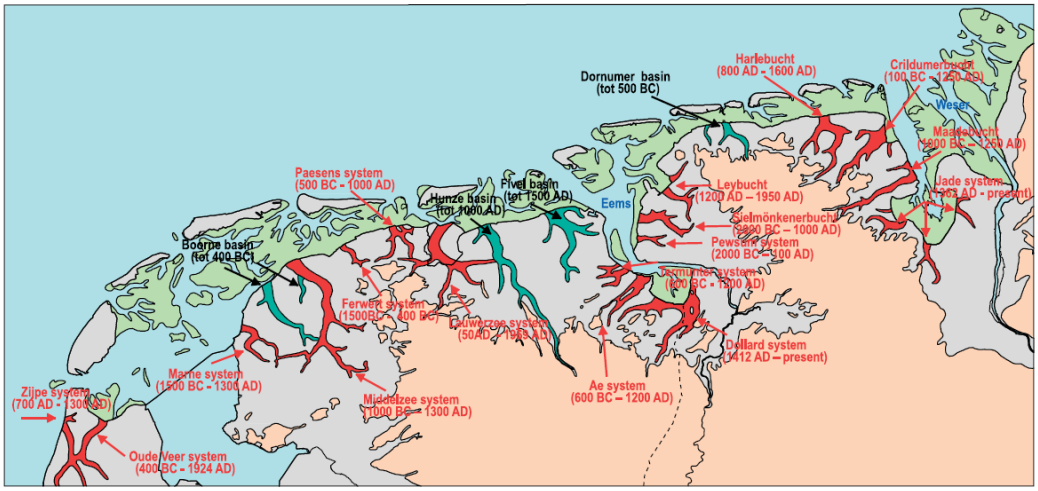

FIGURE 6: ACTIVE TIDAL SYSTEMS ALONG THE WADDEN SEA COAST BETWEEN 2400 AND 600 BP (VOS & KNOL 2015).

One of the natural causes for these more frequent Late Holocene transgressions is the increase in tidal energy within the tidal basins. The coastal progradation and inland migration of the barrier complexes led to a steeper land-sea gradient of the Wadden Sea basin which enhanced tidal ranges (Vos & van Kesteren 2000). Another natural cause for these Late Holocene transgressions is the lateral migration of the barrier islands along the northern coast. A tidal inlet system prevents the formation of coastal peatland. However, behind the barrier complexes, depositional environments were less dynamic such that salt marshes and peatlands existed. With the lateral shift of the barrier complexes, former stable coastal peatlands could become inundated and became vulnerable to erosion (Vos & Knol 2015). This newly created accommodation space increased water depth, tidal prism and thus tidal ranges so that inland located peatlands were naturally drained (Van der Spek 1994). This drainage enhanced further natural compaction and oxidation, resulting in subsidence.

At the same time (2500 BP), humans started settling in the supratidal zone (Vos & Knol 2015, Pierik *et al.* 2017). Especially the supratidal levees that were naturally higher regions and therefore safe during storm surges were attractive for settlement. To further prevent flooding, the supratidal levees were raised by adjacent sediments, creating the typically inhabited dwelling mounds (in Dutch, 'terpen in Friesland' or 'wierden in Groningen') (Vos & Nieuwhof, 2021; Figure 7). Artificial dug canals drained the bordering fertile coastal peatlands and enabled agriculture but reinforced shallow subsidence (Pierik *et al.* 2017)

Both the natural and the anthropogenic causes for increased shallow subsidence led to the creation of extra accommodation space. Sediments from these Late Holocene active ingression systems are lithostratigraphically referred to as the Naaldwijk Formation, Walcheren Layer, predominantly consisting of heavy clay (Kiestra 2000, Stouthamer *et al.* 2020). The loading by this new deposition increased peat compaction, further reinforcing subsidence. These positive feedback mechanisms by increasing tidal volume and accommodation space resulted in transgressions of large parts of northeast Groningen during the Late Holocene (Pierik *et al.* 2017).

From 1200 AD onwards humans started building dikes to prevent flooding (Vos & Knol 2015). As a consequence, seawater could no longer intrude. Both natural and human-induced compaction led to shallow subsidence landward from the dike. As relative sea-level rise continued, new sediment was deposited at the seaward side of the dike. These series of events repeated and so large parts of former tidal ingressions could be reclaimed (Vos 2015). As each sequence of newly reclaimed land grew with sea-level rise, this reclaimed landscape constitutes of staircases with increasing elevation in seaward direction.

Since the start of cultivation, natural surface water drainage has been accelerated by a large drainage system of ditches and canals. From approximately 1500 AD onwards, surface water drainage is artificially controlled, first

by pumping water out with the use of windmills and later with the use of electrically driven mills. The repetition of groundwater level lowering and enhanced subsidence is the reason that large parts of north-eastern Groningen are located -1 up to -2.5 m below mean sea level

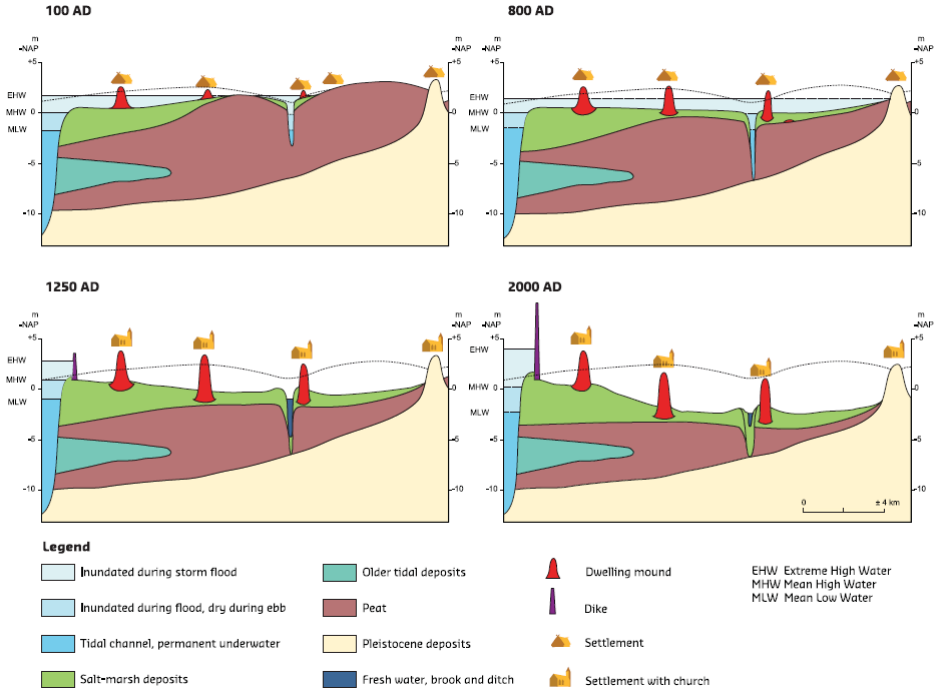

FIGURE 7: SCHEMATIC CROSS-SECTION OF THE COASTAL AREA OF NORTHERN NETHERLANDS FROM 3000 BP TILL PRESENT (VOS & KNOL 2015).

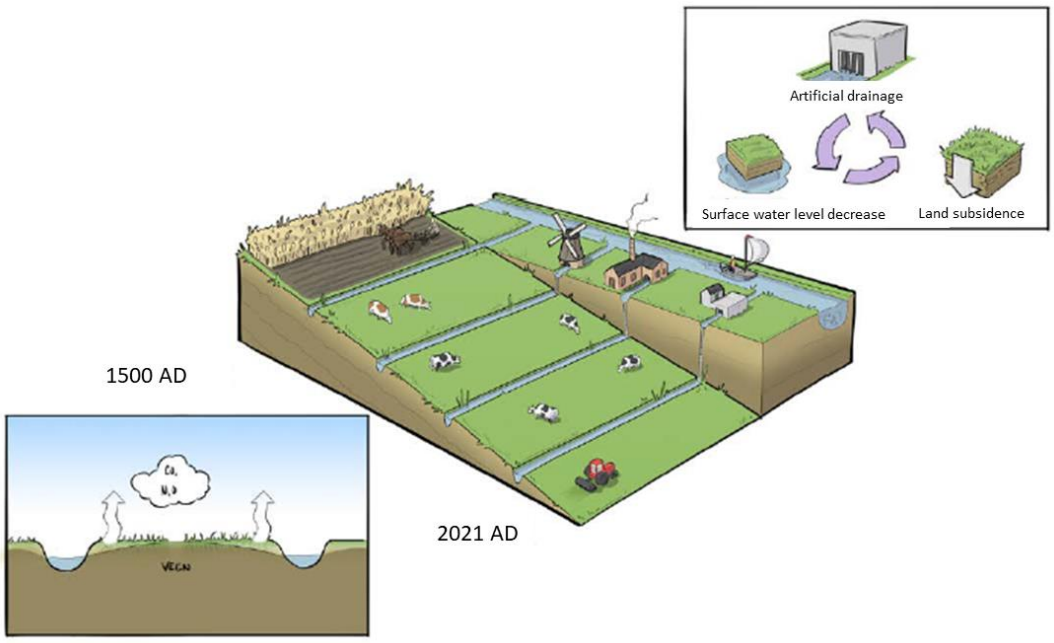

FIGURE 8: SCHEMATIC CROSS-SECTION OF LAND SUBSIDENCE SINCE 500 BP INITIATED BY LAND RECLAMATION AND ARTIFICIAL DRAINAGE (ADAPTED FROM BOS ET AL., 2017).

3. LITERATURE REVIEW ON SHALLOW LAND SUBSIDENCE

This literature review on shallow land subsidence starts with a synthesis on respectively the mechanisms that cause subsidence (section 3.1) and the drivers that could enhance subsidence (section 3.2). The aim is to clarify the processes and associated terminology on which the rest of the thesis is built upon. Thereafter, these mechanisms and drivers will be discussed in terms of spatial and temporal variations, causing differential subsidence (section 3.3). The final section will synthesize the use of groundwater level in shallow subsidence research (section 3.4). A recent Dutch overview report on subsidence by Deltares entitled ''Deltafact Bodemdaling'' provides additional information (Van Asselen *et al.* 2019).

3.1 SUBSIDENCE MECHANISMS

3.1.1 COMPRESSION

Compression is the mechanical compaction of a soil or rock matrix (Fitts 2002, Van Asselen *et al.* 2009). The total vertical stress (σ) consists of two components; the matrix forces between the grains or effective stress (σ') and the pore fluid pressure (μ) (Terzaghi, 1943; Figure 10). The effective stress is the force exerted on the surface of the interconnected solid matrix (Van Asselen *et al.* 2009). The pore fluid pressure is the force of the fluid in the pores of a medium that act on the total surface (Fitts 2002).

$$\sigma = \sigma' + \mu \tag{1}$$

Compression can be subdivided into *primary compression* and *secondary compression* (Figure 11;Figure 10). Primary compression is considered as a mechanical compaction due to an increase in the effective stress between the grains (Van Asselen *et al.* 2009, Koster *et al.* 2018). Secondary compression (also referred to as *creep*) however, is a reorganisation of the matrix structure under constant effective stress and indicates an internal viscous response of the grains resulting in deformation(Le *et al.* 2012). The increase in effective stress for primary compression can be the result of two possibilities; either the total vertical stress increases (assuming pore pressure remains constant) or the pore pressure decreases (assuming total vertical stress remains constant)(Figure 11). The total vertical stress can naturally increase by active deposition, or artificially by applying a load at the surface (Van Asselen *et al.* 2009). A decrease in pore fluid pressure can be differentiated in terms of the type of fluid that is present in the pores. Water comprises the pores for the saturated subsurface at shallow depth, however at greater depth (> 1000 m) also hydrocarbons and oil may be present in the pores of the subsurface. (Fokker *et al.* 2018). This literature review will further focus on the shallow compression mechanisms that are a result of changes in the water pressure.

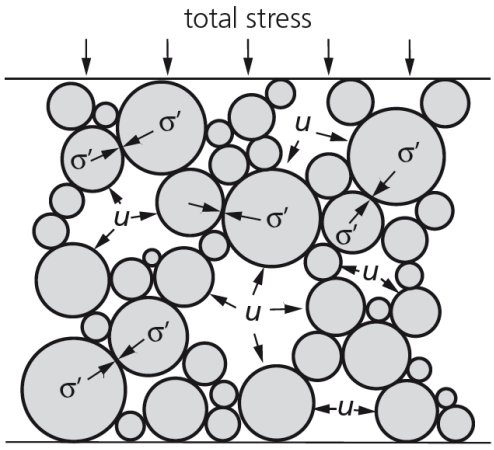

FIGURE 9:SCHEMATIC REPRESENTATION OF THE EFFECTIVE STRESS BETWEEN GRAINS AND FLUID PRESSURE IN THE PORES (VAN ASSELEN *ET AL.* 2009)

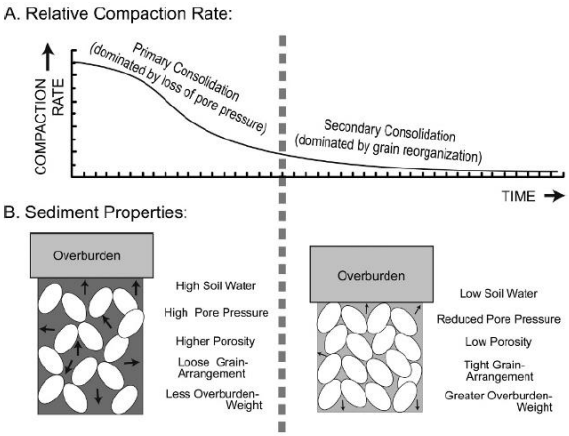

FIGURE 10: DEVELOPMENT OF THE RELATIVE COMPRESSION RATE AND THE SEDIMENT PROPERTIES THROUGH TIME (YUILL *ET AL.* 2009).

In the saturated zone, various reasons can cause the water pressure to decline. *Consolidation* is referred to as the process where over pressured pore water is expulsed from the pores and the sediment structure reaches a new equilibrium between the water pressure and the weight of the overburden (Van Asselen *et al.* 2009). The term consolidation, however, does in specific refer to expulsion of water from fine-grained sediments since the low permeability increases the duration of the consolidation process, referred to as the *consolidation time* (Van Asselen *et al.* 2009, 2019). An extreme type of consolidation is *autocompaction*, where thick, impermeable layers at large depths (>300 m) still consolidate. Rates of this autocompaction are for most parts of the Netherlands extremely small, in the order of 0.1 mm/year (Kooi *et al.* 1998). A natural cause for a declining water pressure can be a declining groundwater table as a consequence of a drop in relative sea level (Van Asselen *et al.* 2009). Human-induced examples for declining water pressures are the artificial lowering of the groundwater table or extraction of water from aquifers(see 3.2)(Van Asselen *et al.* 2009).

In the unsaturated zone close to the surface, evapotranspiration creates negative pore water pressure of the soil moisture, referred to as the matrix potential (M. Hendriks 2010, Fokker *et al.* 2019). When the matrix potential increases, for example by stronger evapotranspiration, the vertical effective stress will increase as well, resulting in *shrinkage* of the top layer (Bronswijk 1989). Parts of this shrinkage are reversible, such as differences throughout a year, driven by seasonal changes in evapotranspiration. However, *irreversible shrinkage* rearranges the soil structure such that the porosity after swelling has decreased compared with the porosity prior to shrinkage.

The potential compression of a layer, or *compressibility,* is determined by 1) the matrix/soil properties 2) the thickness of the compressible layer 3) the pore water pressure. All three factors eventually influence the exerted effective stress (Van Asselen *et al.* 2009, Stouthamer *et al.* 2020). Soil properties that influence the compressibility are texture, permeability, porosity, density and organic matter content (Van Asselen *et al.* 2009). In general, coarse-grained soils consisting of gravel and sand are nearly incompressible, clay soils are moderately compressible and peat soils are most compressible (Van Asselen *et al.* 2009, Yuill *et al.* 2009, Higgins 2016).

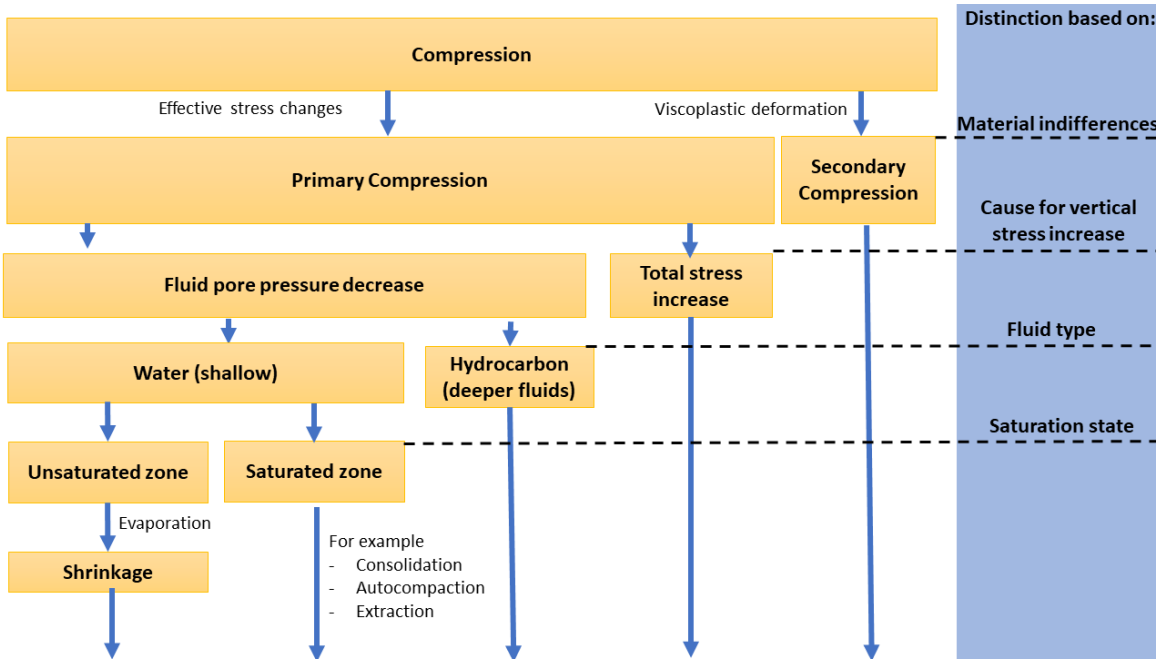

FIGURE 11: SUBDIVISION OF THE COMPRESSION MECHANISMS AND ASSOCIATED TERMINOLOGY. THIS FIGURE IS USED TO STRUCTURE DIFFERENT (SUB-) COMPONENTS OF COMPRESSION AND CAN BE CONSULTED AS GUIDANCE WHILE READING THIS PARAGRAPH.

3.1.2 PEAT OXIDATION

Peat oxidation is the decomposition of organic matter into smaller organic or inorganic matter such as carbon dioxide, methane and nitrogen. When the oxygen that acts as the oxidizer in the oxidation reaction originates from the atmosphere, the peat oxidation process is known as aerobic decomposition. However, organic matter can also decompose under anaerobic conditions in the saturated zone. For example, oxygen from the biomass itself such as nitrate and sulphate might function as an oxidizer (Brouns 2016, Van Asselen *et al.* 2019). Aerobic decomposition is approximately ten times faster than anaerobic decomposition, although this ratio varies for different types of peat (Scanlon & Moore 2000).

Peat oxidation can result in subsidence because of two reasons. Firstly, organic matter that decomposes into atmospheric gasses, such as carbon dioxide and methane, causes a loss of mass (Figure 12). Secondly, decomposition degrades the fabric structure of the peat into smaller organic compounds that can be structured more efficient to fit into a smaller volume. In contrary to shrinkage, peat oxidation is always irreversible. The decomposition rate is determined by biotic factors such as (1) the organic matter content (2) the type of peat (3) the presence of soil bacteria and by abiotic factors such as (4) the oxygen availability (5) the soil temperature (6) the pH (Brouns 2016).

A saturated subsurface lacks the supply of atmospheric oxygen and can only decompose anaerobically. Oxygenation, the process where sediment becomes exposed to oxygen, of former non-oxygenated deeper situated peat can double decomposition rates, as the permeability of 'fresh' peat is still relatively high (Frolking *et al.* 2001, Brouns *et al.* 2014). Oxygenation is hindered when a peat layer is covered by a less porous layer such as clay (Brouns *et al.* 2014). However, preventing the supply of oxygen by a covering clay layer barely occurs, as a consistent sealing function of a clay layer is most often interrupted by the existence of cracks or macropores (personal communication Van Den Akker). An admixture of clastic material such as clay during peat formation could reduce the potential for peat oxidation. Brouns et al. (2014) found higher decomposition rates for eutrophic peat compared with oligotrophic peat. However, varying decomposition rates for different types of peat are rather unknown and more research into this topic is required. For the sake of simplicity, the temperature, pH and presence of soil organisms will be neglected in this study as their contribution is rather small or still unknown.

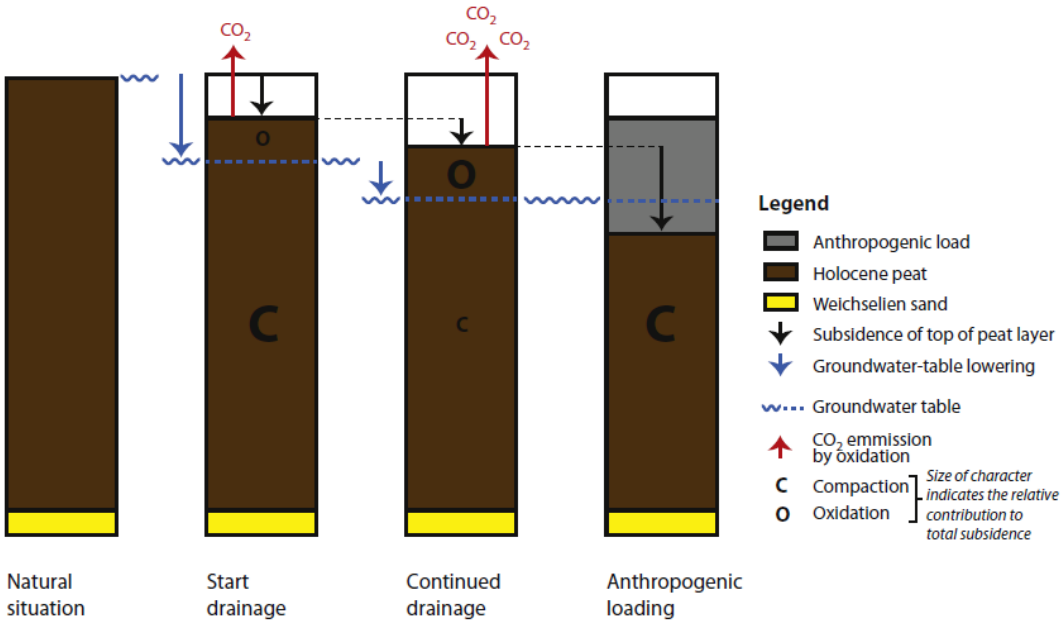

FIGURE 12: SCHEMATISATION OF VARIATIONS IN THE DOMINANT SUBSIDENCE MECHANISM THROUGH TIME (VAN ASSELEN *ET AL.* 2018)

3.1.3 GEOLOGICAL SUBSIDENCE

A couple of other, subordinate subsidence mechanisms contribute to the total vertical ground movement and are sometimes referred to as background subsidence. These subordinate mechanisms will be discussed briefly.

NEOTECTONICS

Tectonic subsidence can be the consequence of basin or local tectonics. The Netherlands is located in the sedimentary North Sea Basin, formed by differential tectonics between northwest and southern Europe during the Tertiary (Stouthamer *et al.* 2020). The tilting of this basin results in differential vertical movement in the Netherlands, ranging from an uplift of 0.015 mm/year and subsidence of 0.06 mm/year (Kooi *et al.* 1998, Hijma & Kooi 2018). The study area in Groningen experiences no subsidence or even a minor uplift (maximum 0.015 mm/year) due to the basin tectonics(Figure 13). This value is at least a factor two or even three smaller than the current measured vertical movement (Figure 2). Moreover, the study area is not influenced by local tectonics, as the Roer Valley Graben is located more than a hundred kilometres away (Cohen 2003)

ISOSTASY

Isostasy is considered as the balance in pressure of the asthenosphere. Spatial differences in the pressure component can cause flow of the liquid asthenosphere and thereby result in differential vertical movement of the surface. Differential pressure gradients may be a consequence of differential loading by ice (referred to as glacio-isostatics) or water (hydro-isostatics). The high viscosity of the asthenosphere delays the restoration of the balance in pressure, meaning that subsidence or uplift may continue for hundreds or thousands of years after (additional) loading has ended (Cohen 2003, Stouthamer *et al.* 2020). Glacio-isostatics in the Weichselian caused an uplift of the Netherlands referred to as the forebulge, a phenomenon acting in the area surrounding the glacier. After glacier retreat during the Late Pleistocene and early Holocene, the glacio-isostatic rebound caused subsidence of the Dutch surface level. This glacio-isostatic subsidence is largest in northern Netherlands with maximal glacio-isostatic uplift(Stouthamer *et al.* 2020). Present isostatic subsidence rates for our study area in Groningen are approximately 0.2 mm/year (Hijma & Kooi, 2018; Kooi et al., 1998;Figure 14).

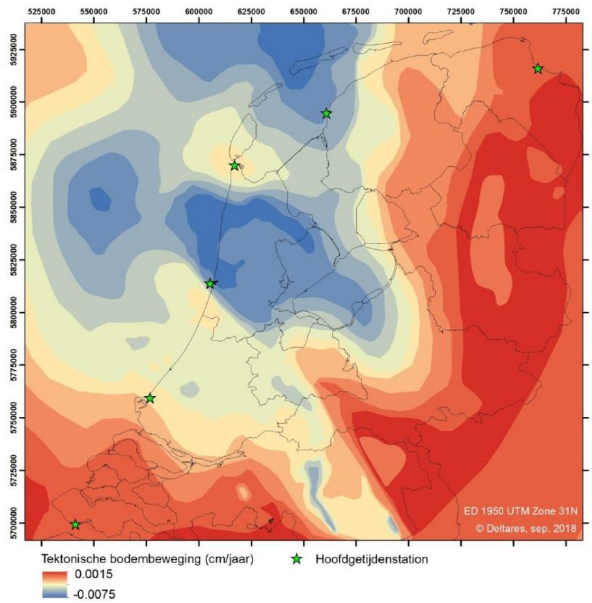

FIGURE 13: TECTONIC MOVEMENT IN CM/YEAR: BLUE INDICATES A DECLINE AND RED INDICATES TECTONIC HEAVE (HIJMA & KOOI 2018).

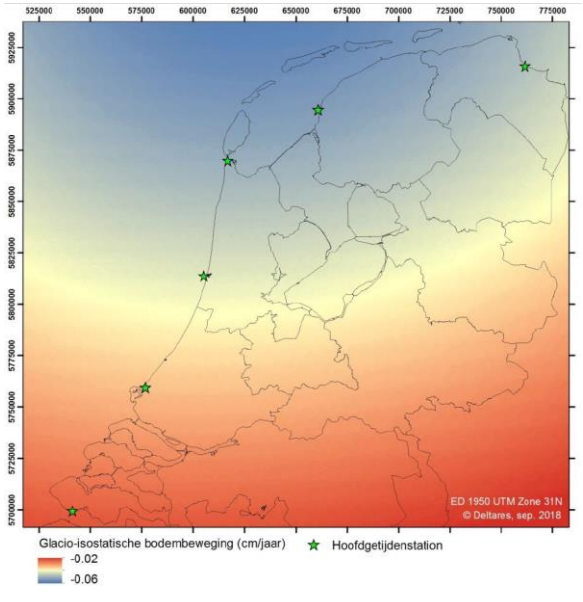

FIGURE 14: GLACIO-ISOSTATIC MOVEMENT IN CM/YEAR (HIJMA & KOOI 2018).

3.2 Subsidence Drivers

3.2.1 Surface water drainage

Cultivated land requires a regulated groundwater table (Bos *et al.* 2017). As our study area is located below mean sea level (see 2.3), land has to be drained to maintain an optimized groundwater table. Without proper water management, the research would slowly flood by the addition of ground-, river and rainwater. However, excess water is stepwise pumped towards the sea by a system of ditches, canals and pumping stations. Because of pressure head differences between groundwater and surface water, changes in surface water management indirectly influence the groundwater level (Fitts 2002). Lowering the surface water level forces the groundwater table to decline (M. Hendriks 2010), which accelerates subsidence. First, the drop in groundwater level can oxygenate peat and trigger extra aerobic decomposition (Brouns et al., 2014; Figure 12). Second, the disappearance of water decreases the pore pressure and enhances compression (Terzaghi 1943). Surface water drainage controlled by seasonal differences in groundwater levels oxygenates parts of the soil that become aerated annually. However, drastic surface water lowering could oxygenate former non-oxygenated, 'fresh' sediments which further accelerates subsidence (Brouns *et al.* 2014).

3.2.2 Hydrocarbon fluid withdrawal

The withdrawal of hydrocarbon decreases the pore fluid pressure (*depletion)* and thereby increases the vertical effective stress between grains within the extraction reservoir (Terzaghi 1943). The extraction initiates deep compression and so the overburden and surface elevation subside (Van Thienen-Visser *et al.* 2015, Fokker *et al.* 2018). The withdrawal of hydrocarbon from the Groningen gas field started in 1963 (Van Thienen-Visser *et al.* 2015) and recent governmental policy is intended to end the extraction within 10 years (Rijksoverheid 2021). The generated subsidence by hydrocarbon withdrawal depends on the depth and size of the reservoir, the extraction volume, and the historic extraction (NAM 2020). The latter because there is a delay between the gas extraction and the measured subsidence at the surface (Van Thienen-Visser *et al.* 2015). The subsidence by deep compression is characterized by a circular depression (Figure 3). Currently measured subsidence rates by hydrocarbon withdrawal vary between 5 mm/year at the centre of the extraction well to <1 mm/year tens of kilometres away from the centre (NAM 2020). The subsidence by hydrocarbon withdrawal since the start of the gas extraction in the research area varies between 25 and 30 cm (NAM 2020).

3.2.3 Subordinate drivers

Salinity

Seepage of saltwater from the sea reduces the aerobic decomposition rate (Brouns *et al.* 2014). The brackish-saline interface is at the study area is located more than 100 meters deep and is therefore not likely to influence the groundwater of the shallow subsurface (Oude Essink & De Louw, 2014; Figure 15).

Loading

Natural compression of shallow deposits can be accelerated by applying an additional load at the surface, since the extra weight will increase the total vertical stress (Terzaghi 1943). Accelerated subsidence due to loading occurs predominantly in urban areas with a high density of buildings and infrastructure (Laarhoven 2017). Loading is purposefully applied in construction work to trigger subsidence, reducing the future subsidence potential. However, this thesis investigates subsidence in rural areas with minor (urban) loading. Only sporadic ditch damping may have accelerated subsidence locally, which is considered during fieldwork preparation.

Groundwater extraction

Groundwater extraction from the subsurface decreases the hydrostatic pressure of the concerned aquifer and enhances compression (Minderhoud *et al.* 2017). In many low lying urbanized areas around the world, the largescale extraction for drinking water or irrigation is an important driver (Higgins 2016, Minderhoud *et al.* 2017, Koster *et al.* 2018). The most proximal groundwater extractions in northeast Groningen are located several tens

of kilometres away (Commissie bodemdaling n.d.). This thesis assumes that groundwater extractions do not significantly contribute to total measured subsidence. However, there is insufficient scientific knowledge on the effect of groundwater extraction and subsidence to substantiate this statement

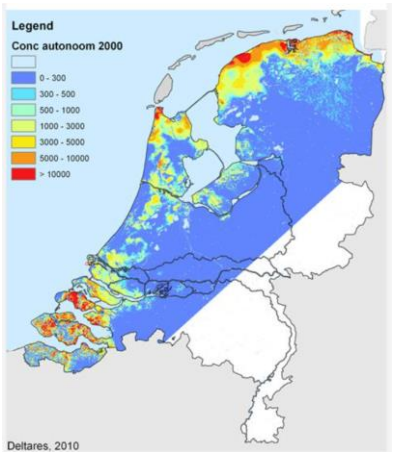

FIGURE 15: OVERVIEW MAP OF POSSIBLE SALINE SEEPAGE IN THE NETHERLANDS (OUDE ESSINK & DE LOUW 2014).

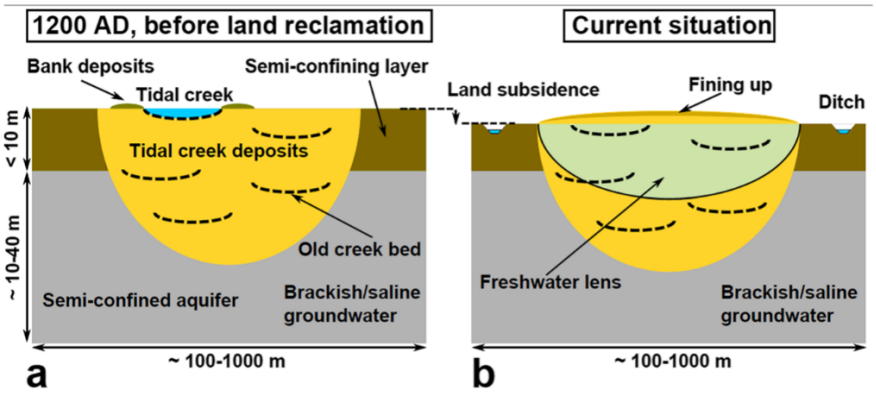

FIGURE 16: DIFFERENTIAL SUBSIDENCE AFTER THE LAND RECLAMATION LEADING TO AN INVERSION IN LANDSCAPE (PAUW *ET AL.* 2015).

3.3 DIFFERENTIAL SHALLOW SUBSIDENCE

The previous paragraphs discussed subsidence mechanisms and drivers as individual acting contributors to total vertical movement. However, a subsidence signal can be the consequence of various active subsidence mechanisms. This paragraph considers the reasons for spatial and temporal differences in shallow subsidence.

HETEROGENEITY

Two important factors contribute to a heterogeneous subsurface in Groningen. First, the relief of the Pleistocene surface created a differential thickness of Holocene deposits (Stouthamer *et al.* 2020). Second, the dynamic tidal system caused a local variety in sediment material comprising this Holocene subsurface (Kiestra 2000), determining spatial differences in water content, porosity and permeability over a relatively short distance (Van Asselen 2010). Heterogeneity is expected to affect subsidence in the shallow subsurface. First, aerobic decomposition is limited by the amount of peat in the unsaturated zone. Therefore, regions with peat close below the surface are prone to peat oxidation (Brouns *et al.* 2014). Second, the higher water content of peat enables more expulsion of pore water, increasing the compression potential. Though, the low permeability of clay could delay the effect of consolidation, such that compression in clay can continue long after the compression of peat already ended (Koster *et al.* 2018).

HISTORIC SUBSIDENCE

Historic subsidence affects the subsidence potential. (Van Asselen 2010, Stouthamer & Van Asselen 2015). Previous peat oxidation increased the relative clastic fraction in the peat, reducing the potential for future peat oxidation (Fokker *et al.* 2019). Both compression and oxidation reduce the porosity and permeability of fine sediment over time, suggesting that recently deposited sediments are more compressible (Van Asselen, 2010; Figure 11). For example, just after reclamation of subaqueous deposits, the compressibility of these recently aerated sediments is still high and can contribute significantly to the total subsidence (Fokker *et al.* 2019). Over time, the layer becomes more compact, reducing the compressibility for future subsidence. This thesis on subsidence in Groningen considered shrinkage as a minor contributor to shallow subsidence, as the compressibility of the unsaturated zone is expected to have decreased significantly since the first artificial drainage around 1500 AD (Pierik *et al.* 2017). In northeast Groningen, historic subsidence due to a discontinuous subsurface can be distinguished in the landscape. Former tidal creeks are nowadays slightly higher elevated, referred to as *relief inversion* (Stouthamer et al., 2020; Figure 15). It is hypothesized that this differential

subsidence pattern is the result of coarser-grained deposits in former tidal creeks that have been less prone to subsidence over the last hundreds of years.

DYNAMIC WATER TABLE CONDITIONS

Groundwater levels vary because of seasonal and annual differences in atmospheric conditions. Higher evapotranspiration and less precipitation lower the groundwater level in the (late) summer, increasing the subsidence potential (J. J. H. Van den Akker *et al.* 2007). Artificial drainage by active water management reduces the natural dynamics by adapting the surface water levels throughout the year. Surface water levels in summer are raised to initiate lateral groundwater flow from the ditches to surrounding land, whereas the direction of flow reverses in winter when groundwater has been fed by increased precipitation (Bos *et al.* 2017). Present climate change reinforces the extremes of the natural dynamics in groundwater level fluctuations, increasing the subsidence potential. Longer summer droughts can induce compression and decompose former non-oxygenated peat (Brouns *et al.* 2014, Kooi & Erkens 2020). Climate warming increases the occurrence of 'dry' years and associated extreme low groundwater levels, such as in 2016, 2018, 2019 and 2020 (Voosen 2021)

Not only temporal but also spatial differences in groundwater level cause differential subsidence. Depending on the moment in time, groundwater levels either increase or decrease exponentially perpendicular to bordering surface water. The extremes in groundwater level increase with distance from an open water body, causing a non-uniform subsidence rate over, for example, the length of a farming parcel (J. J. H. Van den Akker *et al.* 2007, Bos *et al.* 2017). Besides, water authorities in northeast Groningen have divided the land into designated regions, to which they allocate surface water levels to optimize surface water drainage. This regional water management creates a local varying thickness of the unsaturated zone, affecting subsidence. Lastly, the groundwater level might vary locally due to several additional factors such as macropore flow, vegetation and irrigation.

3.4 INCORPORATING GROUNDWATER LEVELS IN SUBSIDENCE RESEARCH

First, the incorporation of the groundwater levels in subsidence research depends on the general research strategy. Shallow subsidence research can be differentiated in studies that model historic subsidence (Hoogland *et al.* 2012, R. Hendriks *et al.* 2014, Fokker *et al.* 2015, 2019, Erkens *et al.* 2016) or potential/future subsidence (J. J. H. Van den Akker *et al.* 2007, Stouthamer & Van Asselen 2015, Koster *et al.* 2018, Kooi & Erkens 2020). Some studies manage to model both historic as potential subsidence (Van Asselen *et al.* 2018). Research on historic subsidence benefit from the fact that historic hydrological and meteorological measurements can be consulted. Some studies used historic surface water levels as an indicator for historic groundwater levels (Hoogland *et al.* 2012), whereas other studies have deployed an additional model for the development of the groundwater level through time (R. Hendriks *et al.* 2014, Fokker *et al.* 2015, 2019). Studies that model future or potential subsidence have either predicted future groundwater levels (Koster *et al.* 2018) or managed to neglect groundwater levels by focussing on another important indicator of future shallow subsidence such as the sediment density (Stouthamer & Van Asselen 2015, Van Asselen *et al.* 2018). Recently, Kooi & Erkens (2020) incorporated predicted seasonal fluctuations of future groundwater levels.

Second, the degree of detail in modelling groundwater levels is determined by the aerial extent of the study. Vertical, one-dimensional subsidence research can accurately mimic groundwater levels through time (Kroes *et al.* 2017). However, two or three-dimensional subsidence models will have to incorporate differential groundwater levels, besides temporal variations. Some studies that investigate subsidence over long time periods on a national scale do not consider groundwater levels, as in these situations the effect of groundwater is of minor importance (Erkens *et al.* 2016). Van den Akker et al. (2007) considered extreme conditions in the subsurface saturation state by an empirical relation between yearly lowest groundwater levels and oxidation. Unfortunately, these empirical relations do not consider compression and were only derived for locations containing solely peat or a small coating of clay on top of peat. The heterogeneous subsurface of northeast Groningen does rarely match these criteria.

4. MATERIALS AND METHODS

4.1 GENERAL APPROACH

Several research strategies were combined to achieve the main objective of this thesis *to quantify historic, shallow subsidence in the Groningen gas field since 1963 using a differential subsurface saturation state based on a dynamic groundwater level.*

Since already existing subsidence models did not fit the desired goal to incorporate a dynamic groundwater level, this thesis chose to develop a new subsidence model in which the occurrence of shallow subsidence mechanisms relies on the differential subsurface saturation state. The establishment of such a subsidence model required the incorporation of dynamic groundwater levels. Therefore, this study used the SWAP-model to obtain daily groundwater levels. Both the SWAP-model as the subsidence model required a substantial amount of input parameters. Most of these parameters could be obtained by a data inventory of online databases. All the remainder required parameters were obtained by a field study in Nieuwolda and Appingedam (Figure 17).

The method section is structured as follows. First the available data (materials) is gathered and assembled through a data inventory of online databases (section 4.2; Subobjective 1). Next, daily groundwater levels will be modelled with use of the SWAP-model (section 4.3). A comparison between modelled and measured groundwater levels will allow to assess the potential and reliability of the modelled groundwater levels (Subobjective 2). Subsequently, the modelled groundwater levels will be incorporated in a newly developed model that quantifies subsidence in the shallow subsurface (section 4.4). Deploying the model for a location in the field study area and for a future scenario is used to validate the model capabilities (Subobjective 3). Additional research strategies to quantify historic subsidence will be determined by investigating historical measurements from the data inventory (section 4.5; Subobjective 4). Finally, additional required parameters needed to achieve these objectives were be obtained by a field study in Nieuwolda and Appingedam (Section 4.6). Complementary, the detailed investigation of the local subsurface in Nieuwolda allowed an investigation of the effect of subsurface heterogeneity on shallow subsidence (Subobjective 5).

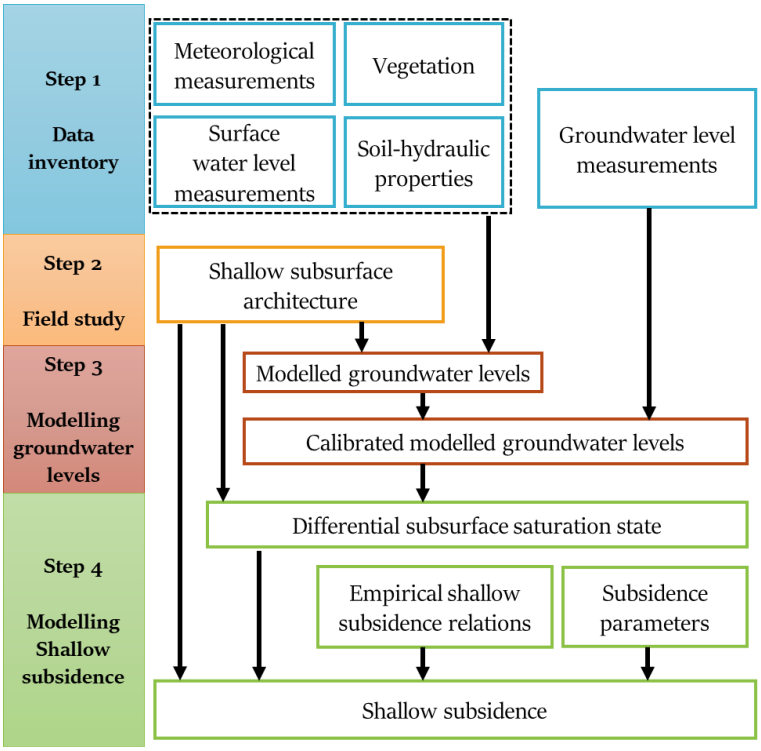

FIGURE 17: FLOW CHART OF THE GENERAL RESEARCH STRATEGY AND COMPLEMENTARY METHODS.

4.2 MATERIALS

Various sources are consulted in the search for required data. The qualitative criteria that were set for the data selection are discussed. The available data is most often acquired for the research area of northeast Groningen.

SURFACE LEVEL

A great amount of historic surface level measurements obtained before 1982 are stored in a digital database entitled ''Tophoogte MD'' (Table 1). The surface level measurements were obtained by the digitalisation of old maps. These maps contained elevation contour lines that were created by a spatial interpolation of aerial photographs with some manual measurements as reference (personal communication Ramon Hanssen). The surface level measurements for our study area in northeast Groningen were documented to be obtained in 1963/1964. However, it is not certain whether this document date is the moment that the aerial photographs were taken or the data when the maps were digitalized (may be a difference of some tens of years). Additionally, due to two interpolation techniques applied in the creation of these surface-level measurements, the exact inaccuracy of these surface-level measurements is rather unknown. However, a study by de Greeff et al. (2019) assumes an accuracy of approximately 30 cm. More recently, LiDAR-operations created the surface elevation for location in Groningen in 1998 (AHN1), 2009(AHN2) and in 2019(AHN3) (Table 1).

	Tophoogte MD	**AHN1**	**AHN2**	**AHN3**
Production year	1963-1964	1997-1999	2009	2019
Method	Spatial interpolation of aerial photographs to elevation contour lines	LiDAR	LiDAR	LiDAR
Data type	Point	Raster	Raster	Raster
Source	UU Database	PDOK	PDOK	PDOK
Accuracy [minimal 70% of the measurements]	Unknown, depend on spatial interpolation technique (approximated +/- 30 cm)	20 cm	10 cm	10 cm
Accuracy [minimal 99.5% of the measurements]	Unknown (approximated+/- 30 cm)	50 cm	20 cm	20 cm
Measurement density	Once every 10.000 m2	Once every 25 m2	Once every 0.25 m2	Once every 0.25 m2

TABLE 1: CHARACTERISTICS OF THE SURFACE ELEVATION MEASURE CAMPAIGNS IN THE NETHERLANDS.

LITHOLOGY

Since the start of the gas extraction, several parties have performed hand drillings. Most of the lithological core descriptions have been gathered by the Dutch Geological Survey (TNO), publicly available at DINOloket (Data en Informatie Nederlandse Ondergrond) or the online application of the BRO (Basisregistratie Ondergrond). The registered core descriptions in the research area since 1963 have been qualitatively investigated for their potential usage in shallow subsidence research. This qualitative selection was based on criteria concerning 1) the age of the hand drilling, 2) the spatial density of performed hand drillings 3) the total depth, 4) the detail in texture determination, 5) the vertical sampling resolution, 6) the groundwater level dynamics. Several, historical core projects in the research area were assessed as valuable for future usage (Figure 18).

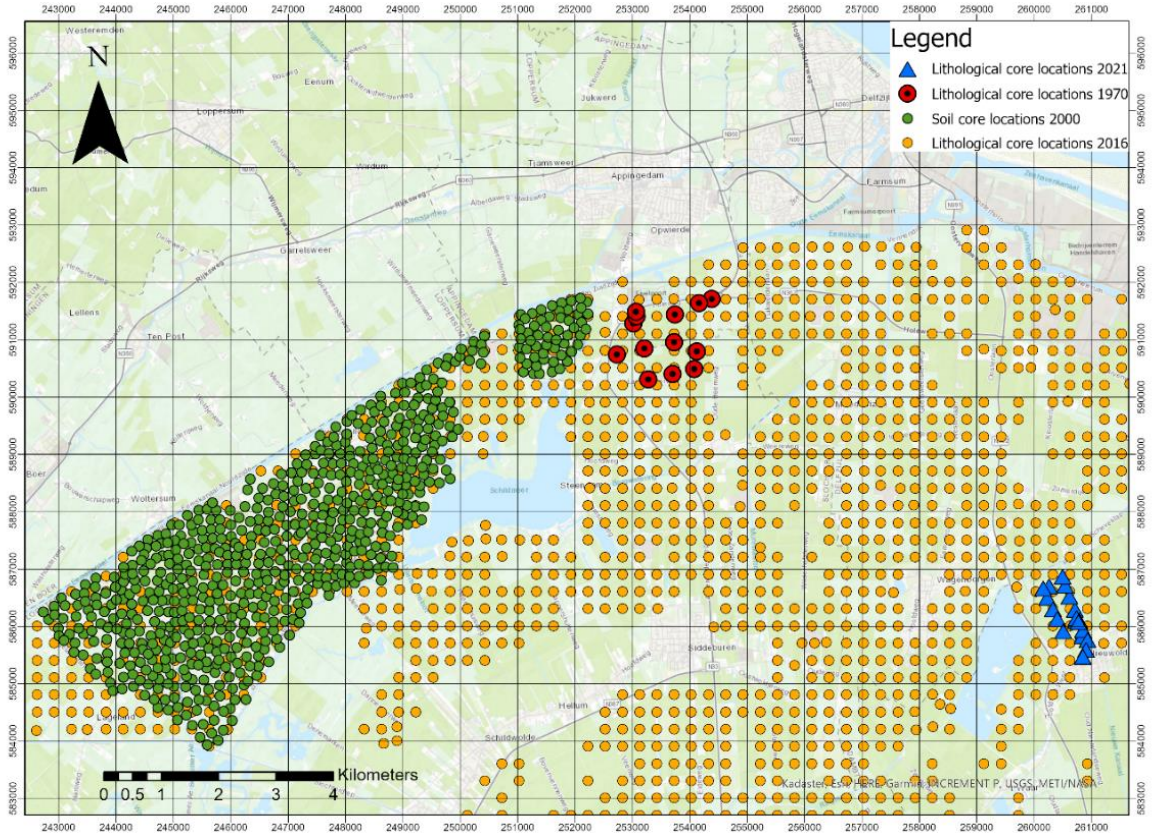

FIGURE 18: CORE LOCATIONS FROM PREVIOUS CORE PROJECTS IN AND AROUND THE RESEARCH AREA IN NORTHEAST GRONINGEN.

GROUNDWATER AND SURFACE WATER LEVEL

Historic groundwater and surface water level measurements could be obtained from the database DINO-loket (TNO) or by the online data portal maintained by water authority Hunze & Aa. Moreover, the webpage grondwatertools.nl contains already pre-analysed groundwater level series for some of the same measurement locations of the DINO-loket database. Additional, recent data concerning groundwater and surface water levels were provided by water authority Hunze & Aa through personal communication with A. Bartelds.

Measured groundwater levels were obtained by a pressure transmitter placed in a tube at a specific depth below surface level. The measured hydraulic head might differ from the actual phreatic groundwater level (Hendriks, 2010). Differences between the actual phreatic groundwater level and the measured hydraulic head are mainly determined by the filter depth. This study only used measured hydrostatic pressures whenever the pressure transmitter was placed within one meter below the expected phreatic groundwater level, allowing to assume that consulted, measured hydrostatic pressures always correspond with phreatic groundwater level measurements. The open data portal of the water authority Hunze & Aa provided among others seasonal prescribed surface water levels for the requested land parcel in Groningen (**Error! Reference source not found.**). Additionally, this database indicates the location of precipitation measurements, pumping stations, open water bodies and ditches. Desired groundwater level series can be requested for any monitoring well from the DINO-loket database maintained by TNO (**Error! Reference source not found.**).

SOIL-HYDRAULIC PROPERTIES

Soil hydraulic functions in the SWAP-model, such as the Richards equation and Mualem van Genuchten relations, require sediment characteristics regarding the permeability and saturation state (Bakker et al., 2019; Fitts, 2002). This study used fitted soil-hydraulic properties for different soil textures that were obtained by a long record of measurements from Wageningen Environmental Research on hydraulic properties, in Dutch referred to as the

'Staringreeks' (Bakker et al., 2019). Dr. M. Heinen (WUR) provided a database containing individual hydraulic properties of 999 sediment samples from 1964 onwards (Figure 19). First, all the individual samples were differentiated in terms of age. The measurements before 2012 were excluded because it is undetermined whether and how the hydrological measurements were performed. Subsequently, hydraulic properties were only used for sediment in the subsurface in the field study area, comprising soft and weak clay, eutrophic and oligotrophic peat, and loam (Appendix 7). Finally, improbable saturated hydraulic conductivities were excluded whenever these values where ten times larger than their expected value, based on a qualitative judgement by the author. Finally, this method yielded averaged soil-hydraulic properties for different texture groups (Table 2). The study by Bakker et al., 2019) gives additional information regarding the reliability of each soil-hydraulic property.

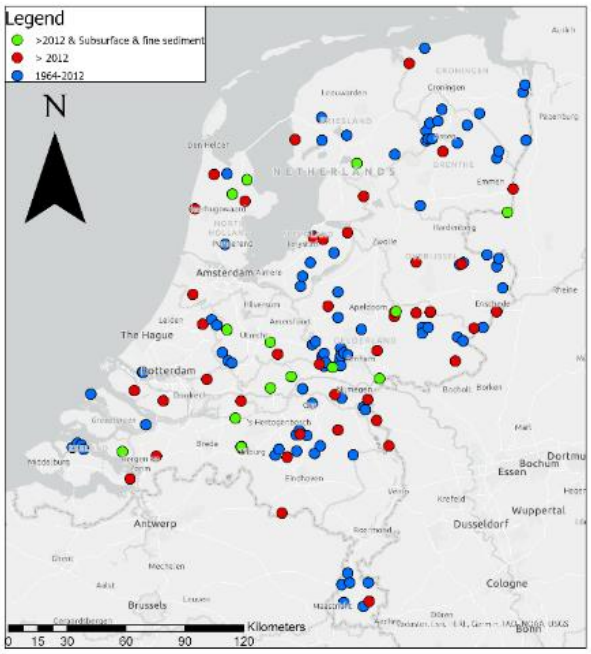

FIGURE 19: LOCATIONS OF SEDIMENT SAMPLES USED TO OBTAIN SOIL-HYDRAULIC PROPERTIES. ALL BLUE LOCATIONS ARE SEDIMENT SAMPLES OBTAINED BEFORE 2012. BOTH THE RED AND GREEN POINTS ARE SAMPLES OBTAINED AFTER 2012. THE GREEN POINTS INDICATE SAMPLES OF FINEGRAINED-DEPOSITS THAT MATCH THE TEXTURE GROUPS OF SEDIMENT OBSERVED IN OUR FIELD STUDY AREA.

Texture group	Residual Saturated water content	Saturated Water content	Alpha	N	L exp	Fitted hydraulic conductivity	Measured Hydraulic conductivity	Bulk density	Organic matter content
Unit	*cm3/cm3*	*cm3/cm3*	*cm*	-	-	*cm day*	*cm/day*	*mg/cm3*	*%*
Zware zavel	0.00	0.454	0.0135	1.174	6.44	11.43	437.45	1492.5	2.15
Lichte klei	0.06	0.451	0.0118	1.237	3.13	2.36	729.83	1470.0	2.37
Matig zware klei	0.00	0.639	0.0074	1.117	-4.00	1.28	198.23	968.0	8.43
Zeer zware klei	0.03	0.567	0.0125	1.072	-10.00	1.34	1.67	1197.3	3.97
Oligotroof veen	0.00	0.919	0.0060	1.325	5.50	1.17	6.27	154.5	94.68
Mesotroof en eutroof veen	0.00	0.770	0.0033	1.376	0.00	17.39	89.20	421.5	68.10

TABLE 2: SOIL-HYDRAULIC PARAMETERS REQUIRED IN THE SWAP-MODEL FOR EVERY TEXTURE GROUP PRESENT IN THE STUDY AREA.

4.3 MODELLING DYNAMIC GROUNDWATER LEVELS

The SWAP-model (Soil-Water-Atmosphere-Plant) is used to model groundwater levels. SWAP is an ecohydrological, process-based, one-dimensional model developed by Wageningen University & Research that simulates the transport of water, solutes and heat in variably saturated soils (Kroes *et al.* 2017). SWAP does not contain a modelling environment but is executed as a batch file in a command prompt. The code is written in Fortran language. Kroes et al. (2017) provide additional theoretical information on incorporated soil and subsurface processes. Besides, an additional more practical manual was built during this thesis for future hands-on guidance while modelling in SWAP (Appendix 10). First, the basic principle of modelling in SWAP will be summarized (section 4.3.1), followed by the determination of the soil-hydraulic properties (section 4.3.2). Subsequently, the key decisions that were made while modelling are addressed (section 4.3.3). Then, the strategy for the calibration of the modelled groundwater levels is explained (section 4.3.4). Finally, the consultation of the model for a sensitivity analysis is clarified (section 4.3.5).

4.3.1 MODEL DOMAIN, STRUCTURE AND PROCESSES

Vertically, the SWAP-model reaches from the vegetation cover to several meters below the groundwater level (Kroes et al., 2017; Figure 20). Meteorological data and potential irrigation serve as input at the surface, whereas the user can select various forms of hydraulic heads or fluxes at the lower boundary. The flow of water in the saturated zone uses Darcy's Law and the concept of hydraulic head (Fitts, 2002; Hendriks, 2010). The extraction of soil moisture by the roots of vegetation can be implemented. In the unsaturated zone, the flow of water is calculated with use of the Richards equation, which incorporates the dependency of the hydraulic conductivity on the variable volumetric moisture content through time (Fitts 2002, Kroes *et al.* 2017). In the horizontal direction, the model simulates lateral drainage in the saturated zone with the use of analytical drainage formulas.

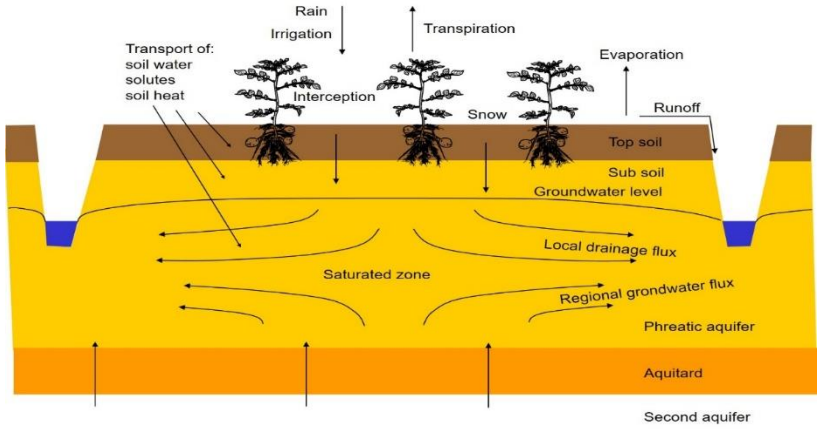

FIGURE 20: SWAP-MODEL DOMAIN AND ASSOCIATED PROCESSES REGARDING THE FLOW OF WATER THROUGH THE SUBSURFACE (KROES *ET AL.* 2017).

4.3.3 KEY MODEL DECISIONS

The structure of this section corresponds with SWAP's main input file, including meteorology, vegetation, soil water, lateral drainage and the bottom boundary. The most important decisions and associated uncertainties while modelling in SWAP will be addressed. All the parameters that were set can be consulted in Appendix 8.

METEOROLOGY

Meteorological input for the SWAP-model was conducted from a KNMI-weather station in Eelde, located 30 kilometres from the study area (KNMI 2021). This study assumed that the atmospheric conditions in Eelde match our study area. The measured atmospheric parameters were converted to serve as input for the SWAP-model (Table 3). The atmospheric data lacked absolute humidity measurements Hum (kPa) required in the SWAP-model. Therefore, the saturated vapour pressure Svp (kPa) was calculated from the average air temperature T_{air} (Kelvin) and the relative humidity RH (-), yielding the absolute humidity (Tetens 1930, Kroes *et al.* 2017).

The temporal resolution of meteorological measurements determines the resolution of the model results. Therefore, daily meteorological measurements used in this study yielded daily groundwater levels.

$$Hum = \frac{RH}{100} * Svp = \frac{RH}{100} * 0.611^{\frac{17.27*T_{air}}{T_{air}+237.3}} \quad (2)$$

SWAP meteorological parameters	Description	Unit	Notation	Corresponding KNMI column
Station	Station number	-	'number'	
DD	Day	-	integer	YYYYMMDD
MM	Month	-	integer	YYYYMMDD
YYYY	Year	-	integer	YYYYMMDD
RAD	Global radiation	kJ/m2	1 decimal	Q
Tmin	Minimum temperature	Celsius	1 decimal	TN
Tmax	Maximum temperature	Celsius	1 decimal	TX
HUM	Humidity	kPa	2 decimals	TG
WIND	Windspeed	m/s	1 decimal	FG
RAIN	Daily precipitation	mm	1 decimal	RH
ETref	Evaporation	mm	1 decimal	EV24
WET	Duration precipitation per day	days	4 decimals	DR

TABLE 3: REQUIRED METEOROLOGY PARAMETERS AND ASSOCIATED MEASUREMENTS FROM A WEATHER STATION.

VEGETATION

Vegetation can intercept precipitation, transpire water vapour and extract water by their roots (Kroes *et al.* 2017). The vegetation cover was obtained during the field study. Personal communication with the landowner of the field study area provided information on the land cover between 2016 and 2020. Vegetation was incorporated by adding additional crop files for the required types of vegetation (maize, wheat, grass, etc.) that were already developed by WUR. The timing of crop emergence and harvest were included based on the landowners' memory.

SOIL WATER

Layers were vertically discretised on a cm-resolution and were divided into multiple compartments. The number of compartments decreases with depth, because surficial and frequently unsaturated compartments require multiple along with more complex computations (Kroes *et al.* 2017). Every discretized layer was assigned to a soil-physical layer containing associated soil-hydraulic properties (Table 2). Layer thickness is a constant when modelling in SWAP, meaning that changes in layer thickness, such as shallow subsidence or swelling, could not be incorporated. Therefore, layers are assumed to be constant through time. Snowfall and frost were neglected while modelling in SWAP during this study, since the occurrence of snowfall and frost is rare and expected to have a minor impact on the eventually modelled groundwater levels. Additionally, hysteresis and macropore flow were neglected due to practical consideration. These phenomena require substantial input of data that were not easily accessible and valued as unfeasible within this thesis.

LATERAL DRAINAGE

This study chose to include lateral drainage through an additional file considering drainage and infiltration resistances. Surface water level measurements from a nearby pumping well at the Nieuwolda field study area were incorporated (Figure 21). Drain spacing was obtained by measuring the distance between ditches using satellite imagery. The depth of the ditches with respect to the surface level was measured using a measuring pole during the field campaign. An additional drainage level was incorporated to simulate interflow in the most

surficial 30 cm (Kroes *et al.* 2017), in order to reduce extreme ponding. This method was recommended by one of the SWAP developers (Dr. R. Hendriks) through personal communication.

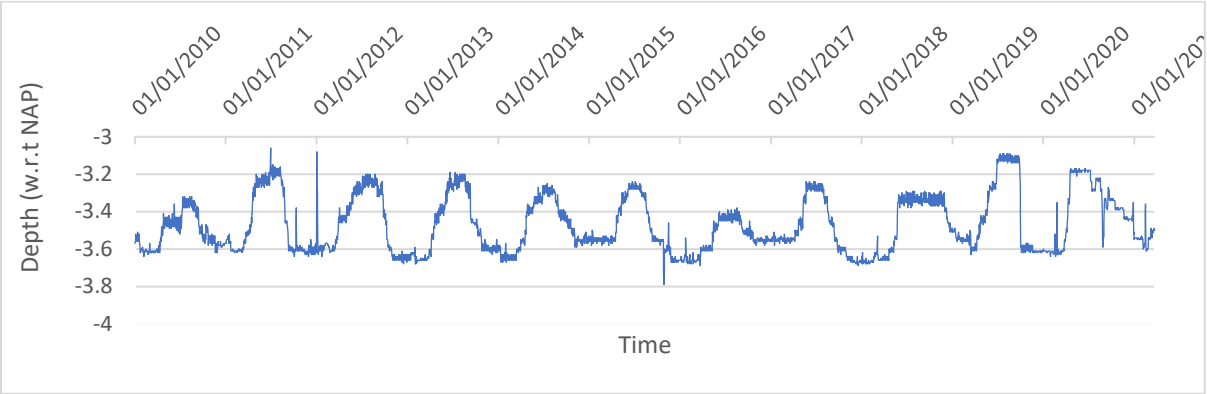

FIGURE 21: SURFACE WATER LEVEL MEASUREMENTS SINCE 2010 FOR THE NIEUWOLDA FIELD STUDY AREA (DINOLOKET.NL, ONDERGRONDGEGEVENS, GRONDWATERMONITORING)

BOTTOM BOUNDARY

The SWAP-model allows several options to calculate the hydraulic state at the bottom boundary of the model. This study chose to calculate the bottom boundary from hydraulic head measurements in the underlain aquifer. The monitoring well in Nieuwolda has measured the hydraulic head in the top of the aquifer (7-8 m below surface) daily since 1992. The hydraulic head at the aquifer is lower than the hydraulic head measurements 2 meters below surface level, indicating a vertical downward flux (*drainage)* year-round.

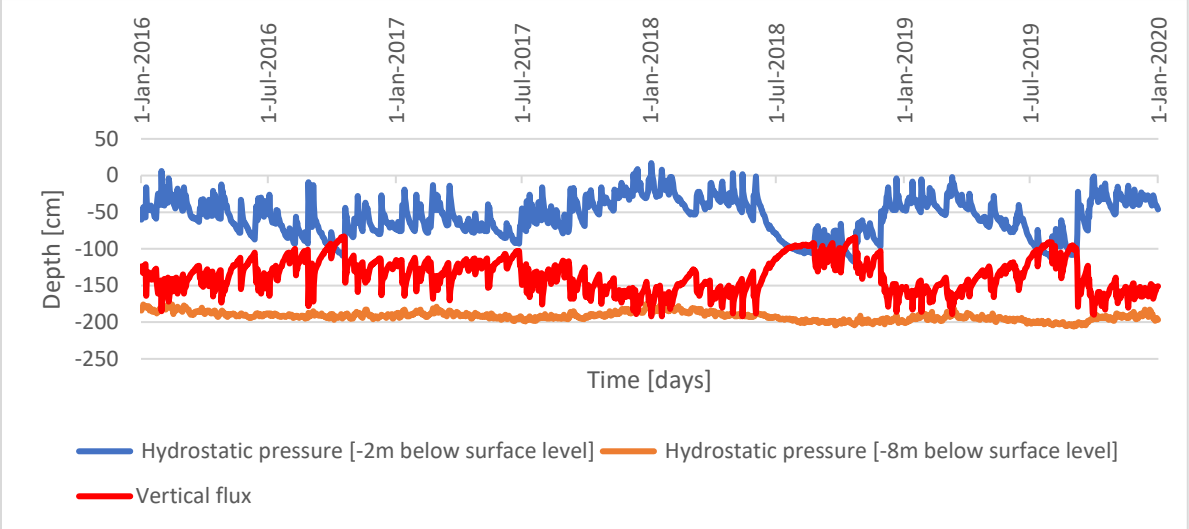

FIGURE 22: A SERIES OF MEASURED HYDROSTATIC PRESSURES FOR TWO LOCATIONS IN THE VERTICAL PROFILE AT THE MONITORING WELL IN NIEUWOLDA (DINOLOKET.NL, ONDERGRONDGEGEVENS, GRONDWATERMONITORING)

4.3.4 CALIBRATION AND VALIDATION

Modelled groundwater levels are calibrated by a comparison with groundwater level measurements from a nearby monitoring well in Nieuwolda. Groundwater levels were measured once every fourteen days between 1992 and 2007, and once a day from 2007 onwards. The pressure transmitter was placed within one meter below the expected phreatic groundwater level, allowing to assume that the measured hydrostatic pressure reflects the actual phreatic groundwater level.

The calibration was performed manually by adapting fitting parameters and investigating changes in the modelled groundwater levels. The quantitative validation is based on the root mean squared error (RMSE) between the measured and modelled groundwater levels, with t = time [days], GW_mea_t = the measured groundwater level [m] at t, GW_mod_t = modelled groundwater level [m] at t and n = the total amount of measurements [days].

$$RMSE = \sqrt{\sum_{t=1}^{n} \frac{(GW\_mea_t - GW\_mod_t)^2}{n}} \quad (3)$$

4.3.5 Model consultation

After model calibration at the monitoring well location in Nieuwolda, the model was deployed to obtain the groundwater levels at two additional locations in the field study area(Figure 23). Deeper hydraulic head measurements in an aquifer were only available at the location of the monitoring well. Therefore, the bottom boundary was determined by a sinusoidal relation for the vertical flux, based on the mean and extremes of the measured vertical flux at the monitoring well. Finally, the effect of seven parameters on the modelled groundwater levels has been investigated through a sensitivity analysis (Table 4). The sensitivity analysis is performed at the monitoring well location, allowing a comparison with groundwater level measurements. The land cover, surface water level and drain spacing were selected for the sensitivity analysis to investigate the effect of environmental factors that are regulated by humans. Other parameters were investigated because these were expected to significantly affect final model results, such as the meteorological input parameters, drainage resistance, vertical resistance and the interflow depth (Table 4).

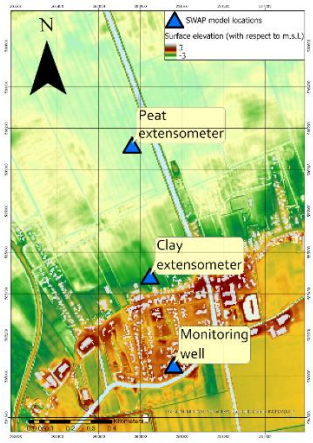

FIGURE 23: LOCATIONS FOR THE SWAP-MODEL CONSULTATION.

Location	Variable	Total runs	Period	Purpose
Monitoring well	-	1	2016-2019	Calibration, model performance
Monitoring well	-	1	1965-2019	Model performance
Peat extensometer	-	2	2016-2019	Input shallow subsidence model
Clay extensometer	-	1	2016-2019	Input shallow subsidence model
Monitoring well	Meteorological input	3	2018-2019	Sensitivity analysis
Monitoring well	Land cultivation	5	2018-2019	Sensitivity analysis
Monitoring well	Surface water level	4	2018-2019	Sensitivity analysis
Monitoring well	Drain spacing	4	2018-2019	Sensitivity analysis
Monitoring well	Horizontal resistance	4	2018-2019	Sensitivity analysis
Monitoring well	Vertical resistance	4	2018-2019	Sensitivity analysis
Monitoring well	Interflow depth	4	2018-2019	Sensitivity analysis

TABLE 4: MODEL RUNS USING THE SWAP-MODEL.

4.4 Modelling shallow subsidence

An empirical, one-dimensional, shallow subsidence model has been developed in MATLAB. The model is built to incorporate groundwater levels dynamics in the computation of shallow subsidence. First, the general model structure will be briefly explained (section 4.4.1). Afterwards, the individual model components will be addressed (section 4.4.2) and finally the model scenarios that were investigated will be presented (section 4.4.3). A practical manual has been developed for future model consultation (Appendix 11).

4.4.1 Model domain and structure

The vertical model domain reaches from the surface level down to the first appearance of an incompressible layer (Figure 24). Deep subsidence does not affect shallow subsidence because the surface level is set as zero and marks the upper limit of the model domain. In fact, groundwater levels are modelled with respect to the surface level, creating a differential saturation state through time.

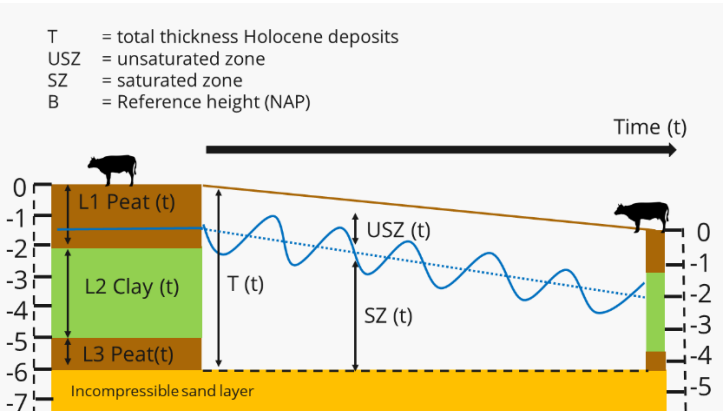

FIGURE 24: SCHEMATIZATION OF THE SUBSIDENCE MODEL PERFORMANCE. THE SURFACE IS MODELLED STATIC TO ACCURATELY MIMIC THE SATURATION STATE OF THE SUBSURFACE THROUGH TIME AND TO EXCLUDE INFLUENCES OF DEEP SUBSIDENCE FROM GAS EXTRACTION.

A lithological profile of the desired location is discretized into layers containing specific parameters. The groundwater levels that were produced using SWAP are incorporated and used to compute the saturation state of every layer at one moment in time. Next the model computes the decrease in layer thickness caused by compression and oxidation for every layer, starting at the top and continuing in downward direction. After calculating the deformation of all layers at one moment in time, the model computes the new thickness of all these layers. These new thicknesses are then used to calculate the deformation at the next timestep. To summarize, the model operates with a double loop. In the first loop subsidence is computed for every discretized layer, in the second loop the deformation is calculated at every moment in time (Figure 25).

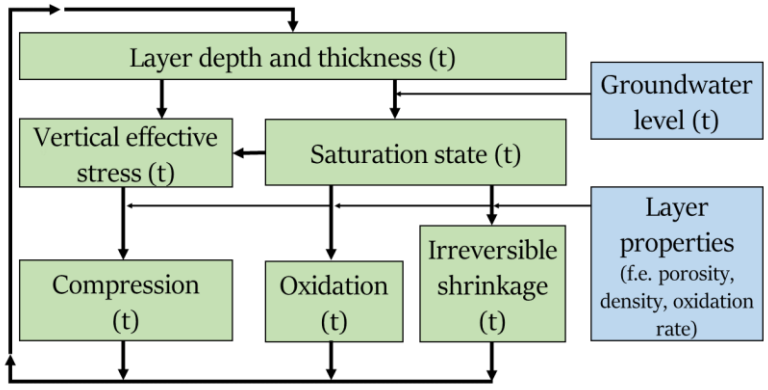

FIGURE 25: FLOW CHART OF THE SUBSIDENCE MODEL METHODOLOGY WITH A LOOP COMPUTING THE SUBSIDENCE IN EVERY LAYER AT ANY MOMENT IN TIME.

4.4.2 MODEL COMPONENTS

The model concepts are based on the model from the study by Fokker et al. (2019). For example, equations regarding the computation of stress and strain, compression and oxidation are similar. One important difference between the models is the computation of the saturation state. The model in this thesis incorporates daily fluctuations in groundwater level, whereas the model by Fokker et al. (2019) uses a gradual decreasing groundwater level. Therefore, the model by Fokker et al. (2019) is not able to compute seasonal or even daily differences in peat oxidation, while the model in this thesis does.

SUBSURFACE PARAMETERIZATION

Lithological parameters are assigned to every discretized layer in the subsurface profile (Table 5). Assigning different parameter values for each layer enables the differentiation between layers with the same texture group but a different subsidence history.

GROUNDWATER LEVEL DYNAMICS

Groundwater levels are incorporated by loading a text file containing the modelled groundwater levels from the SWAP-model. Positive groundwater levels (ponding) are converted to zero, still indicating full saturation of the subsurface. The saturation state is determined by an if-statement indicating whether the layer is either fully saturated, partly saturated, or unsaturated. Layers that were entirely located above the groundwater level were assumed to be completely dry and therefore disposed of water.

STRESS AND STRAIN

The effective stress σ'_{eff} [kg m^-1 s-2] is computed following Terzaghi's Law (see 3.1) by the difference between the total vertical stress $\sigma_{tot,v}$ [kg m^-1 s-2] and the hydrostatic pressure μ [kg m^-1 s-2]. The effective stress is separately computed for the unsaturated (dry) and saturated (wet) part of every layer, using the gravitational constant g [m s-2], the layer thickness h [m], the layer porosity n [-], the density of the grains ρ_{gr} [kg m-3] and the density of water ρ_w [kg m-3]. The contribution of the exerted effective stress by the saturated and unsaturated part within every layer is added and gives the effective stress for every layer. Finally, the total effective stress that a certain layer experiences is the contribution of the total exerted effective stress of all the overlain layers combined.

$$\sigma_{tot,v(wet)} = \Big((1-n) * \rho_{gr} + \rho_w\Big) * g * h \tag{4}$$

$$\sigma_{tot,v\,(dry)} = (1-n) * \rho_{gr} * g * h \tag{5}$$

$$\mu = \rho_w * h \tag{6}$$

$$\sigma'_{eff(dry)} = (1-n) * \rho_{gr} * g * h \tag{7}$$

$$\sigma'_{eff(wet)} = (1-n) * (\rho_{gr} - \rho_w) * g * h \tag{8}$$

$$\sigma'_{eff} = \sigma'_{eff(wet)} + \sigma'_{eff(dry)} \tag{9}$$

$$\sigma'_{tot\,,eff} = \sum_L \sigma'_{eff} \tag{10}$$

COMPRESSION

The model computes compression using the 1D-Koppejan model (Koppejan 1948), differentiating between primary and secondary compression. Δh_{pr} [m] and Δh_s [m] are respectively the decrease because of primary and secondary compression. C_p [m day-1] and C_s [m day-1]] are respectively the primary and secondary compression parameters. t = timestep [days], and $\Delta\sigma$ is the difference in total, vertical effective stress between the former and the current timestep. Note that $\Delta\sigma$ will be positive for a decreasing groundwater level, and

negative for an increasing groundwater level. This stsudy assumed that all the obtained effective stresses were smaller than the preconsolidation stress, based on the fact that there is no average decrease in the measured groundwater level observed. Based on this assumption, the model only accounts for reversible compression.

$$\Delta h_{com} = \Delta h_{pr} + \Delta h_s = \left(\left(\frac{1}{C_p} + \frac{1}{C_s} * \log\left(\frac{1+t}{1}\right)\right) * \ln\left(\frac{\sigma' + \Delta\sigma'}{\sigma'}\right)\right) * h_L \quad (11)$$

PEAT OXIDATION

The model first computes which part of the peat can truly be decomposed. The model considers aerobic peat decomposition such that peat oxidation only occurs under unsaturated conditions. Second, the relative clastic admixture α in peat is excluded from the computation of peat oxidation because only organic matter in peat can be decomposed.

$$\Delta h_{ox,p} = h_p - h_{p,wet} - \alpha * h_{p(t=0)} \quad (12)$$

Next, the actual decrease in thickness due to peat oxidation is approached by an exponential decay function. The exponential decay constant is the oxidation rate v_{ox} [m day-1].

$$\frac{dh_{ox,p}}{dt} = -v_{ox} * t \quad (13)$$

Finally, equation 12 and 13 are combined to compute the decrease in thickness Δh_{ox} due to peat oxidation at any timestep for every layer.

$$\Delta h_{ox} = \left(h_p - h_{p,wet} - \alpha * h_{p,(t=0)}\right) * (1 - e^{-v_{ox} * \Delta t}) \quad (14)$$

Every discretized layer contains a characteristic value for 1) the peat thickness 2) the oxidation rate 3) the relative clastic admixture (Table 5).

4.4.3 MODEL CONSULTATION

The model is only deployed for the peat extensometer location, as the two other modelled locations do not contain peat in the unsaturated zone and are not prone to peat oxidation. Unfortunately, no average decrease in groundwater level is observed at this location during the modelled period (2016-2019). Therefore, only the contribution of peat oxidation will be considered in the quantification of shallow subsidence. The initial thickness is obtained during the field study. The clastic admixture of peat could not be measured but was assumed to be zero, based on the determined organic matter content from the Nieuwolda field study. The peat oxidation rate, bulk density, porosity and, primary and secondary compression parameters are based on values from the study by Fokker et al. (2019). The sediment properties in this publication are obtained for sediment from a study area in Flevoland and will differ from the sediment characteristics from our study area in Nieuwolda. The compressibility of the sediment from the Flevoland study is expected to be larger than the compressibility of sediment in Nieuwolda, due to the only recent reclamation of Flevoland. However, acquiring the necessary properties for sediment from the Nieuwolda study area was not feasible within this thesis.

	Texture	**h_initial**	**V_ox**	**res_clay**	**n**	**rho_gr**	**Prim Com**	**Sec Com**
Unit	-	*m*	*cm m-1 a-1*	-	-	*kg m-3*	*m a-1*	*m a-1*
L1	Clay	0.4	0	0	0.75	1400	9497	42369
L2	Peat	2.3	0.88	0	0.85	1100	2557	23741
L3	Clay	0.2	0	0	0.75	1400	9497	42369
L4	Peat	0.9	0.88	0	0.85	1100	2557	23741
L5	Clay	1.1	0	0	0.75	1400	9497	42369

L6	Loam	1.6	0	0	0.75	1470	9497	42369

TABLE 5: SEDIMENT CHARACTERISTICS PER DISCRETIZED LAYER IN THE SUBSIDENCE MODEL.

First, the model performance is investigated using the sediment properties from Table 5. Next, the effect of the oxidation rate and the relative clastic admixture in the computation of shallow subsidence is investigated through a sensitivity analysis (Table 6). The minimum and maximum oxidation rates used in the sensitivity analysis are based on the same investigated oxidation rates in the study by Koster et al. (2018) varying between 0.5 and 3 cm m-1 year-1. Finally, a future scenario with an averagely linear decreasing groundwater level is investigated to study the model performance for the computation of compression. A sinusoidal groundwater prediction is used to mimic the future seasonal fluctuation in groundwater level for the peat oxidation computation, similar to the study by Kooi & Erkens (2020). The amplitude A [m] is based on the measured groundwater level amplitude at the monitoring well in Nieuwolda. The initial groundwater level GW_{ini} [m] is obtained from the measured groundwater level during the field study. The linear decrease rate β [m]is purely hypothetical.

$$GW\ (t) = A * \sin\left(\frac{2\pi * t}{365.25}\right) - GW_{ini} + \beta * \Delta t \quad (15)$$

$$GW\ (t) = 0.3 * \sin\left(\frac{2\pi * t}{365.25}\right) - 0.5 + (-0.05) * \Delta t \quad (16)$$

	Period	Subsidence mechanisms	Groundwater levels	Variable	Total runs	Purpose
1	2016-2019	Oxidation	SWAP, Averagely constant	-	1	Model performance
2	2016-2019	Oxidation	SWAP, Averagely constant	Oxidation rate	7	Sensitivity analysis
3	2016-2019	Oxidation	SWAP, Averagely constant	Relative clastic admixture	7	Sensitivity analysis
4	2020-2040	Oxidation + Compression	Sinusoidal prediction, Linearly lowered	-	1	Performance modelling compression Predict future shallow subsidence

TABLE 6: MODEL RUNS USING THE SUBSIDENCE MODEL.

4.5 INDIRECT MEASURING, HISTORIC SHALLOW SUBSIDENCE

Apart from modelling subsidence based on groundwater level dynamics, two additional strategies were performed to quantify historic, shallow subsidence since 1963 in the Groningen gas field area. First, a comparison between the thickness of fine-grained deposits from historical and present lithological measurements will indicate differences in the shallow subsurface build-up through time (section 4.5.1). Second, investigating surface-level measurements through time will indicate vertical motion of the surface level since 1963 (section 4.5.2).

4.5.1 INVESTIGATING DIFFERENCES IN LITHOLOGY THROUGH TIME.

The University of Amsterdam obtained the lithology at twenty locations south of Appingedam in September 1970, for which sediment was sampled with a cm-accuracy. These locations were reported in the Dutch national coordinate system (RD). Seven locations of these historical core descriptions were selected to revisit, based on their accessibility and total Holocene sediment thickness. For example, some of the core locations from 1970 were eliminated because land management after 1970 such as road constructions or ditch damping made these locations not suitable for a lithological comparison. The present lithological build-up will be obtained by a field study in Appingedam in March 2021, during which the lithology of the exact same locations will again be

determined with a cm-accuracy. The difference in thickness of fine-grained deposits between 1970 and 2021 will reveal the subsurface deformation within 56 years.

There are some factors that influence the results of this strategy. First, the difference in thickness of fine-grained deposits is used as an indication for the part of the subsurface that has been prone to the shallow subsidence mechanisms of compression and peat oxidation. The transition between (incompressible) sand deposits and fine-grained deposits in 2021 is set as the transition from peaty sand to sandy peat. However, the core description of 1970 did not had such a high resolution texture determination and only discriminated between sand and peat. The error of the results from difference in sampling technique is approximated as 5cm. Second, the core description in 1970 were obtained in September, and the core description in 2021 in March. Due to seasonal fluctuations of the surface level, the subsurface in March(2021) is hypothesized to be more swollen after increased precipitation during winter compared to the subsurface in September (1970). The maximal range in seasonal surface level fluctuation is approximately 5 cm (Van Asselen *et al.* 2020). The total error-bar of these results is therefore approximated as 10cm.

4.5.2 Investigating differences in surface elevation through time.

The surface level measurements from 1963 (Tophoogte MD) and from 2019 (AHN3) were imported into ArcGIS Pro. First, the pixels from AHN3 that overlapped surface level measurements from 1963 were clustered using the Spatial statistics tool, resulting in the measured surface levels of approximately 32.000 data points for both 1963 and 2019. Subsequently, the pixel values from 1963 were subtracted from the pixel values from 2019 using the minus tool in the Spatial analyst toolbox, yielding the total vertical movement of the surface level between 1963 and 2019. Note that the final accuracy of the obtained vertical motion is the combined accuracy of the measurements from 1963 and 2019, which is in the order of 40 cm due to the larger approximated inaccuracy of the measurements from 1963. The large quantity of measurements allows an investigation of the regional differences in the subsidence pattern. The surface motion map will be compared to cross-section obtained from the DINO-loket, allowing to investigate the effect of regional shallow subsurface heterogeneity on subsidence.

4.6 Field study

Additional data on the local subsurface build-up and heterogeneity has been obtained during a one-week field campaign in March 2021. The fieldwork was a joint effort for this Thesis and the PhD research of Chayenne Janssen (Improvement of geophysical models at Holocene and Pleistocene depths, DeepNL-project). The field campaign comprised the following distinctive aims:

1. To determine the local subsurface build-up of Groningen, allowing to investigate spatial differences in lithology and historic, shallow subsidence.
2. To obtain sediment characteristics such as the organic matter content, clastic admixture and porosity required to model groundwater dynamics and shallow subsidence.
3. To determine the lithology of several locations south of Appingedam that have previously been investigated in 1970. Differences in the total thickness of Holocene deposits between 1970 and 2021 will indicate quantify the subsidence in the shallow subsurface over the last 51 years.

Additionally, this field study contribute to the field study objective of Chayenne Janssen to select the potential locations for two extensometers that will measure vertical motion between discretized layers in the subsurface. In the selection of a proper field study area, several criteria were set:

- A location affected by subsidence due to gas extraction of the Groningen gas field (see Chapter 2.1)
- A location with a shallow subsurface comprising fine-grained (peat and/or clay) deposits that is expected to be prone to shallow subsidence (see Chapter 3.2)
- A heterogenous subsurface comprising both surficial peat and surficial clay, allowing a differentiation between different subsidence mechanisms (see Chapter 3.2).

- Sufficient historic data to model groundwater levels. A continuous signal of measured groundwater levels and surface water levels is preferred to calibrate modelled groundwater levels.
- The approval by the landowner to perform the planned field activities.

Online databases on the surface elevation (AHN), the subsurface build-up and regional hydrology (DINO-loket) were used to investigate whether areas of interest met the criteria. Eventually, a field study area north of the city Nieuwolda was selected because this location met all the above mentioned criteria.

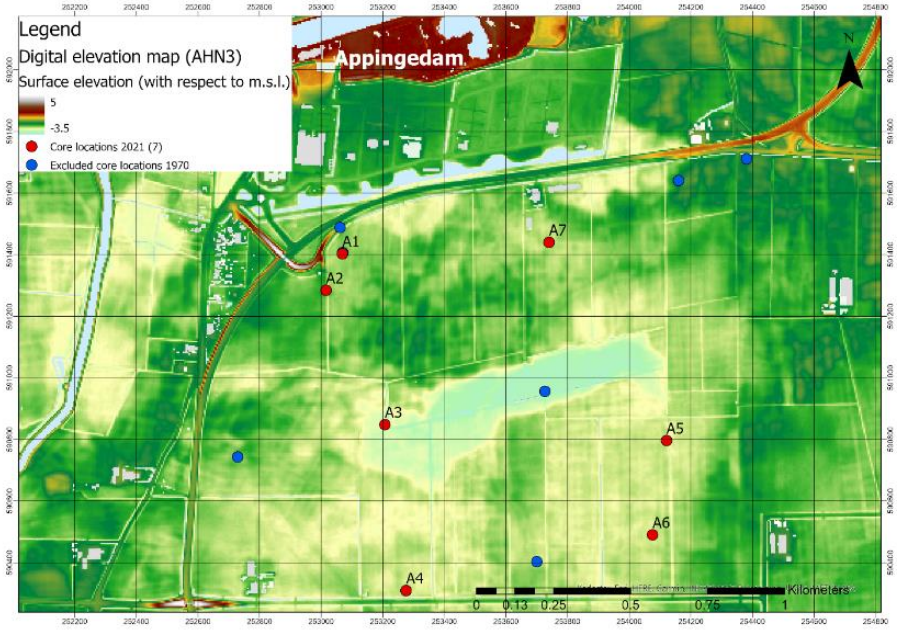

FIGURE 26: A DIGITAL ELEVATION MAP OF THE FIELDWORK AREA IN APPINGEDAM CONTAINING THE CORE LOCATIONS. .

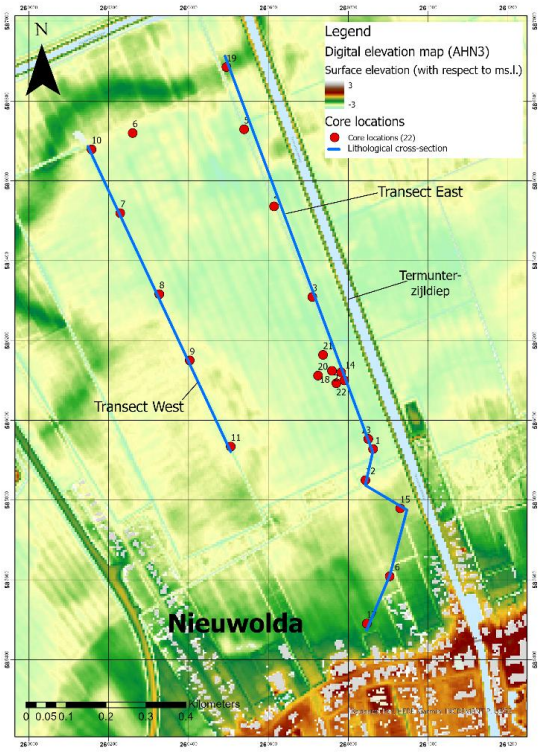

FIGURE 27: A DIGITAL ELEVATION MAP OF THE FIELDWORK AREA IN NIEUWOLDA CONTAINING THE CORE LOCATIONS.

Coring strategy

In the Nieuwolda field study area, hand drillings were performed along two parallel transects that were oriented perpendicular to a creek ridge at the northern end of the farmers parcel (Figure 27). Hand drillings were performed every 200 meters along both transects, indicating differences in the local subsurface build-up of the study area. Drillings were performed until the first appearance of sand at approximately 6-7 meters below surface-level, marking the transition between Holocene and Pleistocene deposits in the study area. The total thickness of Holocene, fine-grained deposits would indicate the part of the shallow subsurface that was prone to compression. The depth of the groundwater level, the amorphousness of peat and the occurrence of ironoxide spots would indicate the part of the shallow subsurface that was prone to peat oxidation. In the Appingedam field study area, seven locations that were already investigated in September 1970 by the University of Amsterdam were revisited (Figure 26; Appendix 4).

Lithology and stratigraphy

The Edelman hand auger has been used from the surface down to the groundwater level. Downwards, the saturated zone allowed the usage of a 1 m long gauge. The sediment cores from the Nieuwolda field campaign were sampled at ten-centimetre intervals by investigating the texture, relative organic matter content, colour, redox status, plant remains and the relative calciumcarbonate content. Additionally, specific characteristics such as the presence of anthropogenic compounds, ironoxide spots and layer transitions were described as well. Lithological transitions in the Appingedam field campaign were determined with a cm vertical resolution. The clastic texture determination was based on the Dutch classification scheme, defined by de Bakker & Schelling (1966) adjusted by Berendsen (2005). Additionally, the relative organic matter content has been determined with the organic matter classification scheme by de Bakker & Schelling (1966) and adjusted by Stouthamer & Berendsen (2001).

Analysis

Based on the texture classification, stratigraphical position and layer transition a lithological cross-section for transect west and east were made. Moreover, a lithogenetic cross-section for both transects could be created by combining the lithological cross-section and the presented geological background, in which deposits are divided into clastic tidal deposits that originate from formerly active tidal creeks and organic deposits from bordering coastal plain peatlands (see Chapter 2). Differences in the subsurface build-up and present surface elevation, such as the elevated creek ridge, are used to investigate the effect of local shallow subsurface heterogeneity on subsidence.

5. RESULTS

This section presents the results of this thesis. First, the modelled groundwater levels are presented and compared to groundwater level measurements (section 5.1). Second, the results of the subsidence model with incorporated groundwater level dynamics are presented (section 5.2). Third, the results of additional research strategies to quantify subsidence are presented (section 5.3), differentiating between the use of lithological and surface-level measurements. Finally, the lithological and lithogenetic cross-section that were obtained from the field study in Nieuwolda will be presented and interpreted for their Holocene development.

5.1 MODELLED GROUNDWATER LEVELS

Groundwater levels were modelled using SWAP at three locations in and around the Nieuwolda field study area. First, the general model performance is explained by comparing modelled and measured groundwater levels (section 5.3.1). Second, the model results for the potential extensometer locations are presented (section 5.3.2). Third, the results of a sensitivity analysis on seven model parameters are presented (section 5.3.3).

5.3.1 GENERAL MODEL PERFORMANCE

The SWAP-model was used to mimic daily groundwater level dynamics. The results presented in this paragraph are meant to indicate the overlap between the measured and modelled groundwater levels. The analysis will be presented both quantitatively by addressing the root-mean-square-error (RMSE) and the mean-error (ME), but also qualitatively by describing a trend or misfit between the measurements and model results.

Figure 28 shows the groundwater level measurements and model results for the period of 2016-2019. First, the RMSE-value indicates an averaged error of 22.2 cm between the measurements and model results. On average, the modelled groundwater levels are 7 cm lower compared to the measured groundwater levels. In general, the model seems to mimic daily fluctuations fairly well. For example, an abrupt increase in groundwater level during an extreme rainfall event is measured and modelled at the same moment in time. Moreover, the decrease in groundwater level during the infiltration after precipitation is modelled most often with the same rate compared to measurements. Seasonal and even yearly groundwater dynamics can also be observed Figure 29. The trend in low groundwater levels during summer droughts is well simulated for all the four investigated years.

Although the model seems to mimic the general trend in fluctuating groundwater level, there are various moments when there is a clear error between measured and modelled groundwater levels. Several types of these deviations were observed and are discriminated, allowing an individual explanation and possible improvement for future usage.

First, the magnitude of an abrupt increase in groundwater level sometimes differ between the measured and modelled groundwater levels. For example, around August 2018 the model shows a considerable groundwater level rise of 60 cm(Figure 28). Although the timing of this increase coincides with the measurements, the measured groundwater level rise is only 20 cm. From this moment on, the model seems to mimic the extremes and magnitudes in groundwater level fluctuations fairly well for the subsequent months of September, October, and December. However, due to the one large deviation from August 2018, the modelled groundwater levels appear approximately 50 cm higher in the soil profile during all three subsequent months. This example shows that one error in the groundwater level computation can create a misfit between measured and modelled groundwater levels for three entire months. Other examples of such errors that seem to have a great impact on the outcome of the model results can be observed around June 2017 and September 2019. Second, the model seems to compute lower groundwater levels during periods with continuously high groundwater levels (Figure 28). More specific, when measured groundwater levels are within the surficial 30 cm of the subsurface for a longer time period, such as in the winter of 2017, the model incorrectly computes lower groundwater levels. Additionally, Although the extremes in the groundwater level fluctuations match the extremes in measured groundwater levels, the model continues to underestimate the groundwater levels for the first half-year of 2018.

Third, minor fluctuations in measured groundwater levels are sometimes 'missed' by the model computations. For example in March 2019, the modelled groundwater level continuously decreases, whereas the measured groundwater level slightly increases.

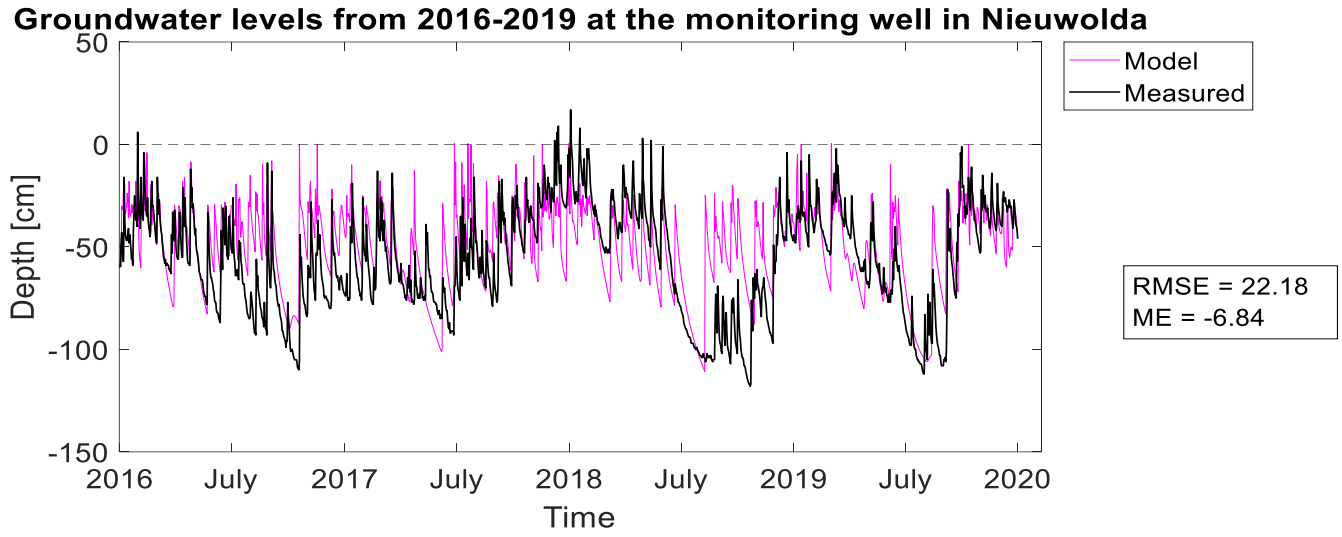

FIGURE 28: MODELLED GROUNDWATER LEVELS BETWEEN 2016 AND 2019 AT THE MONITORING WELL IN NIEUWOLDA.

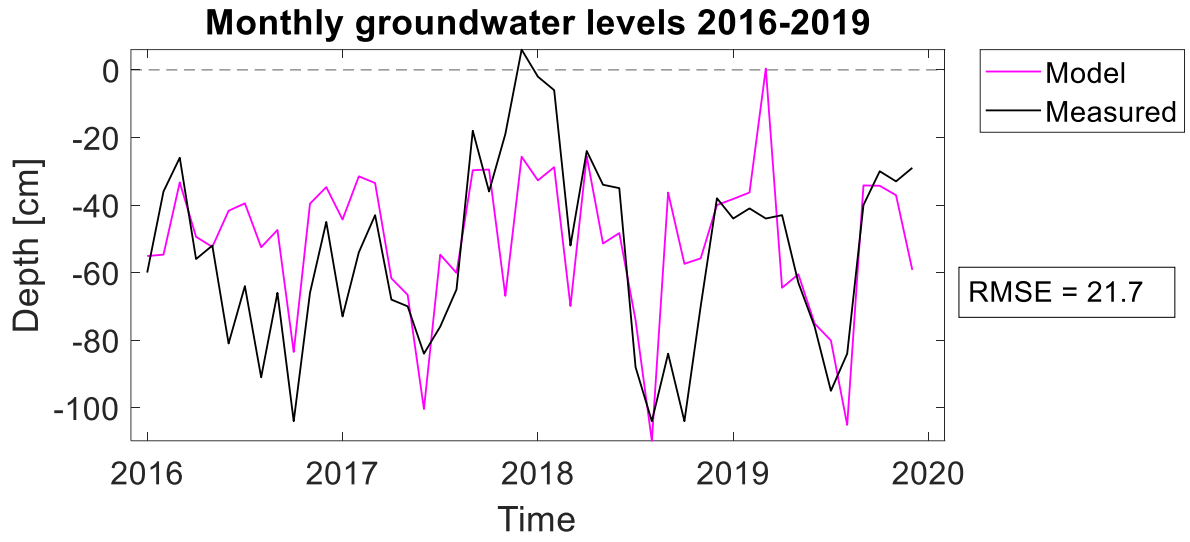

FIGURE 29: MONTHLY AVERAGES OF MODELLED GROUNDWATER LEVELS BETWEEN 2016 AND 2019 AT THE MONITORING WELL IN NIEUWOLDA.

5.3.2 MODEL USAGE FIELDWORK AREA NIEUWOLDA

The two designated extensometer locations at the fieldwork area in Nieuwolda were used to investigate the recent historic groundwater levels between 2016 and 2019. Note that there are no groundwater level measurements available for a comparison at these locations. The analysis of the modelled groundwater levels is purely qualitative, describing interesting features in the differential groundwater saturation.

Figure 30 shows the modelled groundwater levels at the peat extensometer location for the situation with and without drains, allowing to analyse the effect of the drains on the groundwater level. First, the model shows a significant drop in groundwater level during the summer. This decrease in groundwater level coincides with the period that wheat has been sown and starts growing at this location. The uptake of soil water by the roots of

wheat is large, and together with already sparse precipitation rates, the groundwater level significantly drops. When the wheat is harvested in October, the groundwater level increases again and fluctuates around -80 cm below surface level. Groundwater levels would have dropped 10 to 20 cm deeper without the presence of subsurface drains in summer. The presence of subsurface drains decreases the extremes in groundwater level.

Figure 31 shows the modelled groundwater levels for the clay extensometer location. This location is situated 20 m from a bordering ditch. Despite rainfall events, the mean groundwater level varies around -160 cm below surface level. The surface water level in this ditch varies around -180 cm below surface level and influences the surrounding groundwater levels.

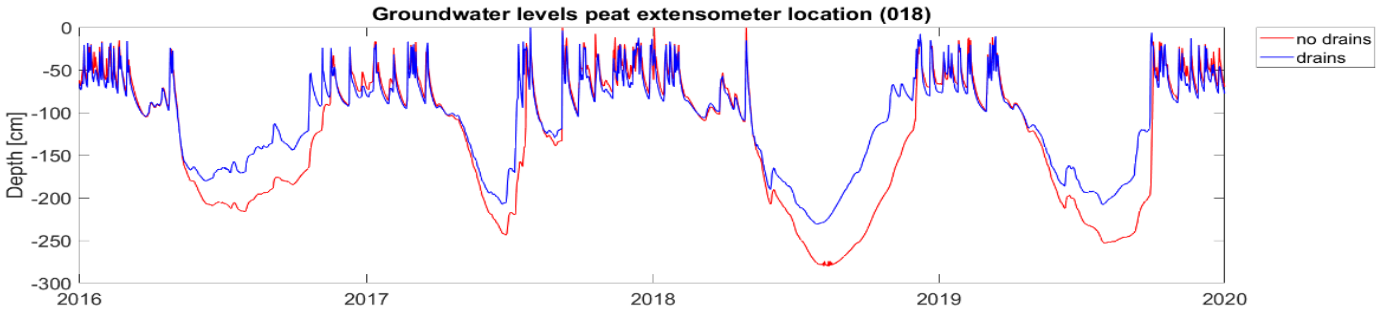

FIGURE 30: MODELLED GROUNDWATER LEVELS BETWEEN 2016 AND 2019 AT THE POTENTIAL PEAT EXTENSOMETER LOCATION IN THE NIEUWOLDA FIELD STUDY AREA.

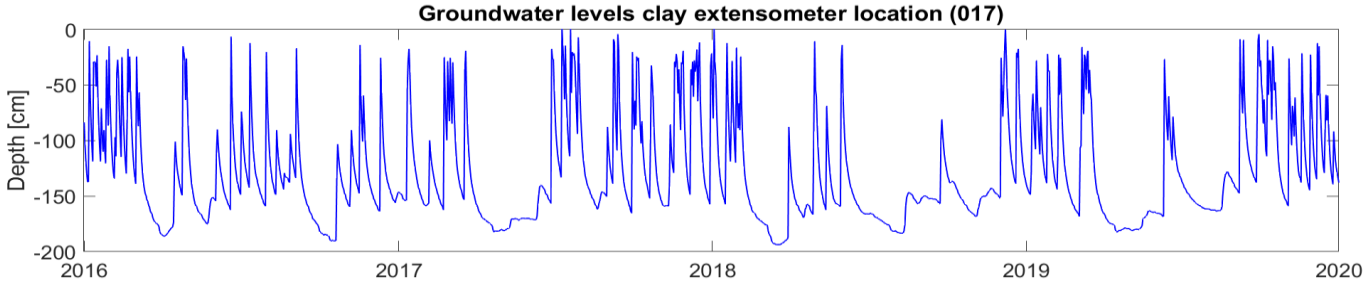

FIGURE 31: MODELLED GROUNDWATER LEVELS BETWEEN 2016 AND 2019 AT THE POTENTIAL CLAY EXTENSOMETER LOCATION IN THE NIEUWOLDA FIELD STUDY AREA.

5.3.3 SENSITIVITY ANALYSIS

As indicated in section 5.3.1, the model performs adequately. However, the SWAP-model obtains over 200 parameters that all influence the final result. This paragraph presents the effect of seven parameters that were thought to affect the final modelled groundwater levels.

Figure 32 depicts the groundwater levels that were modelled using a different meteorology station and associated meteorological input parameters. Although all three stations show approximately the same seasonal trend, there are large differences in the time and magnitude of groundwater level changes. For example, in August 2019 the modelled groundwater levels from weather station De Bilt indicate an extreme rise in groundwater level, whereas this increase is less significant for Nieuw Beerta and even absent for weather station Eelde. The weather condition in winter are more consistent for the observed weather stations, whereas rainfall events in the summer show a greater variety. In general, the maximal difference in RMSE of 2.2 cm between the investigated weather stations is relatively small.

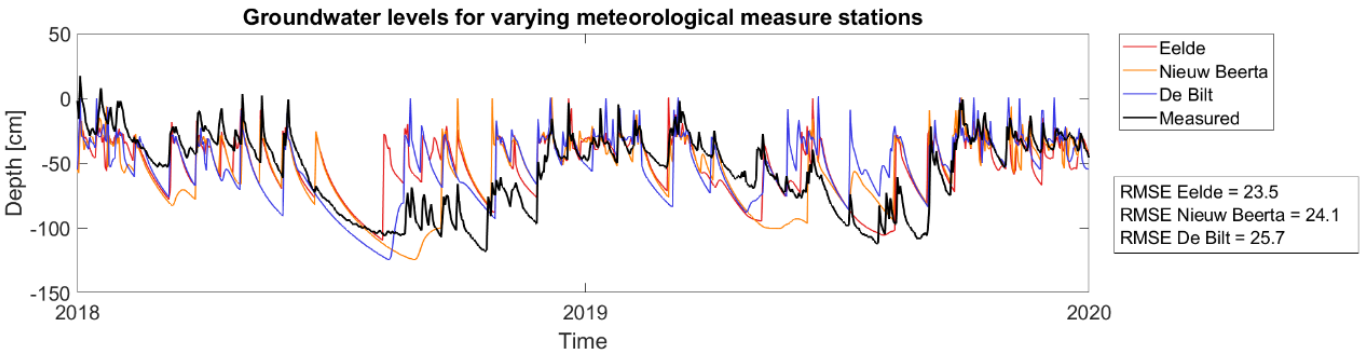

FIGURE 32: MODELLED GROUNDWATER LEVELS IN 2018 AND 2019 FOR VARYING METEOROLOGICAL INPUT PARAMETERS.

A total of five scenarios with different or lacking vegetation cover were investigated to indicate the effect of the land cover (Figure 33). A bare soil or grass cover shows a very similar groundwater level pattern, comparable to the measured groundwater levels. However, the growth of different types of crops changes the groundwater level dynamics enormously. The growth of potatoes, maize, and wheat all depict a gradual decreasing groundwater level during summer, by the uptake of soil water from the roots of these plants. Wheat appears to extract the most soil water, followed by maize, and potatoes.

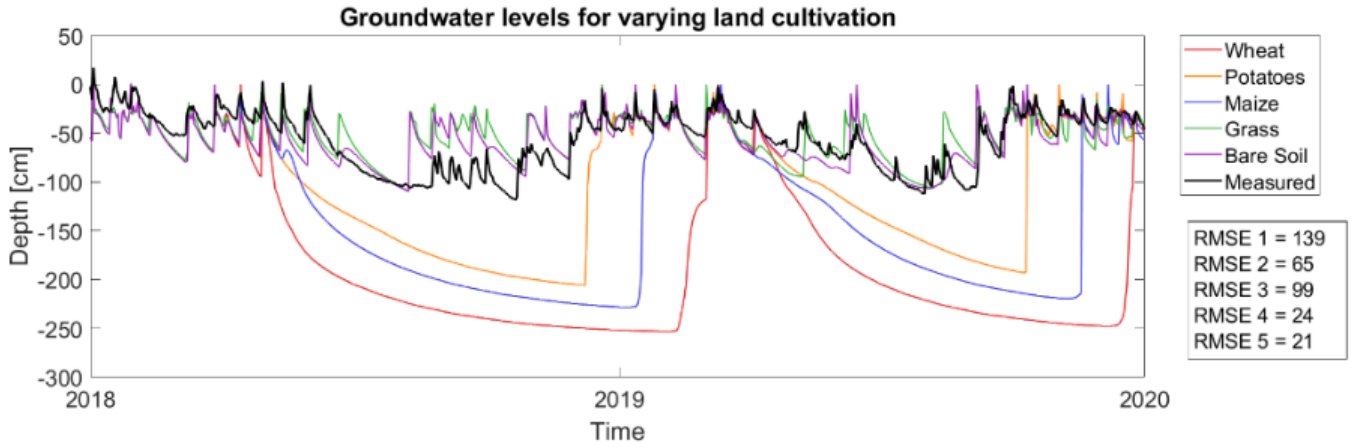

FIGURE 33: MODELLED GROUNDWATER LEVELS IN 2018 AND 2019 FOR VARYING LAND CULTIVATION

Figure 34 shows the effect of the surface water level in bordering surface water on the modelled groundwater level. The proximal Termunterzijldiep-canal is located at 60 meters from the Nieuwolda monitoring well. Interestingly, the modelled groundwater levels for different distances only deviate maximally 10cm. The surface water level has an insignificant impact on the modelled groundwater levels for this situation. Also, the effect of the distance between proximal surface water and the monitoring well on the modelled groundwater levels has been investigated in Figure 35. Also distance changed the modelled groundwater levels only a few centimetres and also has a minor impact on the modelled groundwater levels.

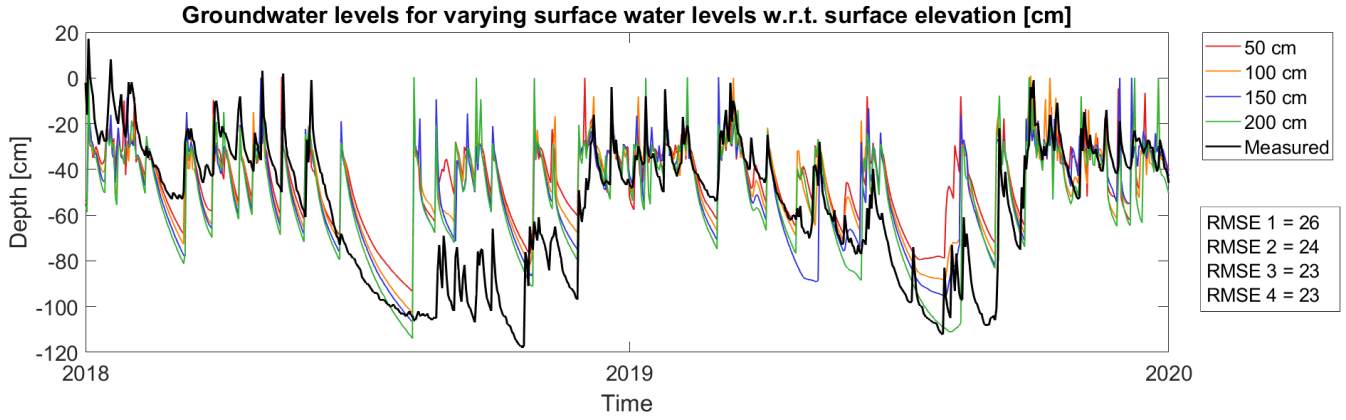

FIGURE 34: MODELLED GROUNDWATER LEVELS IN 2018 AND 2019 FOR VARYING SURFACE WATER LEVELS IN BORDERING SURFACE WATER.

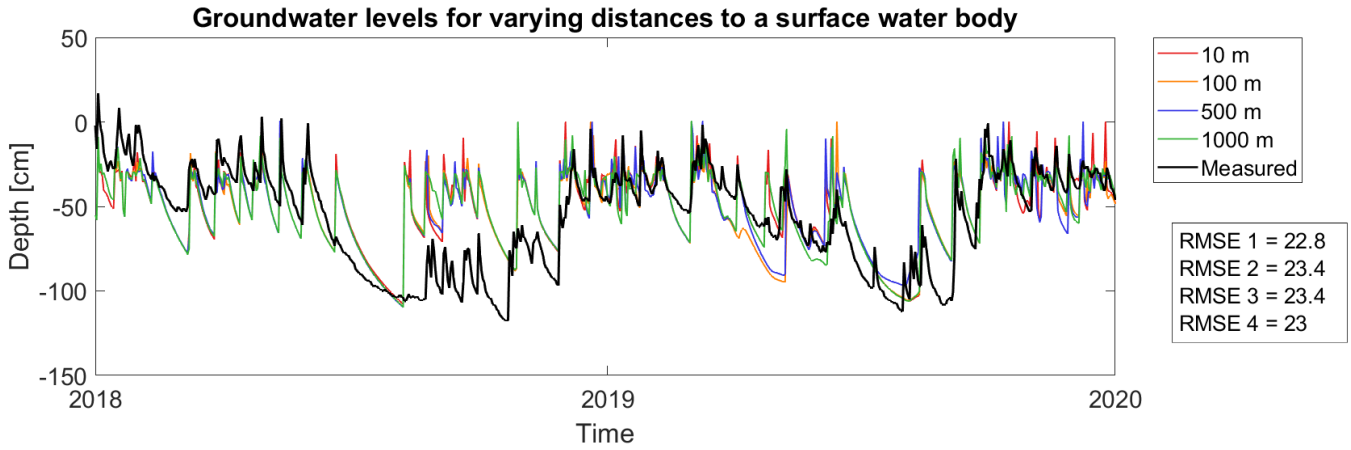

FIGURE 35: MODELLED GROUNDWATER LEVELS IN 2018 AND 2019 FOR VARYING DISTANCES TO NEARBY SURFACE WATER.

The next three investigated parameters were unknown beforehand and had to be obtained during a qualitative calibration. Figure 36 shows that a smaller hydraulic resistance lowers the modelled groundwater levels. The effect of the hydraulic resistance on the modelled groundwater levels relies on the direction of the vertical flux. At the monitoring well there is a vertical, downward flow of groundwater at any moment in time (Figure 22). The vertical hydraulic resistance parameter reduces this downward flux. Therefore, decreasing the vertical hydraulic resistance enhances drainage and lowers the modelled groundwater level.

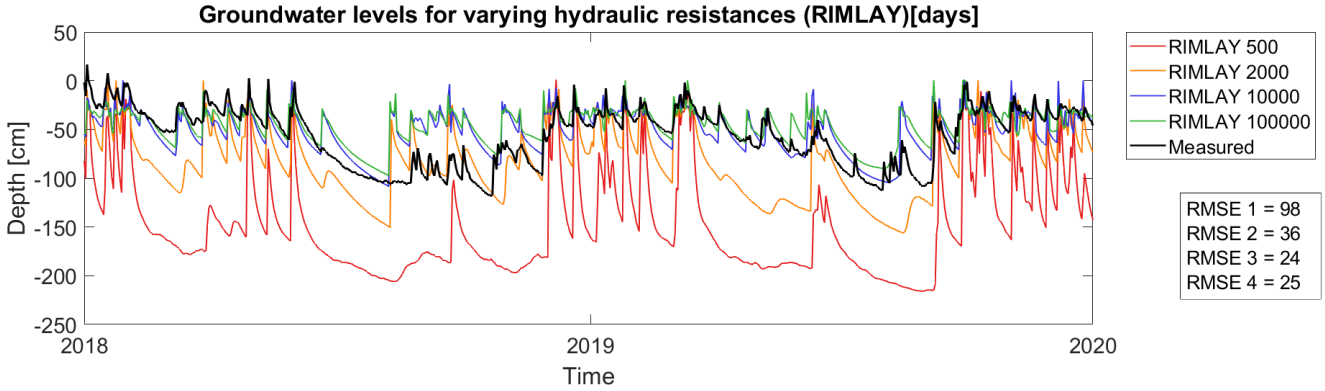

FIGURE 36: MODELLED GROUNDWATER LEVELS IN 2018 AND 2019 FOR VARYING HYDRAULIC RESISTANCES

Moreover, the drainage resistance (DRARES) accelerates or delays the horizontal groundwater flux. Figure 37 indicates that decreasing the horizontal drainage resistance lowers the modelled groundwater levels in this situation. However, it is important to be aware of the modelled surface water level in the bordering open water body. In this case, the surface water level in the proximal Termunterzijldiep canal is -156 cm below the surface level at the monitoring well location An extremely small horizontal drainage resistance allows an almost instantaneous exchange of water with the open water body, such that the groundwater level would ultimately approach -156 cm when decreasing the drainage resistance. Differences between a drainage resistance of 10.000 and 100.000 (days) however are small. For these scenarios, the resistance is already this high that horizontal groundwater exchange has become insignificant.

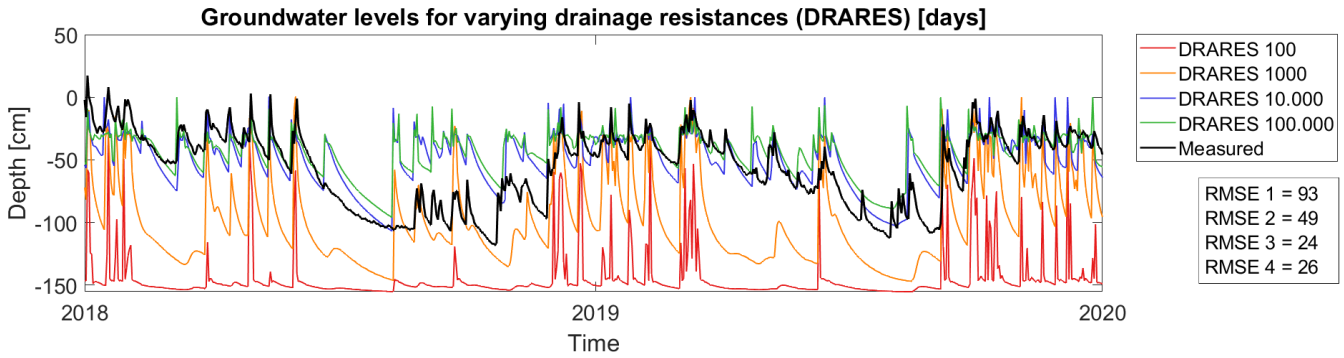

FIGURE 37: MODELLED GROUNDWATER LEVELS IN 2018 AND 2019 FOR VARYING DRAINAGE RESISTANCES

Finally, the effect of the surficial, horizontal interflow depth on the modelled groundwater levels is investigated (Figure 38). Expanding the interflow depth lowers the modelled groundwater levels increases, because more horizontal drainage with only minor resistance is allowed. A small interflow compartment of 10 cm creates a relatively good correspondence with measured groundwater level during the winter months with increased precipitation.

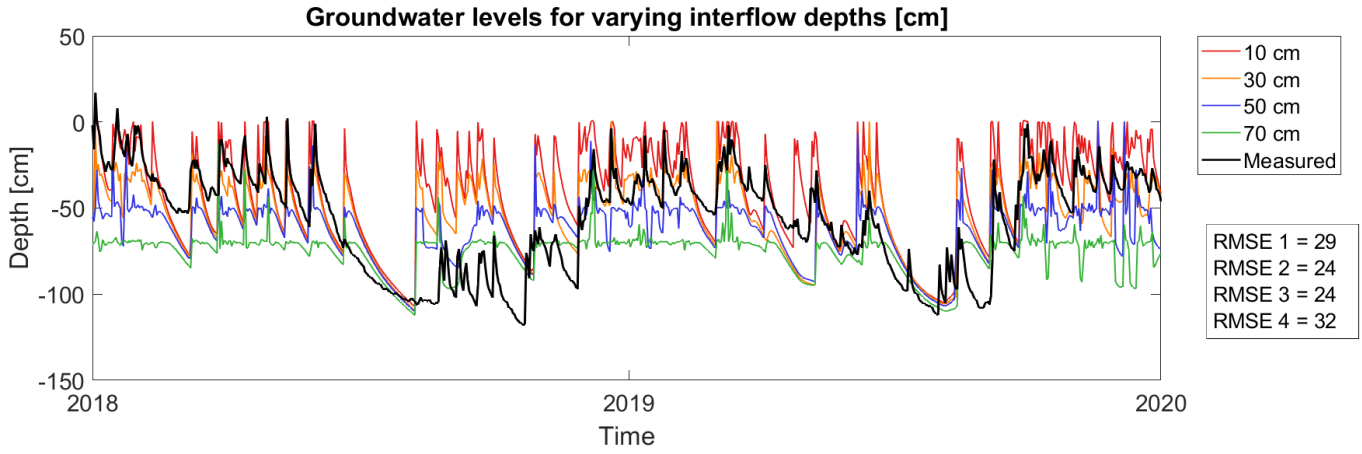

FIGURE 38: MODELLED GROUNDWATER LEVELS IN 2018 AND 2019 FOR VARYING INTERFLOW DEPTHS.

5.2 MODELLED SHALLOW SUBSIDENCE

The prior modelled groundwater levels were incorporated in an empirical subsidence model that quantifies shallow subsidence. This paragraph presents various possibilities of consulting this developed subsidence model. Results in this section are all obtained at the potential peat extensometer location in the Nieuwolda field study area.

5.2.1 HISTORIC SUBSIDENCE

Figure 39 shows the shallow subsidence because of peat oxidation between 2016 and 2019. Peat is constantly oxygenated in summer and partly saturated during winter. Lower groundwater levels in summer correspond with increased absolute subsidence by oxidation, as the thickness of the column of oxygenated peat is larger such that more peat oxidizes. The increased peat oxidation causes the total sediment thickness to decrease faster. A clear pattern of a fast decrease in total thickness during summer and a more gradual decline during winter is observed. The total subsidence is approximately 2.0 cm between 2016 and 2019, yielding a shallow subsidence rate of 0.5 cm per year.

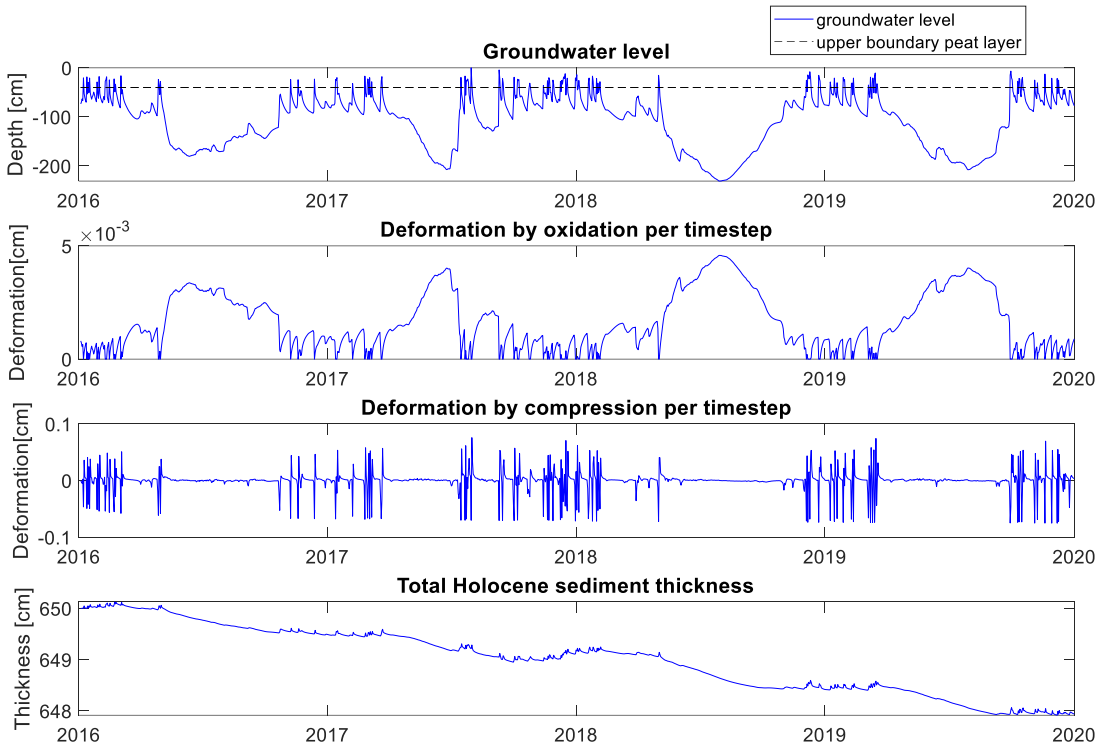

FIGURE 39: MODELLED GROUNDWATER LEVELS INCORPORATED IN THE SUBSIDENCE MODEL TO QUANTIFY SHALLOW SUBSIDENCE.

The modelled shallow subsidence in Figure 39 is strongly determined by the oxidation rate and the clastic admixture within the peat. The effect of these parameters on the modelled deformation is further investigated by performing a sensitivity analysis. Figure 40 shows the development of the total sediment thickness using seven different oxidation rates. The effect of incorporating different oxidation rates on the computation of shallow subsidence causes especially differential subsidence rates during the summer when more peat can be oxidized (Figure 40). Table 7 depicts the variation in computed shallow subsidence between minimal and maximal oxidation rates. Absolute modelled shallow subsidence ranges from 1.4 to 9.7 cm within four years for different oxidation rates, and associated absolute subsidence rates vary between 0.35 and 2.44 cm per year.

Figure 41 shows the effect of using a different clastic admixture in peat on shallow subsidence. Modelled shallow subsidence decreases from 2.44 to 0.21 cm when relative clastic admixture increases from 0 to 90 %(Table 8). The total absolute subsidence due to oxidation decreases because only organic matter can be decomposed. Note that peat with a clastic admixture of more than 50% is actually no longer defined as peat since peat is in this situation no longer the dominant texture group. However, the organic matter within the sediment can still oxidize and thereby contribute to shallow subsidence. These scenarios are especially of interest for the abundant organic clays in the research area.

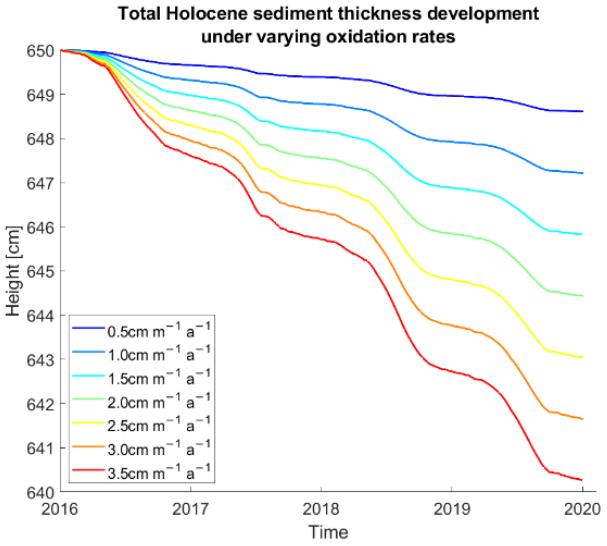

FIGURE 40: MODELLED TOTAL THICKNESS OF HOLOCENE DEPOSITS BETWEEN 2016 AND 2019 FOR VARYING OXIDATION RATES. A HIGHER OXIDATION RATE CAUSES MORE SUBSIDENCE BY OXIDATION.

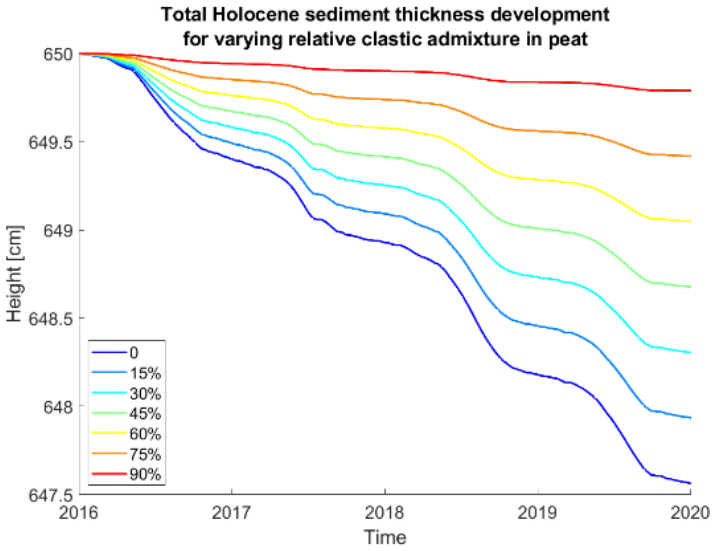

FIGURE 41: MODELLED TOTAL THICKNESS OF HOLOCENE DEPOSITS BETWEEN 2016 AND 2019 FOR A VARYING RELATIVE CLASTIC ADMIXTURE IN PEAT. MORE CLASTIC ADMIXTURE REDUCES THE SUBSIDENCE POTENTIAL.

Oxidation rate	subsidence by oxidation	Subsidence rate due to oxidation
0.5 cm m-1 a-1	1.4 cm	0.35 cm a-1
1.0 cm m-1 a-1	2.8 cm	0.70 cm a-1
1.5 cm m-1 a-1	4.2 cm	1.04 cm a-1
2.0 cm m-1 a-1	5.6 cm	1.39 cm a-1
2.5 cm m-1 a-1	7.0 cm	1.74 cm a-1
3.0 cm m-1 a-1	8.4 cm	2.09 cm a-1
3.5 cm m-1 a-1	9.7 cm	2.44 cm a-1

TABLE 7: MODELLED SHALLOW SUBSIDENCE BETWEEN 2016 AND 2020 USING DIFFERENT OXIDATION RATES, BASED ON THE SAME MINIMAL AND MAXIMAL VALUES USED IN A STUDY BY KOSTER ET AL (2018).

Relative clastic admixture	Absolute subsidence by oxidation	Subsidence rate due to oxidation
0 %	2.44 cm	0.61 cm / year
15 %	2.07 cm	0.52 cm / year
30 %	1.70 cm	0.42 cm / year
45 %	1.32 cm	0.33 cm / year
60 %	0.96 cm	0.24 cm / year
75 %	0.58 cm	0.15 cm / year
90 %	0.21 cm	0.05 cm / year

TABLE 8: MODELLED SHALLOW SUBSIDENCE BETWEEN 2016 AND 2020 USING A DIFFERENT RELATIVE CLASTIC ADMIXTURE IN PEAT.

5.2.2 FUTURE SCENARIO

A future scenario was modelled in which a predicted sinusoidal fluctuating groundwater level that linearly declines by 5 cm per year was used to compute future shallow subsidence. Compression initiated by an increase in effective stress was included.

Figure 42 contains four subplots that show respectively the development in; 1) groundwater level, 2) the subsidence by oxidation per timestep, 3) subsidence by compression per timestep and 4) total Holocene sediment thickness representing total shallow subsidence. Subplot 1 contains both the linearly decreasing fluctuating groundwater level used to compute the oxidation and the averaged, linear lowering groundwater level used to compute compression. The observed subsidence by oxidation in subplot 2 is in the order 0.001 cm per timestep [day], which is 0.4 cm per year. The observed deformation by compression in subplot 3 however is in the order of 0.000007 cm per timestep [day] and thus 0.003 cm per year. The averaged ratio in absolute subsidence rate between oxidation and compression is therefore approximately 143:1. The combined contribution of oxidation and compression shows a drop of 5 cm within the next 20 years, corresponding with a shallow subsidence rate of approximately 0.2 cm per year.

Figure 43 depicts the deformation per timestep for primary and secondary compression individually. Figure 43 is used to describe the development and the relative contribution of primary and secondary compression, rather than the absolute value of either one of these mechanisms. Right after the start, the compression is only a result of the primary compression, as the model assumes that the subsurface has not experienced any historic compression yet. As the primary compression is triggered, the secondary compression starts to increase exponentially. The primary compression decreases throughout the modelled period, as the total thickness constantly decreases due to the combined effect of the compression and oxidation from the former time step. As less sediment is available to be compressed, the newly yielded absolute deformation by primary compression will be lower compared to the prior timestep. At approximately 2025, the maximal deformation by compression is achieved. This moment coincides with the change in the dominant relative contribution from primary compression to secondary compression. From this moment on the relative contribution of secondary compression increases until the end of the modelled period.

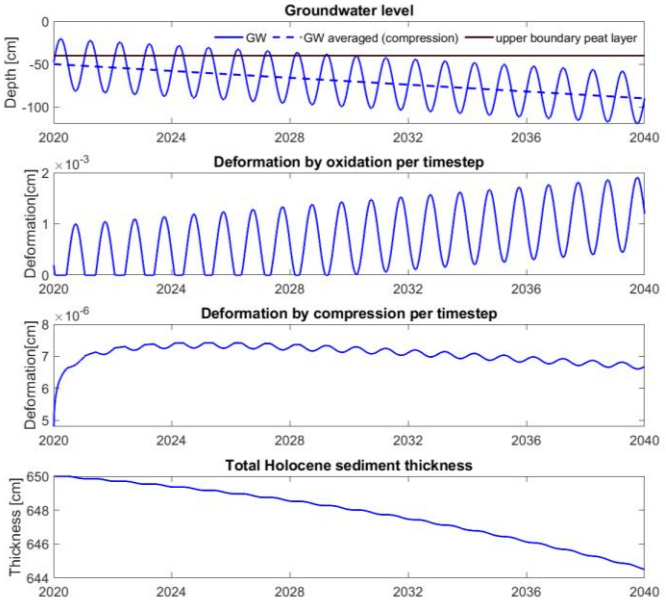

FIGURE 42: INCORPORATED SINUSOIDAL AND LINEARLY DECREASING AVERAGED GROUNDWATER LEVEL PREDICTIONS BETWEEN 2020 AND 2040 USED TO COMPUTE FUTURE SUBSIDENCE IN THE SHALLOW SUBSURFACE BY COMPRESSION AND OXIDATION.

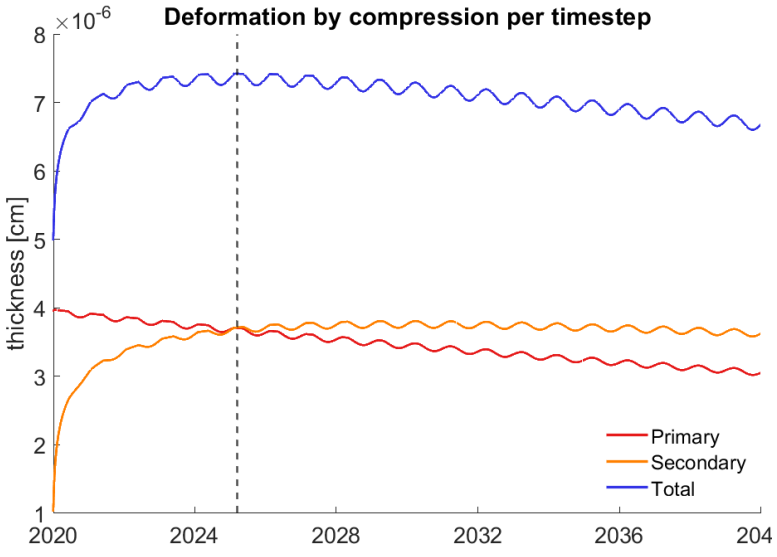

FIGURE 43: THE CONTRIBUTION OF PRIMARY AND SECONDARY COMPRESSION TO TOTAL COMPRESSION FOR MODELLED FUTURE SUBSIDENCE BETWEEN 2020 AND 2040.

5.3 INDIRECT, MEASURED SHALLOW SUBSIDENCE

5.3.1 LITHOLOGICAL MEASUREMENTS

The fieldwork study in Appingedam allowed comparing the total thickness of Holocene deposits between 1970 and 2021 at seven locations (Figure 44). Sand deposits from the Late Pleistocene were situated at a depth ranging from -2.5 up to -4.5 m below surface level. The determined lithology in 1970 and 2021 is similar at location 1-6, with a basal peat layer overlain by a surficial clay layer (Figure 44). Only location 7 deviates and indicates rather an opposite lithology in 2021 compared to 1970. This difference can be explained by a human error in the lithological core description of location 7 from 1970. The core description seems to have reported a peat layer as a clay layer and vice versa (Appendix 4). Location 7 is still incorporated in the quantitative analysis because the error did not affect the documented total thickness of Holocene deposits.

The total thickness of the Holocene sediment column between 1970 and 2021 decreased several tens of centimetres at location 2, 3, 4, 5 and 7 (Figure 45). At location 1 and 6 the total thickness appears to have increased since 1970 by almost 20 cm. On average the measurements indicate an average decrease in total thickness between 1970 and 2021 by 10 cm. Location 3,4 and 5 shows the largest decrease in thickness varying between 20 and 40 cm since 1970. Interestingly, at these locations the surficial clay layer is relatively small of only 40-60cm such that peat is situated relatively shallow in the subsurface. Moreover, the most surficial 20-40 cm consists of amorphous peat. Apart from the absolute deformation, the relative deformation indicates the contribution of deformation compared to the initial total thickness. The total thickness of Holocene deposits between 1970 and 2021 appears to have been decreased by 3% on averagely. Finally, the total deformation within 51 years has been used to determine the deformation rate per year. This shows an averaged subsidence rate of 0.2 cm per year.

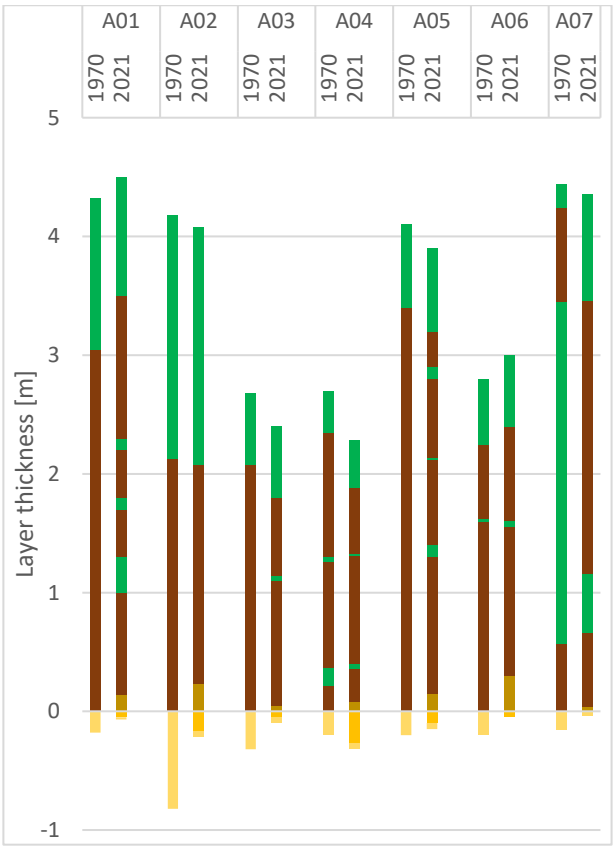

FIGURE 44: THE LITHOLOGICAL BUILD-UP OF SEVEN LOCATIONS SOUTH OF APPINGEDAM FOR 1970 AND 2021. THE X-AXIS MARKS THE TRANSITION FROM SAND TO FINEGRAINED DEPOSITS, SINCE THE TOTAL THICKNESS OF FINE-GRAINED DEPOSITS INDICATE THE PART OF THE SUBSURFACE PRONE TO SHALLOW SUBSIDCENCE.

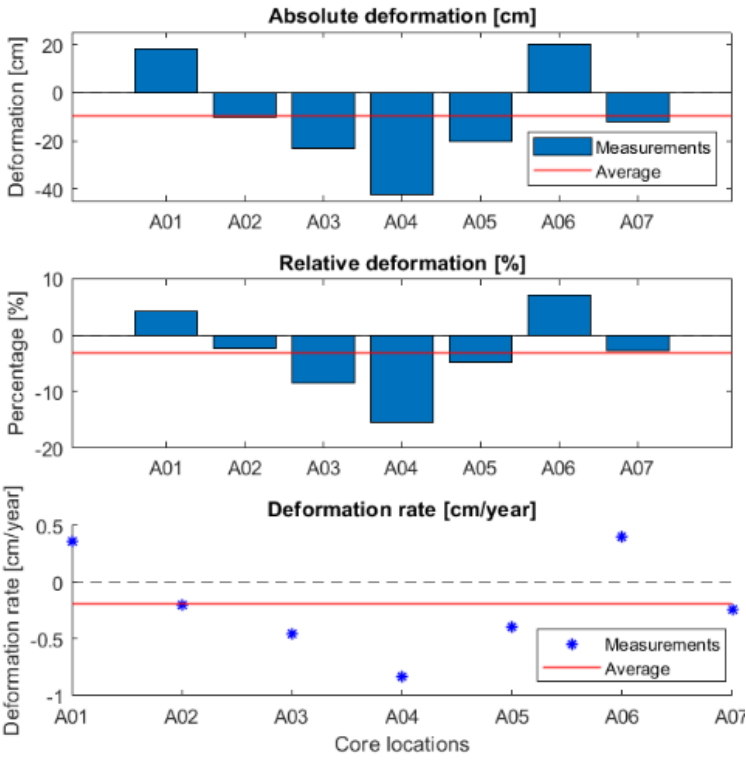

FIGURE 45: ABSOLUTE AND RELATIVE DEFORMATION IN HOLOCENE DEPOSITS BETWEEN 1970 AND 2021 APPINGEDAM.

5.3.2 SURFACE-LEVEL MEASUREMENTS

The difference in surface elevation between 1963 and 2019 has been quantified for approximately 32.000 locations (Figure 46). The vertical motion varies predominantly between 20 and 70 cm, yielding an averaged total subsidence rate between 0.35 and 1.25 cm/year. Deep subsidence by the gas extraction is assumed to decrease gradually in eastern direction (away from the centre of extraction). Local deviations in the total subsidence pattern are therefore assumed to be the result of mechanisms in the shallow subsurface.

The cross-sections from the GeoTOP-model indicate larger subsidence rates between 1963 and 2019 for regions with increasing thickness of fine-grained, Holocene deposits. At the southern end of cross-section A, for example, Holocene deposits are absent, since Pleistocene sand deposits are situated at or close below surface level (Figure 47). This region between the villages of Slochteren-Siddeburen-Oostwold shows only minor differences in surface elevation between 1963 and 2019. However, succeeding in northern direction along transect A, the thickness of clay and peat deposits that overlay aeolian sand deposits increases. The obtained total vertical motion of this region around the Schildmeer is also larger (Figure 46). A similar pattern is observed at cross-section B (Figure 47). East of the Hondshalstermeer, around the field study area of Nieuwolda, the shallow subsurface consists of 6-8 m of Holocene, fine-grained deposits. Total measured subsidence from the surface motion map in this region are relatively large and vary between 40 to 60 cm in 56 years, corresponding with 0.7 to 1 cm/year. However, in western direction along transect B, two locations are distinguished with no or very few fine-grained deposits. These location correspond to minimal subsidence rates from the surface motion map. Also prior reclaimed land at the north and eastern borders with the Wadden Sea show a minimal subsidence rate varying between 10- 30 cm in 56 years (Figure 46).

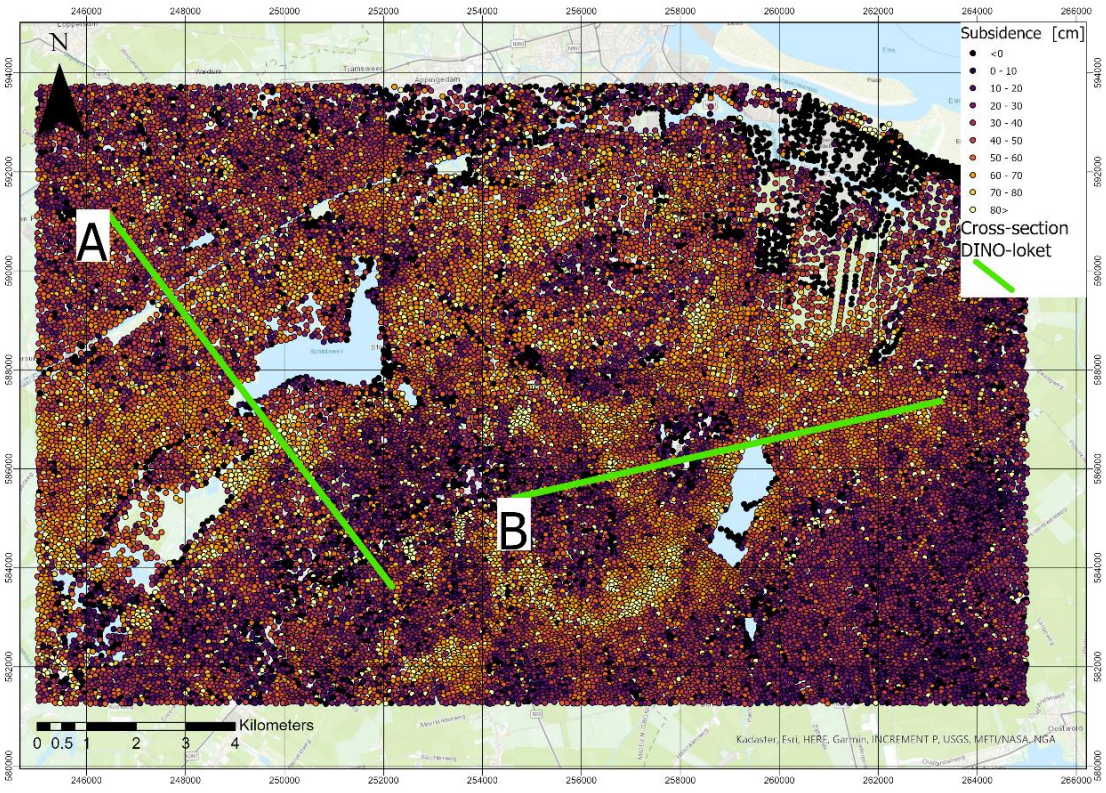

FIGURE 46: OVERVIEW OF THE TOTAL VERTICAL SURFACE MOTION BETWEEN 1963 AND 2019. THE MAP WAS CREATED IN GIS BY SUBTRACTING PIXEL VALUES OF SURFACE LEVEL MEASUREMENTS OBTAINED/PRODUCED IN 2019 AND 1963. THE CROSS-SECTIONS FROM FIGURE 47 ARE INDICATED.

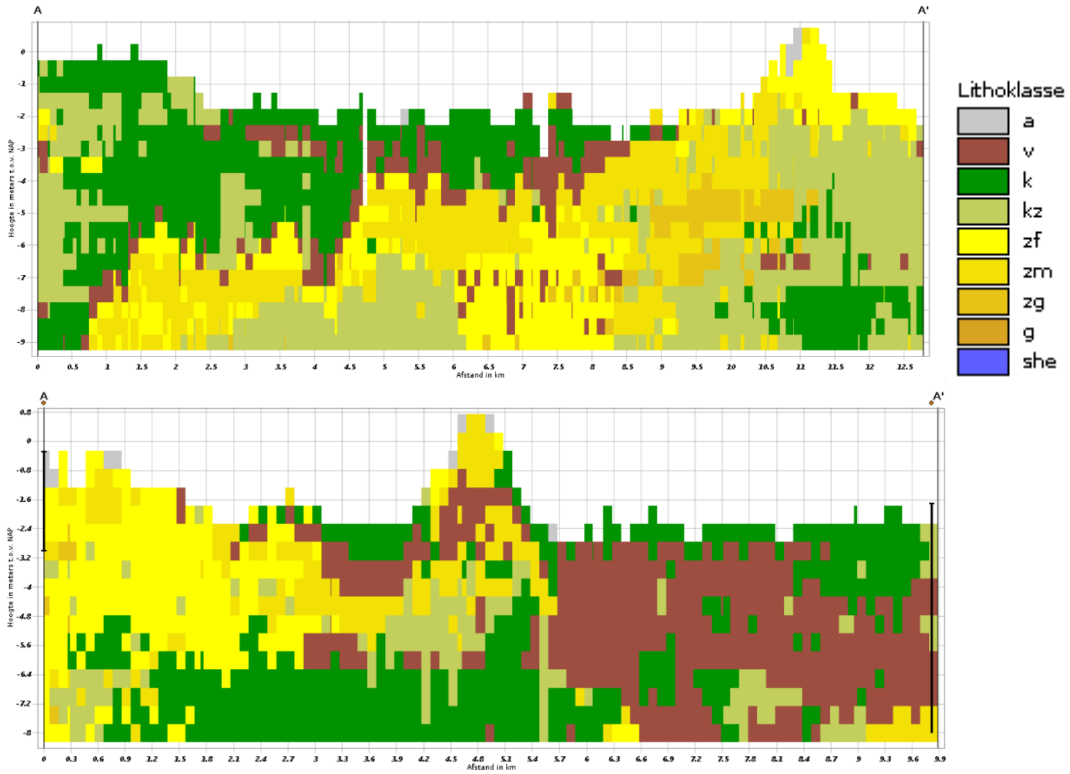

FIGURE 47: GEOLOGICAL CROSS-SECTIONS FROM TWO TRANSECTS AT THE SURFACE MOTION MAP OF FIGURE 46, INDICATING THE DIFFERENTIAL HOLOCENE SEDIMENT THICKNESS IN THE RESEARCH AREA. THE CROSS-SECTIONS WERE OBTAINED USING DINO-LOKET (TNO). **TOP (A)** NORTHWEST-SOUTHEAST TRANSECT FROM GARRELSWEER TO SIDDEBUREN **BOTTOM (B)** EAST-WEST TRANSECT FROM SIDDEBUREN TO WOLDENDORP.

5.4 LOCAL, HETEROGENEOUS SHALLOW SUBSURFACE

The created lithological and lithogenetic cross-sections will be discussed in terms of the development through time, generally from bottom to top. The lithological observations and corresponding morphological interpretations are consecutively discussed for every successive stage. All ages are in calibrated years before present (cal yr BP).

TRANSECT EAST

The former Pleistocene surface is located -8 to -9 m below NAP and consists of very fine, well-rounded sand. The aeolian sand deposits are overlain by a relatively small, eutrophic, compact peat layer ranging from 0.2 to 0.5 meter in thickness (Figure 48). Distinctive coloured horizons are distinguished right on top of the sand deposits (Figure 52A). Based on the lithological composition, spatial extent and profile this transition is interpreted as a well-developed paleosoil that formed on the former Pleistocene surface. The black, organic sand layer marks the eluviated soil-horizon, where minerals were leached downward. The observed underlain sand deposits were still yellowish and were interpreted as the illuviated soil horizon.

The gradual transition towards eutrophic peat marks the transgression of this Pleistocene surface into a coastal plain peatland. This first rise in groundwater level as a consequence of sea level rise occurred between 7500 and 7000 BP (De Haas *et al.* 2018). Successive stages in the organic matter in peat further confirm this interpreted drowning system, where wood peat (alder trees) gradually shifts towards sedge and reed peat. At the northern side of the transect this drowning phase continues and the clastic admixture of clay increases. The basal peat layer is overlain by a 1 to 2 m thick compact clay layer containing many reed plant remains. These fine, tidal deposits are interpreted as supratidal flat deposits from the first Holocene, large tidal inundation system I between 7000 and 4750 BP (De Haas et al., 2018; Vos & Knol, 2015; Figure 33). At that time, sediment supply to the tidal basin exceeded the accommodation space created by sea level rise. The quantity of plant remains in the

clay deposits varies, indicating varying phases of tidal dominance. At core location 202102018 coarser-grained loam deposits were observed between -8 and -9 m below NAP (Figure 48; Figure 52D). These loam deposits were interpreted as subtidal deposits from a tidal creek system. According to the absence of distinctive paleosoil horizons at this location, the subtidal channel is thought to have eroded parts of the formerly Pleistocene surface. It is interpreted that a northern located tidal creek system delivered the clay deposits, since the thickness of the tidal deposits increase in northern direction (Figure 48). At core location 202102017 the supratidal flat deposits from tidal inundation system I are absent, probably because this region was further located from the most nearby tidal creek system and received minor clastic input.

Succeeding, the tidal deposits from tidal inundation system I are overlain by 3 to 4-meter peat. This transition is situated approximately 7 m below NAP and is gradual from clay to organic clay and finally eutrophic peat, indicating the coastal progradation of this tidal system. Due to the location of peat in the subsurface profile, the peat is thought to be deposited between 4750 and 2600 BP (Vos & Knol 2015). The eutrophic peat predominantly comprises reed, and sporadically sedge and wood remains such as a twig (Figure 52G). The different peat composition is interpreted as small alternations between terrestrial or coastal phases during peat formation. In the centre of the cross-section, parts of this peat body are situated above the lowest groundwater level and are regularly exposed to oxygen from the atmosphere. Within this larger sedimentological peat body, several smaller clay lenses are present. These clay lenses vary in thickness from 10 up to 70 centimetres, and in spatial extent from 200 up to more than 500 meters wide. The alternations between peat and clay are mostly gradual. The clay lenses are interpreted as tidal inundations originating from local tidal creeks into the coastal plain peatland. Four tidal inundations systems (II, III, IV, V) were determined based on the vertical position of the clay lenses within the lithological profile. Horizontally oriented wood remains indicate that vegetation was still present in these supratidal flats (Figure 52C). The tidal inundations must have occurred between 4750 BP and 2600 BP, although local tidal inundations II, III and V cannot be linked to a tidal creek system that deposited the (organic) clays. Sporadically, there are abrupt transitions with very small laminated clay layers [0-20 cm], indicating a temporal increase in tidal flooding events (Figure 52B)

The lithology at location 202102019 differs greatly from the main subsurface build-up of this transect (Figure 48). First, the clay deposits from -4 up to -9m below NAP contain minor or no plant remains. Second, the clay deposits are not as compact as the observed clay deposits from the other core descriptions. Third, this location seems to be elevated approximately 1m above main, local topography. Fourth, the Pleistocene paleosoil is absent in the underlain sand deposits. Instead, there is a very abrupt transition between the clay and sand deposits. These observations led to the interpretation that a former tidal creek was present at this location. This tidal creek system is marked as tidal inundation IV. Because the absence of plant remains and the appearance of soft clay starts from -4m below NAP and continues downward to -10 m below NAP, it is hypothesized that this tidal creek had a maximum channel depth of 6m. Interestingly, based on the channel depth the tidal creek system would be quite powerful and therefore possible to transport coarse-grained sediments such as loam or fine sands. This formerly active, energetic tidal channel is therefore thought to have been abruptly abandoned and eventually filled with soft clay in a low energetic system.

Finally, the peat deposits are overlain by a continuous clay layer that covers the entire transect (Figure 48). The clay layer has a maximum thickness of 2.5 meters at the southern side of the cross-section and reduces within in northern direction over approximately 200 meters horizontal distance to a thickness of approximately 1 meter. The clay deposits are admixed with coarser-grained sediment and contain fewer plant remains compared with deeper located clays. The tidal clay deposits are interpreted as intertidal flat deposits from a recent, large tidal inundation system VI. Because the addition of new sediment was hindered after the building of dikes, this last tidal inundation system must originate from a period just before or during human settlement in this region (De

Haas *et al.* 2018). This tidal inundation seems to correspond with the active tidal system Ae between 2600 and 800 BP (Vos & Knol 2015), partly initiated by human interference during early settlement (Figure 6).

The surface level is currently situated between -1.5 and -3 m below NAP. Because the last sediments are expected to have been deposited at or around mean sea level, the region has been prone to subsidence. Moreover, a differential subsidence pattern can be distinguished. In general, the observed historic subsidence increases in northern direction to half of the transect. Succeeding, the surface level remains moderately constant, except for the former tidal creek. This differential subsidence pattern can be explained by the appearance of surficial peat in the shallow subsurface. As the mean groundwater level is fairly constant over the entire transect and the thickness of the surficial clay layer decreases in northern direction, the thickness of regularly oxygenated peat increases towards the north. The centre region with more surficial peat has experienced more peat oxidation and is lower elevated. Additionally, the recently active former tidal creek in the cross-section has experienced substantially less historic compression compared to the surrounded clay, and is therefore currently higher elevated within the landscape, referred to as relief inversion.

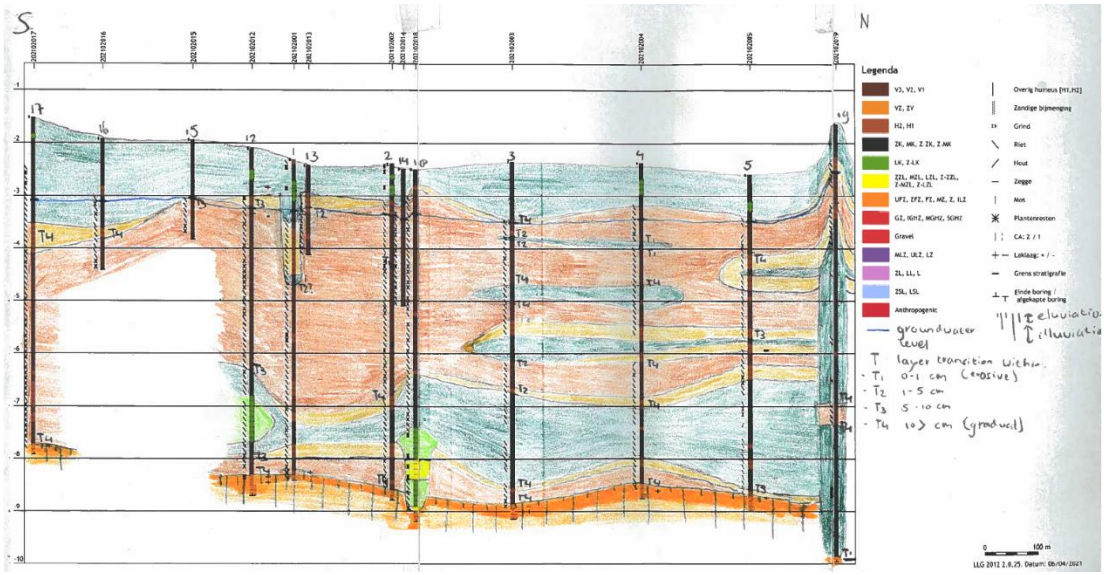

FIGURE 48: LITHOLOGICAL CROSS-SECTION OF TRANSECT EAST IN THE NIEUWOLDA FIELD STUDY AREA.

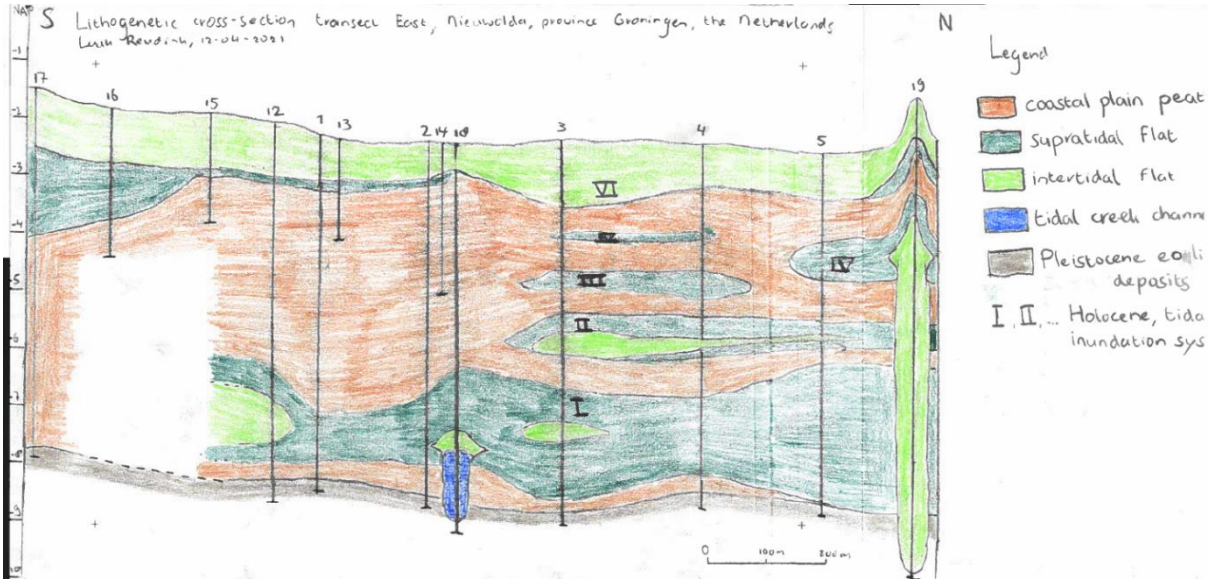

FIGURE 49: LITHOGENETIC CROSS-SECTION OF TRANSECT EAST IN THE NIEUWOLDA FIELD STUDY AREA.

TRANSECT WEST

A total of five core descriptions were used in the production of the lithological and lithogenetic cross-section of the western transect (Figure 50; Figure 51). Transect west shows a very similar subsurface composition compared to the eastern transect. Therefore, the western lithological and lithogenetic cross-sections will only be discussed in terms of similarities and differences compared to the eastern transect.

The large scale tidal deposits from tidal inundation system I are rarely present in the western transect. Based on the depth, the thickness and the spatial extent of the clay deposits at the northern end of this cross-section, these deposits are thought to originate from the same tidal inundation system as number I from transect east. However, in the western cross-section, two successive stages can be differentiated within this tidal inundation system, indicating two phases of a more energetic system in which coarser sediment was deposited. This sediment is interpreted to be deposited in the intertidal zone, because plant remains are absent during these more energetic phases (Figure 51).

Succeeding, two almost continuous clay lenses were distinguished at respectively -4 and -5 m below NAP. Based on the vertical position, the spatial extent and the thickness, the upper and lower clay lense can be interlinked to respectively tidal inundation system V and III from transect east (Figure 49; Figure 51). Finally, the one-meter thick, surficial clay layer present at the surface corresponds to tidal inundation system VI from transect east.. Transect west seems to have experienced similar historic subsidence based on the elevation of the present topography.

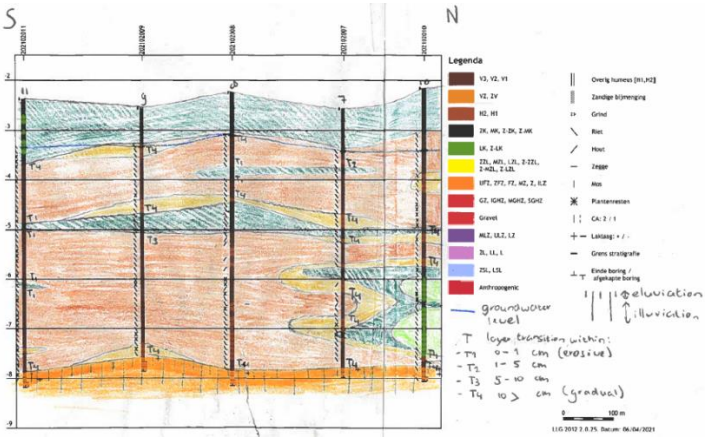

FIGURE 50: LITHOLOGICAL CROSS-SECTION OF TRANSECT WEST IN THE NIEUWOLDA FIELD STUDY AREA.

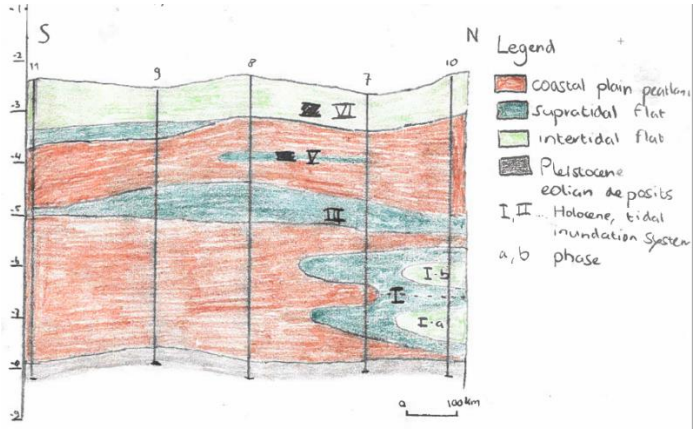

FIGURE 51: LITHOGENETIC CROSS-SECTION OF TRANSECT WEST IN THE NIEUWOLDA FIELD STUDY AREA.

Number	A	B	C	D	E
Core	001	002	017	018	014
Location					
Depth	6.00-6.50m	2.00-2.50m	5.50-6.00m	5.50-6.00m	?

FIGURE 52 SEDIMENT FROM THE NIEUWOLDA FIELD STUDY **A)** PALEOSOIL CONTAINING DISTINCTIVE COLOURED HORIZONS **B)** ABRUPT TRANSITION BETWEEN PEAT AND LAMINATED CLAY **C)** HORIZONTAL ORIENTED WOOD REMAINS IN ORGANIC CLAY DEPOSITS **D)** COARSER-GRAINED LOAM DEPOSITS **E)** HORIZONTAL ORIENTED, PINK COLOURED ALDER WOOD REMAIN **F)** PURE PEAT CONTAINING VERY LITTLE CLASTIC ADMIXTURE **G)** REED PEAT AROUND THE GROUNDWATER LEVEL.

6. DISCUSSION

In this section the results are discussed and compared to related studies. First, a qualitative analysis reflects on individual results and associated thesis objectives and aims (section 6.1). Second, the different research strategies to quantify shallow subsidence in Groningen since 1963 will be synthesized (section 6.2). Third, the effect of a heterogenic subsurface on shallow subsidence is discussed by combining the results of the field study and the created surface motion map of the research area (section 6.3). Fourth, limitations of the conducted methods and the effect of research simplification on the final results are discussed (section 6.4). Finally, the recommendations for future research are presented (section 6.5), followed by the relevance of this MSc thesis to society (section 6.6).

6.1 ACHIEVING THE THESIS GOALS / QUALITATIVE ANALYSIS OF THE RESULTS

6.1.1 ASSESSMENT OF MODELLING DAILY GROUNDWATER LEVELS USING SWAP

In this thesis, the modelled daily groundwater level dynamics largely correspond with measured groundwater levels. SWAP proved to be valuable to model groundwater levels that serve as input for a shallow subsidence model incorporating a differential saturation state of the shallow subsurface. Modelled groundwater levels are suitable to incorporate in shallow subsidence models as long as the trend, the extremes and the average of the modelled groundwater levels match the groundwater level measurements. This assessment is based on both qualitative and quantitative arguments. First, the general trend of modelled groundwater level dynamics corresponds with the measured groundwater level fluctuations. Second, the extremes in modelled groundwater levels match the extremes in measured groundwater levels. Third, the mean error of a modelled groundwater level series can be reduced to only a few centimetres. The most important error of the modelled groundwater levels is the magnitude of a change in groundwater level, creating deviations between measured and modelled groundwater levels that may continue for several days or even months. The deviation between measured and modelled groundwater level in winter can be explained by the interflow relation within the soil water flow computations. Whenever the groundwater level is within 30 cm below the surface level, the model allows horizontal outflow with minor drainage resistance. The intention for allowing interflow is to reduce abrupt increases in groundwater level after heavy rainfall. One of the disadvantages however is that the model appears to be unable to model continuous higher groundwater levels whenever this is observed. Possibly, this might be reduced by addressing a different interflow depth throughout the year.

Regarding the reliability, using SWAP to model groundwater levels has proved to be valuable only for approximately the last ten years. The limiting factor of this assessment was not the availability of historic meteorological measurements, but rather the accessibility of historic surface water levels and land cultivation. For example, knowledge on previous emergence and harvest of crops can almost only be obtained from the landowner, creating a dependency on the accuracy of a landowners archive. Moreover, information on measured surface water levels before 2010 are lacking or simply not easily accessible. This significantly decreases the reliability of modelled groundwater levels, as more assumptions on required parameters have to be made. Therefore, modelling daily groundwater levels for longer periods is unsuitable for quantifying historic subsidence. This problem can be minimized by using measurements with a temporal resolution of months or years as input for the SWAP model.

The sensitivity analysis showed that the horizontal and vertical drainage resistances have the largest effect on the modelled groundwater levels (Figure 36; Figure 37). The importance of these drainage parameters also explains why the surface water level (Figure 34) and distance to surface water (Figure 35) had a minor influence on the model output. The optimal drainage resistance from the calibration was relatively high, reducing the exchange of water with bordering surface water. Possibly, the surface water level and distance to proximal surface water might affect modelled groundwater levels at other locations. The qualitative calibration to obtain the drainage resistances relied on a qualitative estimation by the person performing the calibration on the

plausibility of the calibrated parameter value. Preferably, the actual horizontal and drainage resistances can be acquired or measured in the field. However, more knowledge on the parameterization of these drainage resistances is needed. This could be obtained from follow-up research or a closer collaboration with SWAP developers or experts.

Finally, calibrating modelled groundwater levels through a comparison with groundwater level measurements from a monitoring well need to be performed carefully. The monitoring well measures the hydrostatic pressure close to the surface, and there may be a discrepancy with the actual phreatic groundwater level. Besides, most of the hydrostatic pressures were measured with respect to the surface level. The surface elevation, however, is most often measured only once, during the installation of the monitoring well. After time the surface elevation vertically changes, for example through shrinkage and swelling of the shallow subsurface. This is especially a problem in Groningen, as the gas extraction has caused a significant drop in surface elevation of approximately 0.5 – 1 cm per year. The reliability of the measured groundwater level series, therefore, reduces over time. Preferably, there is a continuous calibration between groundwater level and surface elevation measurements to optimize the actual saturation state of the shallow subsurface.

6.1.2 Assessment of modelling shallow subsidence

The model was tested at the potential peat extensometer location with a thick, surficial peat layer situated at 50 cm below surface level. The model succeeded in computing a differential saturation state of the subsurface through time (Figure 39). The occurrence of oxidation based on the differential saturation state is as expected, with increased oxidation in summer due to lower groundwater levels. This is in accordance with previous research on oxidation that incorporates groundwater level dynamics (Brouns *et al.* 2014). Through a lack of measurements on sediment properties (clastic admixture in peat, preconsolidation stress, oxidation rate, compression parameters) the subsidence model could not be calibrated. The sensitivity analysis highlighted the importance of the used oxidation rate, where the minimum and maximal oxidation rate yielded an absolute difference of approximately 9 cm in the calculated shallow subsidence by oxidation within four years. However, most studies used or found oxidation rates varying between 0.5-1.5 cm m-1 year-1, causing a shallow subsidence rate for this location varying between 0.25-1 cm/year (Van der Meulen *et al.* 2007, Brouns *et al.* 2014, Fokker *et al.* 2019). Another important aspect on computation of compression is the assumption that the modelled effective stresses were always lower than the preconsolidation stress. This assumption was based on the fact that no average groundwater level was observed but also simply because there was no data on the preconsolidation stress for this subsurface. The long summer droughts of 2018 and 2019 could have created effective stress larger than the preconsolidation stress, causing irreversible compression and initiating secondary compression of this part of the subsurface.

6.1.3 Assessment of using historical measurements for shallow subsidence quantification

Comparing the thickness of fine-grained deposits through time appeared useful to get an idea of the order of magnitude of historic, shallow subsidence rates. However, the field campaign required to obtain the present-day lithological build-up is time-consuming. Moreover, the presence and accessibility of detailed, historical measurements in the research area is an important limiting factor. The reliability of the results of this method would have been improved if the lithological build-up was obtained at/around the same date throughout the year, excluding seasonal fluctuation of the surface-elevation through shrinkage and swelling.

The value of historical surface-level measurements relies on the large quantity and the high spatial density, rather than the absolute value of single measurements. This is due to the rather unknown inaccuracy of the surface-level measurements of 2019. Obtaining the vertical motion between 1963 and 2019 based on these surface-level measurements is however not time-consuming. and give a good insight in regional differences in historic, vertical motion. Most important is that subsidence caused by deeper compression within the gas reservoir causes a small

spatial gradient in subsidence rates. Deviations on this (expected) deeper subsidence pattern can be used to detect regions prone to subsidence in the shallow subsurface.

Despite the discussed large error of individual measurements of the surface motion data, some conclusions can still be drawn (Figure 46). The NAM found that historic subsidence since 1963 initiated by the gas extraction varies between 22 and 30 cm for this research area (NAM, 2020; Figure 3). Subtracting the contribution of the gas extraction from the total obtained surface motion in this same period yields a residual subsidence signal. Note that the computed deep subsidence by the gas extraction from studies by the NAM were determined by 'stable' bench marks. The inaccuracy of quantified deep subsidence is therefore also included in the deduced shallow subsidence rate. A detailed study on the obtained deep subsidence rates from the NAM studies could better indicate this included inaccuracy. Excluding human-interfered locations such as road constructions or excavations, the residual subsidence signal reflects the absolute shallow deformation. Moreover, geological subsidence due to basin tectonics and isostatic movement are also included in this residual subsidence signal, but are neglected because of their expected minor impact on total vertical motion (see 3.1.3).The residual subsidence signal varies regionally between 0 and exceptionally 50 cm in 56 years, corresponding to shallow subsidence rates between 0 and maximal 0.9 cm/year. The regional shallow subsidence rates from Bodemdalingskaart 1 yield shallow subsidence rates between 0 and maximally 0.4 cm/year. (Bodemdalingskaart.nl 2020). A detailed investigation in the exact method how these rates were obtained could explain the differences in the obtained shallow subsidence rates between both methods

6.2 SYNTHESIS ON HISTORIC, SHALLOW SUBSIDENCE QUANTIFICATION IN GRONINGEN

	Methodology	**Time period**	**Absolute shallow subsidence**	**Error-bar**	**Shallow subsidence rate**
1	Modelling subsidence using dynamic groundwater levels	2016-2019 (4 years)	2 cm	Oxidation rate most important uncertainty (most likely between 0.5 – 1.5 cm m-1 year-1)	0.5 cm / year *± 1.0 cm*
2	Using lithological measurements	1970-2021 (51 years)	Averaged 10 cm	(± 15 cm)	0.2 cm / year *± 0.3 cm*
3	Using surface-level measurements	1963-2019 (56 years)	Vary between 0 to 60 cm	(± 40 cm), needs to be investigated in more detail!	0 – 1.1 cm/year *± 0.7 cm*

TABLE 9: THREE DIFFERENT RESEARCH STRATEGIES TO QUANTIFY HISTORIC SHALLOW SUBSIDENCE IN THE GRONINGEN GASFIELD AREA SINCE 1963. NOTE THAT THE SHALLOW SUBSIDENCE RATES ARE ALL IN THE ORDER OF SOME MILLIMETERS PER YEAR.

The three different research strategies all yielded subsidence rates in the same order of magnitude of several millimetres per year. These subsidence rates are, although slightly smaller, in accordance with previous studies on historic shallow subsidence in the western Netherlands (Hoogland *et al.* 2012, Koster *et al.* 2018, Fokker *et al.* 2019). Some studies have shown significantly higher subsidence rates, in the order of several tens of millimetres per year (Higgins 2016, Van Asselen *et al.* 2018). However, groundwater extractions greatly contributed to the total subsidence in the study of Higgins (2016) and Van Asselen et al. (2018) investigated historic subsidence over longer time periods of hundreds of years, where the compressibility of fine-grained deposits was larger.

6.3 THE EFFECT OF A HETEROGENIC SUBSURFACE ON HISTORIC SUBSIDENCE

The effect of a heterogeneous shallow subsurface on subsidence was studied 1) by comparing regional differences in historic, vertical motion with lithological cross-sections and 2) by investigating local differences in the shallow subsurface build-up and surface level from the field study in Nieuwolda.

The lithological cross-sections from DINO-loket indicated that locations with a thick layer of fine-grained deposits overlaying the (incompressible) sand deposits show larger historic, shallow subsidence rates. Moreover, the shallow subsidence rates were larger when the thicker peat layers were situated in the shallow subsurface, which

is in accordance with Stouthamer & Van Asselen (2015) and Van Asselen et al. (2018).The development of two lithological cross-sections visualized the local heterogeneity of the Nieuwolda field study area. Two important theories for a differential surface elevation were based on the local subsurface build-up. Firstly, the locations with a thicker peat layer situated in the unsaturated zone currently have a lower surface elevation. This observation emphasizes the importance of oxidation for shallow subsidence, which is in accordance with Van den Akker et al. (2007) and Van Asselen et al. (2018). Secondly, the land surface at the location of the former tidal creek is elevated above local topography. This could be explained by the lithology which contains relatively thick clay layers at the former tidal creek and relatively large amounts of peat in the surrounding area. This would indicate that the shallow subsidence potential of clay is lower than peat, which corresponds with the regional analysis of the surface motion map. However, an alternative explanation is the age of the Holocene sediments at the location of the creek ridge. These deposits belong to a more recent tidal creek channel and are therefore younger. That is why these deposits had less time to consolidate (Van Asselen *et al.* 2009). The observed differential subsidence may also be the result of the two explanations combined, and more research is required to differentiate between the discussed explanations.

These theories rely on the assumption that there was no or minor local relief just after the first initiation of shallow subsidence. This assumption enabled the usage of the local topography as an indication for differential historic shallow subsidence. However, local differences in topography at the start of the reclamation could also (partly) explain the current position of the surface level, rather than historic subsidence.

6.4 Research simplifications and limitations

Modelling groundwater levels in SWAP

SWAP is a complex model that incorporates many processes and thereby many parameters. Although the opportunities of consulting SWAP are numerous, a detailed understanding of the parameterization is required to benefit from these opportunities. Because this was the first consultation of SWAP by the author, the investment in the parameterization of the subsurface and associated flow of water was time-consuming. For the sake of simplicity, various processes that affect the saturation state of the subsurface were neglected when modelling groundwater levels, such as macropore flow and hysteresis. Nevertheless, macropore flow and hysteresis are expected to significantly affect the infiltration of water (Hendriks, 2010). Accurately modelling macropore flow and hysteresis was unfortunately assessed unfeasible within the frame of this MSc research.

There were no soil-hydraulic properties known for sediment at or nearby the study area in Nieuwolda. Instead, the soil-hydraulic properties used to model groundwater levels were obtained by averaging the values of soil-hydraulic properties for similar texture groups throughout the Netherlands (Bakker et al., 2019; Figure 21). This method was considered to obtain the most reliable soil-hydraulic properties required in the SWAP-model. However, averaged soil-hydraulic properties will undoubtedly differ from the actual soil-hydraulic properties of sediment in the study area. Moreover, all the measured soil-hydraulic properties in the study by Bakker et al. (2019) were obtained from sediment samples of the surficial two meter of the subsurface. These soil-hydraulic properties were also assigned to sediment at greater depth in this research. Sediment characteristics at greater depth, however, will be different compared to surficial sediment for almost all required parameters such as the density, saturated conductivity and saturated water content. Although these limitations were known beforehand, there are simply no other soil-hydraulic properties available for sediment at greater depth.

Finally, one important limitation of modelling groundwater levels in SWAP is the inability to model a differential thickness of discretized layers. The saturation state, however, is not only determined by the position of the groundwater level but also by vertical changes in the subsurface. Preferably, the SWAP-model could incorporate deformation mechanisms such as oxidation, compression, shrinkage and swell to compute a new thickness and vertical position at the next time step, comparable to the developed subsidence model in this MSc research. This has already been accomplished for oxidation, by combining SWAP with the ANIMO-model (Kroes *et al.* 2017). A

study by Van Den Akker et al (2017) used ANIMO to compute the emission of greenhouse gasses. The decrease in mass because of the emission is used to compute the deformation within the associated peat layer. However, this method requires the measurements of greenhouse gas emissions that was simply not feasible for this MSc thesis.

Finally, the layer discretization in SWAP was based on core descriptions from the performed field study of this research in 2021. The lithological profile of 2021 might differ from the actual lithology at the start of the modelled period in 2016.

CALIBRATING MODELLED GROUNDWATER LEVELS

The calibration in this research was very time-consuming as every individual parameter had to be adapted manually to investigate the model output. Therefore, only a few of the set parameters could be calibrated. An automatic calibration, however, would optimally calibrate all the unknown parameters. An automatic calibration could be performed with the use of models such as PEST or R (personal communication R. Hendriks) but requires a good analysis of the quality and plausibility of the obtained parameter values. Such an automatic calibration would be useful as the final step in the calibration, to fine-tune parameter values. Automatic calibration of SWAP parameters could not be performed within the framework of this MSc thesis.

MODELLING SHALLOW DEFORMATION USING THE DEVELOPED SUBSIDENCE MODEL

Although an empirical formula for irreversible shrinkage has been incorporated in the model, there was insufficient data on parameters required to quantify irreversible shrinkage. Besides, the compression computation in the model is based on the Koppejan 1D method. Although this method incorporates a time-independent (primary compression) and time-dependent (creep) strain, the scientific approach to quantify compression is already much more advanced (Bjerrum 1967, Den Haan 1994). Moreover, historic compression has been ignored by neglecting the preconsolidation stress experienced since reclamation. Therefore, compression modelled in this MSc research is very simplified but was the first step of a subsidence model that can quantify compression based on dynamic groundwater levels.

6.5 RECOMMENDATIONS AND FUTURE RESEARCH

MODELLING GROUNDWATER LEVELS USING SWAP

1. In collaboration with WUR, soil-hydraulic properties of the subsurface at the location of the extensometer could be obtained. Both parties might benefit from such collaboration because it would generate rather accurate subsurface parameters that could directly be compared to the deformation signal measured by the extensometer. Moreover, a similar collaboration with WUR could be agreed upon to measure greenhouse gas emissions at the extensometer location. The emission can be converted into a decrease in mass by peat oxidation and allows a direct comparison with actual deformation measurements.
2. A future sensitivity analysis using SWAP could investigate the effect of soil-hydraulic properties on the modelled groundwater levels. This sensitivity analysis requires detailed research on the usage of soil-hydraulic properties in the computation of flow of water through the subsurface in SWAP.
3. The potential of the SWAP-model is enormous and this MSc research has only used the basics to model groundwater levels. Follow-up research could step-by-step incorporate more features of the SWAP-model possibilities. The first mechanisms that should be considered in such future research are macropore flow and hysteresis, as these are expected to influence the saturation state significantly. Furthermore, Dr. Van den Akker (personal communication) highlighted the importance of soil temperature in the decomposition rate of peat. At the nearby weather station of Nieuw Beerta, soil temperature measurements were conducted since 1990 and these might be valuable for future research on peat decomposition in Groningen.

4. An alternative model to mimic groundwater levels in Groningen is the more regional MIPWA-model (Methodology for Interactive Planning for Water Management) from the iMOD module of Deltares. Various parties in the water management of northern Netherlands collaborated to create a regional groundwater model that can predict groundwater levels with a resolution of 25x25 m2 (Berendrecht *et al.* 2007). Just as SWAP, the MIPWA is a process-based model focussing on interactions between plant, atmosphere, soilwater, groundwater and surface water level (Van Walsum *et al.* 2004). One of the advantages of this regional model is that there is a direct connection in water flow between the grid cells. An important difference with SWAP is that the subsurface of the MIPWA-model was created by a direct transfer of the GeoTOP subsurface model.
5. Groundwater level fluctuations could be modelled throughout the day. All the required meteorological parameters for the SWAP model were monitored by KNMI for every hour since 1960. Using this data could obtain temporal fluctuations in groundwater level between day and night based on differential evapotranspiration rates and root uptake. Whenever temporal fluctuations in groundwater levels are significant, differential surface water levels between day and night could be considered for future water management.
6. Finally, laboratory research on sediment samples from the study area could optimize the subsurface parameterization. Sediment properties that could be determined through laboratory research are 1) the volumetric moisture content 2) dry bulk density 3) the clastic admixture 4) Organic matter content (LOI)

MODELLING SUBSIDENCE IN THE SHALLOW SUBSURFACE

1. The compression that is incorporated in the shallow subsidence model is greatly simplified. First, the Koppejan 1D method could be improved through the incorporation of compression equations by Bjerrum (1967) or Den Haan (1994), to increase the credibility of the quantified compression. Second, the preconsolidation stress should be measured and subsequently incorporated. Third, measuring the required compression parameters at the field study area would increase the reliability significantly. The compressibility of sediment samples can be measured in the laboratory using an oedometer test.
2. Very few swell and shrinkage parameters are known for the computation of irreversible shrinkage in shallow subsidence models. The parameters by Fokker et al. (2019) were determined for clay soils that had only recently been reclaimed and still relatively compressible. However, extensometers in Groningen will create a better understanding in the swell and shrinkage mechanisms. Future research could parameterize swell and shrinkage behaviour of different sediment texture groups, allowing the incorporation of these mechanisms at any location.

POTENTIAL OF HISTORICAL MEASUREMENTS

1. The historical soil hand drillings from 1999 between Overschild and Luddeweer could be used to expand the research area when studying groundwater dynamics, because the maximum variability in groundwater level is determined for all of the 697 investigated locations (Kiestra 2000).
2. The 999 lithological core descriptions by the water authority Hunze & Aa could be used to create a regional peat thickness map, indicating vulnerable regions for future peat oxidation.
3. The surface motion map of Figure 46 is produced for northeast Groningen. However, the presence of surface level measurements throughout Groningen allows the production of a similar surface motion map for the entire area influenced by the gas extraction.
4. Moreover, the surface motion map could potentially be coupled to the regional GeoTOP subsurface model by TNO. Instead of investigating rather specific transects, this coupling would allow a direct comparison or cross-reference between the regional shallow subsurface and historic subsidence.

6.6 CONTRIBUTION TO SOCIETY

The negative consequences of subsidence for humankind are manifold and were already addressed in Chapter 1 of this thesis. A better understanding of the subsidence process could open doors for innovative solutions to

reduce or counter these negative consequences. For example, Koster et al (2020) explain how areas proximal to tidal systems, such as this study in Groningen, could potentially be elevated by controlled sedimentation via watercourses that deliver new sediment. This thesis added both qualitative and quantitative understanding on the effect of groundwater level on subsidence in the shallow subsurface. The incorporation of daily groundwater dynamics in an empirical shallow subsidence model could be utilized for future research that will investigate the effect of new water management strategies to reduce future subsidence. Moreover, the effect of a discontinuous shallow subsurface on future subsidence can be used to indicate future vulnerable areas and consider more drastic measures at these locations. This study was the start of an extensive research program aimed at quantifying and disentangling the subsidence signal in Groningen. This thesis supported the selection of two extensometers locations that will measure vertical motion the next tens of years, unravelling the differential subsidence signal.

7. CONCLUSION

This MSc-research aimed to quantify shallow subsidence in the Groningen gasfield area since 1963, using a differential subsurface saturation state based on daily modelled groundwater levels. This was achieved by a literature synthesis, a data inventory and a field study that enabled to model dynamic groundwater levels and subsidence in the shallow subsurface. Combining these results led to the following conclusions, corresponding to subobjectives 2-5 of this thesis:

2) Modelling groundwater levels using SWAP was proven to be valuable in mimicking groundwater level dynamics, since the trend, the extremes and the mean of modelled groundwater levels match groundwater level measurements. The minimal, average deviation between measured and modelled groundwater levels is 20 cm, particularly caused by an error in time and magnitude of a change in groundwater level. Most of the important parameters in the SWAP-model could be obtained from online accessible databases. A sensitivity analysis revealed that modelled groundwater levels greatly rely on the vegetation cover, horizontal and vertical drainage resistances.

3) An empirical, one-dimensional, shallow subsidence model has been developed that incorporates dynamic groundwater levels to compute the differential saturation state of the subsurface through time. Sediment properties are parameterized and can be assigned to discretized layers in the subsurface. The model was deployed for a location in the Nieuwolda field study area with a relatively thick peat layer situated in the shallow subsurface. The model indicated an average shallow subsidence rate of 0.5 cm/year between 2016 and 2019 due to peat oxidation and (reversible) compression. A sensitivity analysis highlighted the importance of the incorporated oxidation rate and clastic admixture in the peat that is used in the computation of peat oxidation.

4) Comparing the thickness of fine-grained deposits in the shallow subsurface in Appingedam between 1970 and 2021 yielded an average shallow subsidence rate of 0.2 cm/year. Locations with amorphous peat and a relatively small, surficial clay layer of only 40-60 cm thick showed larger shallow subsidence rates varying between 0.5-0.8 cm/year. Applying this method to quantify subsidence is largely limited by the presence and accessibility of detailed, historical measurements in the research area.

Subtracting quantified deep subsidence found by the NAM from the total, vertical motion obtained from historical measurements yielded a residual subsidence rate varying between 0-0.9 cm/year. By excluding geological subsidence and human-interfered locations, this residual subsidence signal reflects the absolute shallow deformation. This strategy requires a more detailed investigation on the method how these surface-level measurements were obtained, needed to determine the inaccuracy of subsidence rates. Moreover, the value of using historical surface-level measurements to quantify subsidence relies on the large quantity and the high spatial density, rather than the absolute value of single measurements.

5) Cross-sections obtained from a field study indicated the effect of a local, heterogeneous, shallow subsurface on subsidence. Especially local heterogeneity of the unsaturated zone caused differential subsidence. Locations without peat in the unsaturated zone were slightly elevated compared to locations where peat was situated already 50 cm below surface level. Moreover, locations with recently active former tidal creeks are currently higher elevated, because the subsurface contains coarser sediment that has experienced relatively less historic compression. From the regional surface motion map can be concluded that shallow subsidence rates differ locally as a consequence of a regional, heterogeneous shallow subsurface. Regions without fine-grained deposits overlaying (incompressible) sand deposits showed minor shallow subsidence.

This study was the start of an extensive research program aimed at quantifying and disentangling the subsidence signal in Groningen. The data inventory, model exploration and extensometer site selection will support future research on subsidence in Groningen. Future research can increase the reliability of modelled groundwater levels by including hysteresis and macropore flow, by improving soil-hydraulic input parameters or by incorporating

temporal, differential layer thickness by shallow deformation. The developed subsidence model can be improved by obtaining more detailed compression and shrinkage parameters and/or by improving the incorporated compression computations.

REFERENCES

Akker, J. Van Den, Hendriks, R. & Delft, B. Van. (2017) De organische veenbasis Afbraakprocessen in relatie tot hydrologie.

Akker, J.J.H. Van den, Beuving, J., Hendriks, R.F.A. & Wolleswinkel, R.J. (2007) Maaivelddaling, afbraak en CO2 emissie van Nederlandse veenweidegebieden. *Leidraad Bodembescherming, afl*, **83**, 83.

Asselen, S. Van. (2010) *Peat compaction in deltas*.

Asselen, S. Van, Akker, J.J.H. van den & Kooi, H. (2019) Deltafact: Bodemdaling.

Asselen, S. Van, Erkens, G. & Graaf, F. de. (2020) Monitoring shallow subsidence in cultivated peatlands. *Proc. Int. Assoc. Hydrol. Sci.*, **382**, 189–194, Copernicus GmbH.

Asselen, S. Van, Erkens, G., Stouthamer, E., Woolderink, H.A.G., Geeraert, R.E.E. & Hefting, M.M. (2018) The relative contribution of peat compaction and oxidation to subsidence in built-up areas in the Rhine-Meuse delta, The Netherlands. *Sci. Total Environ.*, **636**, 177–191, Elsevier.

Asselen, S. Van, Stouthamer, E. & Asch, T.W.J. Van. (2009) Effects of peat compaction on delta evolution: a review on processes, responses, measuring and modeling. *Earth-Science Rev.*, **92**, 35–51, Elsevier.

Bakker, G., Heinen, M. & Peters, P.D. (2019) Hydrofysische gegevens van de bodem in de Basisregistratie Ondergrond (BRO) en het Bodemkundig Informatie Systeem (BIS).

Bakker, H. de & Schelling, J. (1966) Systeem van bodemclassificatie voor Nederland. De hogere niveaus. *Grondboor & Hamer*, **20**, 229.

Berendrecht, W.L., Snepvangers, J., Minnema, B. & Vermeulen, P.T.M. (2007) MIPWA: a methodology for interactive planning for water management. *MODSIM 2007 Int. Congr. Model. Simulation. Model. Simul. Soc. Aust. New Zeal.*, pp. 74–80.

Berendsen, H.J.A. (2005) *Fysisch-geografisch onderzoek*, Uitgeverij Van Gorcum.

Bjerrum, L. (1967) Engineering geology of Norwegian normally-consolidated marine clays as related to settlements of buildings. *Geotechnique*, **17**, 83–118, Thomas Telford Ltd.

Bodemdalingskaart.nl. (2020) No Title.

Boothroyd, J.C. (1978) Mesotidal inlets and estuaries. in *Coastal sedimentary environments*, pp. 287–360, Springer.

Born, G.J. Van den, Kragt, F., Henkens, D., Rijken, B., Bemmel, B. Van & Sluis, S. Van der. (2016) Dalende bodems, stijgende kosten. *Planbur. voor Leefomgeving Rapp. 1064*.

Bos, A.P., Gies, T.J.A. & Male, B. van. (2017) *Vormgeven aan Sturen met Water: bodemdaling vertragen in het veenweidegebied met boeren en natuur*, Wageningen Livestock Research.

Bronswijk, J.J.B. (1989) Prediction of actual cracking and subsidence in clay soils. *Soil Sci.*, **148**, 87–93, LWW.

Brouns, K. (2016) The effects of climate change on decomposition in Dutch peatlands: an exploration of peat origin and land use effects. *Utr. Univ. Utrecht, Netherlands*.

Brouns, K., Verhoeven, J.T.A. & Hefting, M.M. (2014) Short period of oxygenation releases latch on peat decomposition. *Sci. Total Environ.*, **481**, 61–68, Elsevier B.V. doi:10.1016/j.scitotenv.2014.02.030

Bungenstock, F. & Schäfer, A. (2009) The Holocene relative sea-level curve for the tidal basin of the barrier island Langeoog, German Bight, Southern North Sea. *Glob. Planet. Change*, **66**, 34–51, Elsevier.

Cohen, K.M. (2003) Differential subsidence within a coastal prism: late-Glacial-Holocene tectonics In The Rhine-Meuse delta, the Netherlands.

Commissie bodemdaling. (n.d.) Bodemdaling door grondwaterwinning.

Erkens, G., Meulen, M.J. Van Der & Middelkoop, H. (2016) Double trouble: Subsidence and CO2 respiration due to 1,000 years of Dutch coastal peatlands cultivation. *Hydrogeol. J.*, **24**, 551–568. doi:10.1007/s10040-016-1380-4

Fitts, C.R. (2002) *Groundwater science*, Elsevier.

Fokker, P.A., Gunnink, J., Lange, G. De, Leeuwenburgh, O. & Veer, E.F. Van Der. (2015) Compaction parameter estimation using surface movement data in Southern Flevoland. *Proc. Int. Assoc. Hydrol. Sci.*, **372**, 183–187. doi:10.5194/piahs-372-183-2015

Fokker, P.A., Gunnink, J.L., Koster, K. & Lange, G. de. (2019) Disentangling and parameterizing shallow sources of subsidence: Application to a reclaimed coastal area, Flevoland, the Netherlands. *J. Geophys. Res. Earth Surf.*, **124**, 1099–1117, Wiley Online Library.

Fokker, P.A., Leijen, F.J. Van, Orlic, B., Marel, H. Van Der & Hanssen, R.F. (2018) Subsidence in the Dutch Wadden Sea. *Geol. en Mijnbouw/Netherlands J. Geosci.*, **97**, 129–181. doi:10.1017/njg.2018.9

Friedrichs, C.T. (2011) Tidal flat morphodynamics: a synthesis.

Frolking, S., Roulet, N.T., Moore, T.R., Richard, P.J.H., Lavoie, M. & Muller, S.D. (2001) Modeling northern peatland decomposition and peat accumulation. *Ecosystems*, **4**, 479–498, Springer.

Greeff, B. de, Wit, J. de & Zwaanswijk, M. (2019) Bodemdaling Sneekermeer West.

Haan, E.J. Den. (1994) Vertical compression of soils.

Haas, T. De, Pierik, H.J., Spek, A.J.F. Van der, Cohen, K.M., Maanen, B. Van & Kleinhans, M.G. (2018) Holocene evolution of tidal systems in The Netherlands: Effects of rivers, coastal boundary conditions, eco-engineering species, inherited relief and human interference. *Earth-Science Rev.*, **177**, 139–163, Elsevier.

Hendriks, M. (2010) *Introduction to physical hydrology*, Oxford University Press.

Hendriks, R., Akker, J.J.H. van den, Jansen, P.C. & Massop, H.T.L. (2014) *Effecten van onderwaterdrains in peilvak 9 van polder Groot-Wilnis Vinkeveen*.

Higgins, S.A. (2016) Review: Advances in delta-subsidence research using satellite methods. *Hydrogeol. J.*, **24**, 587–600. doi:10.1007/s10040-015-1330-6

Hijma, M. & Cohen, K. (2010) Timing and magnitude of the sea-level jump preluding the 8200 yr event. *Geology*, **38**, 275–278, Geological Society of America.

Hijma, M. & Kooi, H. (2018) *Bodemdaling in het kustfundament en de getijdenbekkens*.

Hoogland, T., Akker, J.J.H. van den & Brus, D.J. (2012) Modeling the subsidence of peat soils in the Dutch coastal area. *Geoderma*, **171–172**, 92–97, Elsevier B.V. doi:10.1016/j.geoderma.2011.02.013

Kiestra, E. (2000) Bodemkundig-hydrologisch onderzoek voor de waardebepaling van de gronden in het blok Luddeweer-Overschild van de herinrichting Midden-Groningen, Alterra.

KNMI. (2021) Daggevens van het weer in Nederland.

Kooi, H. & Erkens, G. (2020) Modelling subsidence due to Holocene soft-sediment deformation in the Netherlands under dynamic water table conditions. *Proc. Int. Assoc. Hydrol. Sci.*, **382**, 493–498. doi:10.5194/piahs-382-493-2020

Kooi, H., Johnston, P., Lambeck, K., Smither, C. & Molendijk, R. (1998) Geological causes of recent (~ 100 yr) vertical land movement in the Netherlands. *Tectonophysics*, **299**, 297–316, Elsevier.

Koppejan, A.W. (1948) A formula combining the Terzaghi load compression relationship and the Buisman secular time effect. *Proc. 2nd ICSMFE, Rotterdam, 1948*, **3**, 32–37.

Koster, K., Stafleu, J. & Stouthamer, E. (2018) Differential subsidence in the urbanised coastal-deltaic plain of the Netherlands. *Geol. en Mijnbouw/Netherlands J. Geosci.*, **97**, 215–227. doi:10.1017/njg.2018.11

Kroes, J.G., Dam, J.C. Van, Bartholomeus, R.P., Groenendijk, P., Heinen, M., Hendriks, R.F.A., Mulder, H.M., *et al.* (2017) SWAP version 4, Wageningen Environmental Research.

Laarhoven, S. Van. (2017) *Influence of loading history on subsurface architecture and subsidence potential for the historical city of Gouda, The Netherlands.* Retrieved from https://dspace.library.uu.nl/handle/1874/361337

Le, T.M., Fatahi, B. & Khabbaz, H. (2012) Viscous behaviour of soft clay and inducing factors. *Geotech. Geol. Eng.*, **30**, 1069–1083, Springer.

Maren, D.S. Van, Oost, A.P., Wang, Z.B. & Vos, P.C. (2016) The effect of land reclamations and sediment extraction on the suspended sediment concentration in the Ems Estuary. *Mar. Geol.*, **376**, 147–157, Elsevier.

Meijles, E. (2015) *De ondergrond van Groningen: een geologische geschiedenis*, NAM.

Meulen, M.J. Van der, Spek, A.J.F. Van der, Lange, G. de, Gruijters, S.H.L.L., Gessel, S.F. van, Nguyen, B.L., Maljers, D., *et al.* (2007) Regional sediment deficits in the Dutch lowlands: Implications for long-term land-use options. *J. Soils Sediments*, **7**, 9–16. doi:10.1065/jss2006.12.199

Minderhoud, P.S.J., Erkens, G., Pham, V.H., Bui, V.T., Erban, L., Kooi, H. & Stouthamer, E. (2017) Impacts of 25 years of groundwater extraction on subsidence in the Mekong delta, Vietnam. *Environ. Res. Lett.*, **12**, 64006, IOP Publishing.

NAM. (2020) Bodemdaling door Aardgaswinning.

Nichols, G. (2009) *Sedimentology and stratigraphy*, John Wiley & Sons.

Nichols, M.M. (1989) Sediment accumulation rates and relative sea-level rise in lagoons. *Mar. Geol.*, **88**, 201–219, Elsevier.

Oost, A.P. (1995) *Dynamics and sedimentary developments of the Dutch Wadden Sea with a special emphasis on the Frisian Inlet: a study of the barrier islands, ebb-tidal deltas, inlets and drainage basins*, Faculteit Aardwetenschappen.

Oude Essink, G. & Louw, P. De. (2014) Brackish seepage. Retrieved from https://www.stowa.nl/sites/default/files/assets/DELTAFACTS/Deltafacts E PDF nieuw format/Brakke kwel EN.pdf

Pauw, P.S., Baaren, E.S. Van, Visser, M., Louw, P.G.B. De & Essink, G.H.P.O. (2015) Increasing a freshwater lens below a creek ridge using a controlled artificial recharge and drainage system: a case study in the Netherlands. *Hydrogeol. J.*, **23**, 1415–1430, Springer.

Pethick, J.S. (1984) An introduction to coastal geomorphology, Dept. of Geography, Univ. of Hull.

Pierik, H.J., Cohen, K.M. & Stouthamer, E. (2016) A new GIS approach for reconstructing and mapping dynamic late Holocene coastal plain palaeogeography. *Geomorphology*, **270**, 55–70, Elsevier.

Pierik, H.J., Cohen, K.M., Vos, P.C., Spek, A.J.F. Van der & Stouthamer, E. (2017) Late Holocene coastal-plain evolution of the Netherlands: the role of natural preconditions in human-induced sea ingressions. *Proc. Geol. Assoc.*, **128**, 180–197, Elsevier.

Rijksoverheid. (2021) Afbouw gaswinning Groningen. Retrieved April 16, 2021, from https://www.rijksoverheid.nl/onderwerpen/gaswinning-in-groningen/nieuws/2021/02/11/afbouw-gaswinning-groningen-op-schema

Scanlon, D. & Moore, T. (2000) Carbon dioxide production from peatland soil profiles: the influence of temperature, oxic/anoxic conditions and substrate. *Soil Sci.*, **165**, 153–160, LWW.

Spek, A.J.F. Van der. (1994) *Large-scale evolution of Holocene tidal basins in the Netherlands*, Universiteit Utrecht, Faculteit Aardwetenschappen.

Stouthamer, E. & Asselen, S. Van. (2015) Potential of Holocene deltaic sequences for subsidence due to peat compaction. *Proc. Int. Assoc. Hydrol. Sci.*, **372**, 173–178. doi:10.5194/piahs-372-173-2015

Stouthamer, E. & Berendsen, H.J.A. (2001) Avulsion frequency, avulsion duration, and interavulsion period of Holocene channel belts in the Rhine-Meuse delta, the Netherlands. *J. Sediment. Res.*, **71**, 589–598, SEPM Society for Sedimentary Geology.

Stouthamer, E., Cohen, K.M.C. & Hoek, W.Z.H. (2020) *De vorming van het land: geologie en geomorfologie*, Perspectief uitgevers.

Syvitski, J.P.M., Kettner, A.J., Overeem, I., Hutton, E.W.H., Hannon, M.T., Brakenridge, G.R., Day, J., *et al.* (2009) Sinking deltas due to human activities. *Nat. Geosci.*, **2**, 681–686, Nature Publishing Group.

Terzaghi, K. (1943) Theoretical soil mechanics. johnwiley & sons. *New York*, 11–15.

Tetens, O. (1930) Uber einige meteorologische Begriffe. *Z. Geophys*, **6**, 297–309.

Thienen-Visser, K. Van, Pruiksma, J.P. & Breunese, J.N. (2015) Compaction and subsidence of the Groningen gas field in the Netherlands. *Proc. Int. Assoc. Hydrol. Sci.*, **372**, 367–373, Copernicus GmbH.

Vermeersen, B.L.A., Slangen, A.B.A., Gerkema, T., Baart, F., Cohen, K.M., Dangendorf, S., Duran-Matute, M., *et al.* (2018) Sea-level change in the Dutch Wadden Sea. *Geol. en Mijnbouw/Netherlands J. Geosci.*, **97**, 79–127. doi:10.1017/njg.2018.7

Vink, A., Steffen, H., Reinhardt, L. & Kaufmann, G. (2007) Holocene relative sea-level change, isostatic subsidence and the radial viscosity structure of the mantle of northwest Europe (Belgium, the Netherlands, Germany, southern North Sea). *Quat. Sci. Rev.*, **26**, 3249–3275, Elsevier.

Voosen, P. (2021) Global temperatures in 2020 tied record highs, American Association for the Advancement of Science.

Vos, P.C. (2015) *Origin of the Dutch coastal landscape: long-term landscape evolution of the Netherlands during the Holocene, described and visualized in national, regional and local palaeogeographical map series*, Barkhuis.

Vos, P.C. & Kesteren, W.P. van. (2000) The long-term evolution of intertidal mudflats in the northern Netherlands during the Holocene; natural and anthropogenic processes. *Cont. Shelf Res.*, **20**, 1687–1710, Elsevier.

Vos, P.C. & Knol, E. (2015) Holocene landscape reconstruction of the Wadden Sea area between Marsdiep and Weser: explanation of the coastal evolution and visualisation of the landscape development of the northern Netherlands and Niedersachsen in five palaeogeographical maps from 500. *Netherlands J. Geosci.*, **94**, 157–183, Cambridge University Press.

Vos, P.C. & Nieuwhof, A. (2021) Late-Holocene sea-level reconstruction (1200 BC – AD 100) in the Westergo terp region of the northern Netherlands, **2021**.

Walsum, P.E. V Van, Veldhuizen, A.A., Bakel, P.J.T. Van, Bolt, F.J.E. Van Der, Dik, P.E., Groenendijk, P., Querner, E.P., *et al.* (2004) SIMGRO 5.0. 1; theory and model implementation, Alterra.

Yuill, B., Lavoie, D. & Reed, D.J. (2009) Understanding subsidence processes in coastal Louisiana. *J. Coast. Res.*, 23–36, Coastal Education and Research Foundation 1656 Cypress Row Drive, West Palm ….

Zhou, Z., Ye, Q. & Coco, G. (2016) A one-dimensional biomorphodynamic model of tidal flats: sediment sorting, marsh distribution, and carbon accumulation under sea level rise. *Adv. Water Resour.*, **93**, 288–302, Elsevier.

APPENDIX

APPENDIX: MEASURING SUBSIDENCE: A BRIEF OVERVIEW

Subsidence is a slow process in the order of mm or cm per year (Bodemdalingskaart.nl, 2020) Measuring subsidence must be precise and accurate because of the relatively small order of magnitude. It is a challenge in current research to measure subsidence related to individual mechanisms and thereby disentangling the subsidence signal.

FIELD TECHNIQUES

LEVELLING

Levelling is a method to measure the surface level of a certain position with respect to a reference height using a spirit levelling instrument. Measuring the relative height of one position repeatedly through time provides a subsidence signal (Van Asselen et al., 2020). The reference point is founded in a stable layer, usually the Pleistocene surface underlying Holocene sediments . The reference height in the Netherlands is most often the 'Ducth Ordnance Datum' NAP, that approximately corresponds with the position of sea level. Levelling measurements have an accuracy ranging from mm up to cm (Van Asselen et al., 2019). Levelling in northeast Groningen with respect to a reference height founded in the Pleistocene substrate will only show shallow subsidence of Holocene deposits, while deeper compression of the gas reservoir will not be detected. TOPhoogteMD is a Dutch nationwide elevation database with levelling measurements between 1942 and 1983 (Nationaal Georegister, n.d.).

EXTENSOMETER

An extensometer is a founded measuring instrument that can measure vertical movement of different layers in the subsurface with use of anchors that are stabilized at a specific height. An extensometer can quantify subsidence at one location with an accuracy in the order of mm (Van Asselen et al., 2020). In contrary to levelling, an extensometer is able to disentangle a subsidence signal, differentiating between layers in the vertical direction Extensometers are only recently (2019) applied in the Netherlands (Rouveen) and there contribution to subsidence research is still being investigated, yet promising (Van Asselen et al., 2020)

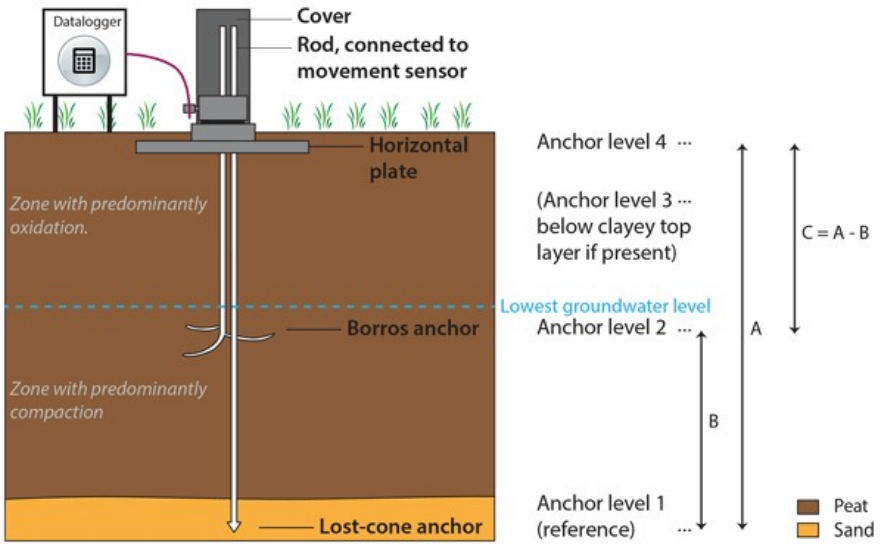

REMOTE SENSING

LIGHT DETECTION AND RANGING (LIDAR)

LiDAR is an air- or spaceborn land survey technique that emits a laser pulse and can measure the distance between the scanning device and the surface level by calculating the travel time (Van Asselen et al., 2020). The surface elevation is obtained by converting the distance to a surface elevation with use of spatial computations.

As the air- or spaceborn device spans a large area, regional or national elevation maps can be acquired. Covering the same region repeatedly over time could indicate differential subsidence. A nationwide survey of the surface elevation has been compiled in an online public database referred to as AHN (Koomen & Maas, 2004)

INTERFEROMETRIC SYNTHETIC APERTURE RADAR (INSAR)

InSAR uses radar images of the earth that are produced with use of a satellite and measures a change in wave phase after reflection of a signal with the surface. Since several tens of radar images are created throughout the year, a change in reflection of the surface can be converted into a vertical movement (Higgins, 2016). InSAR measures only the change in elevation, in contrary to LiDAR that can actually measure an elevation. The obtained vertical movement has an accuracy less than a mm per year and is therefore quite precise, especially in comparison with the accuracy of LiDAR. A disadvantage is that only surfaces that reflect a consistent signal, such as concrete, can be detected. Therefore, the InSAR technique works better for cities and other more densely populated areas compared with rural, cultivated areas. However, sporadic farmhouses or roads can provide a subsidence signal even in these less densely populated regions. A nationwide online database can be publicly consulted to observe and work with InSAR data from the Netherlands (Bodemdalingskaart.nl, 2020).

Boorpunt: 202102001 Namen: 001 Jaar: 2021 Groep: 02 Datum: 13-3-2021

Coordinaten		Hoogte	Diepte
Xco	Yco	Z [m]	[cm]
260862	585928	-2.31	610

KAARTEENHEID	Geomorfogenetische kaart:
Geologische kaart:	Grondwatertrap:
Begroeiingskaart:	Bodemkaart:

Hoogte AHN.
Verwachting 2m kleidek a.d.h.v waterschapsboringen
Potentiële extensometer locatie.

Diepte	Textuur	Org	Plr	Kleur	Redox	Grind	M50	Ca	Fe	GW	M	LKL	Strat	Bijzonderheden
10	MK	H1	r	brgr				0						wortels
20	MK		plr	gr				0	1					wortels
30	MK			gr				0	1					
40	MK			gr				0	1					
50	LK			gr				1	1					
60	LK		plr	gr				1	1					
70	LK			gr				1	1					
80	LK			gr				1						
90	MK			gr				1						schelpfragmenten
100	MK			gr				0		GW				
110	MK			gr				0						#, schelpfragmenten
120	MK		r	gr				0						schelpresten, o2 naar veen
130		V2	r	grbr				0						o2 naar klei,
140	ZK	H2	r	brgr				0						
150	ZK	H1	r	brgr				0						verticale rietstengel
160	ZK	H1	r	brgr				0						verticale rietstengel
170	ZK	H1	r	dbrgr				0						
180	ZK	H1	r	dbrgr				0						#
190	ZK	H1	r	brgr				0						#
200	ZK	H1	r	brgr				0						
210	ZK	H2	r	brgr				0						kleiband 5mm
220	ZK	H1	r	brgr				0						
230	ZK		r	gr				1						
240	ZK		r	gr				1						veen op 2.38,o2
250		V1	r	dbr				0						vezelig, zie foto
260		V1	r	dbr				0						#
270		V1	r	br				0						#, kleiband 5mm
280		V1	r	br				0						
290		V1	r	br				0						
300		V1	r	br				0						
310		V1	r	br				0						
320		V1	r	br				0						
330		V1	r	br				0						#
340	ZK	H2	plr	dbrgr				0						#
350	ZK	H2	plr	dbrgr				0						
360		V2	r	br				0						
370		V2	r	br				0						zwarte banden
380		V2	r	br				0						kleibanden 2 mm
390		V2	r	br				0						
400		V1	r	br				0						# Verloren, gekopieëerd380-390
410		V1	r	br				0						#
420		V1	r	grbr				0						o2 veen-> klei
430	ZK	H2	r	dbrgr				0						
440	ZK	H2	r	dbrgr				0						
450	ZK	H2	r	dbrgr				0						
460		V1	r	dgrbr				0						
470		V1	r	dgrbr				0						
480		V1	rh	grbr				0			M001			#, sample hout?
490	ZK	H1	r	brgr				0						#
500	MK	H1	r	brgr				0						
510	ZK	H0	r	brgr				0						
520	MK	H0	hr	brgr				0			M002			
530	MK	H0	r	brgr				0						
540	ZK	H0	r	brgr				0						zaden (foto)
550	ZK	H1	r	brgr				0						
560	MK	H1	r	brgr				0						# zaadje (foto)
570	ZK	H2	r	dbr				0						#
580		V1	r	br				0						
590		V1	rh	br				0						
600	MK	H1	hr	dgr				0				+		zwarte horizont(7 cm),

Boring: 202102001

Diepte	Textuur	Org	Plr	Kleur	Redox	Grind	M50	Ca	Fe	GW	M	LKL	Strat	Bijzonderheden
610		VZ	r	gr				0						o2 zwart -> zand op 6.07m (Z)

Einde boring: 202102001

Boorpunt: 202102002 Namen: 002 Jaar: 2021 Groep: 02 Datum: 13-3-2021

Coordinaten		Hoogte	Diepte
Xco	Yco	Z [m]	[cm]
260790	586100	-2.39	640

KAARTEENHEID	Geomorfogenetische kaart:
Geologische kaart:	Grondwatertrap:
Begroeiingskaart:	Bodemkaart:

Coordinate 10m accuracy ipv 1m, andere GPS-app

Diepte	Textuur	Org	Plr	Kleur	Redox	Grind	M50	Ca	Fe	GW	M	LKL	Strat	Bijzonderheden
10	MK		plr	brgr				0						
20	MK		plr	brgr				0						
30	LK			brgr				0						
40	MK			brgr				0	1					
50	LK		plr	brgr				0	1					
60	LK			gr				1	1					
70	MK	H0		dbrgr				0						
80	MK	H1	r	dbrgr				0						rietveen
90		V1	r	br				0						
100	ZK	H2	r	br				0		GW				
110		V1	r	dbr				0						#
120		V1	r	dbr				0						
130		V1	r	dbr				0						
140		V1	r	dbr				0						
150		V1	r	dbr				0						
160		V1	r	dbr				0						
170		V1	r	dbr				0						
180		V1	h	dbr				0			M003			#
190		V1	hr	br				0						#, klei 1.85-1.95 (o1)
200	ZK		plr	gr				0						zeer abrupt
210		V1	hr	br				0						stuk hout
220		V2	r	br				0						
230		V2	r	br				0						kleiband 2cm
240		V2	r	br				0						
250		V2	r	br				0						
260		V2	r	dbr				0						#
270		V2	r	lbr				0						#
280		V1	hr	br				0						
290		V2	hr	br				0						
300		V1	r	br				0						
310		V1	r	br				0						
320		V1	r	br				0						
330		V1	r	br				0						
340		V1	r	br				0						#
350	ZK		r	gr				0						# klei-> veen (o1)
360		V1	plr	br				0						
370		V1	r	br				0						
380		V1	r	br				0						
390		V1	hr	br				0						
400		V1	r	br				0						
410		V1	hr	dbr				0						
420		V1	hr	dbr				0						#
430		V1	r	br				0						#
440		V1	r	br				0						
450	ZK	H2	r	brgr				0						graduele overang
460	ZK	H1	r	brgr				0						
470	ZK	H1	r	brgr				0			M004			
480	ZK	H0	r	gr				0						
490	ZK		r	gr				0						
500	ZK		r	gr				0						
510	MK	H0	r	brgr				0						#
520	MK	H0	r	brgr				0						
530	ZK	H0	r	brgr				0						
540	ZK	H1	r	brgr				0						
550	ZK	H1	r	brgr				0						
560	ZK	H2	r	brgr				0						
570		V1	hr	br				0						
580		V1	r	br				0						#
590		V1	r	br				0						#
600		V1	hr	br				0						

Boring: 202102002

Diepte	Textuur	Org	Plr	Kleur	Redox	Grind	M50	Ca	Fe	GW	M	LKL	Strat	Bijzonderheden
610	ZK	H2	hr	br				0						
620		V1	r	br				0						
630		ZV		dbrgr				0				+		zwarte horizont, 5 cm
640		VZ		gr				0						

Einde boring: 202102002

Boorpunt: 202102003 Namen: 003 Jaar: 2021 Groep: 02 Datum: 14-3-2021

Coordinaten		Hoogte	Diepte
Xco	Yco	Z [m]	[cm]
260710	586309	-2.35	680

KAARTEENHEID	Geomorfogenetische kaart:
Geologische kaart:	Grondwatertrap:
Begroeiingskaart:	Bodemkaart:

Bredere bodemhorizonten bovenop Boxtel Fm

Diepte	Textuur	Org	Plr	Kleur	Redox	Grind	M50	Ca	Fe	GW	M	LKL	Strat	Bijzonderheden
10	MK			brgr	o			0						Geroerd
20	MK			brgr	o			0						Geroerd
30	MK			brgr	o			0						Geroerd
40	MK			brgr	o			0	1					
50	MK			gr	o			0	1					
60	MK			gr	o			0	1					
70	MK			gr	o			0	1					schelpfragmenten
80	MK			gr	o			0	1					schelpfragmenten
90	MK			gr	o			0	1					
100	MK			dbrgr	o			0						
110	MK	H0		brgr	o			0						
120	ZK	H2	r	brgr	or			0		GW				Graduele overgang
130		V2	r	br	or			0						
140	ZK	H1	r	brgr	or			0						O2
150	ZK		r	blgr				0						O2
160		V2	r	br				0						Rietveen
170		V1	r	br				0						
180		V1	r	br				0						
190		V1	rh	br				0						Graduele verlanding
200		V1	r	br				0						
210		V1	r	br				0						
220		V2	r	lbr				0						1 cm kleiband
230		V1	r	br				0						Graduele overgang (O4)
240	ZK	H0	r	gr				0						
250	ZK	H0	r	gr				0						
260	ZK	H0	r	gr				0						(O4) 10 cm
270		V1	r	dbr				0						
280		V2	r	dbr				0						
290		V2	r	dbr				0						
300		V2	r	br				0						Rietknoop
310	ZK	H2	r	dgr				0						
320	ZK	H2	r	dgr				0						
330	ZK	H2	r	dgr				0						(O3): 5 cm
340	ZK			gr				0						
350	ZK			gr				0						
360	ZK			gr				0						
370	ZK			gr				0						
380	ZK			gr				0						(O2)
390		V1	r	br				0						
400		V2	r	br				0						
410		V2	r	br				0						
420		V2	r	br				0						
430		V1	r	br				0						
440	ZK	H1	r	gr				0						(O2)
450	ZK	H0	r	gr				0						
460	MK		r	gr				0						
470	MK		r	gr				0						
480	MK		r	gr				0						
490	MK	H0	r	gr				0						
500	MK		r	gr				0						
510	MK			gr				0						
520	MK			gr				0						
530	MK			gr				0						
540	MK		r	gr				0						
550	MK		r	gr				0						
560	MK		r	gr				0						
570	MK		r	gr				0						
580	MK		r	gr				0						
590	MK		r	gr				0						
600	MK			gr				0						

Boring: 202102003

Diepte	Textuur	Org	Plr	Kleur	Redox	Grind	M50	Ca	Fe	GW	M	LKL	Strat	Bijzonderheden
610	MK			gr				0						
620	MK	H0	r	gr				0						(O4)
630	ZK	H2	r	dbrgr				0						
640		V1	r	br				0						
650		V2	hr	br				0						Veen bevat meer hout: landiger
660		ZV	hr	dbr				0				-		
670		VZ		zw				0				+		Br-zw-dbr-zand (O3) horizonten
680	FZ			gr			150-210	0						

Einde boring: 202102003

Boorpunt: 202102004 Namen: 004 Jaar: 2021 Groep: 02 Datum: 14-3-2021

Coordinaten		Hoogte	Diepte
Xco	Yco	Z [m]	[cm]
260614	586536	-2.37	640

KAARTEENHEID	Geomorfogenetische kaart:
Geologische kaart:	Grondwatertrap:
Begroeiingskaart:	Bodemkaart:

Boorlocatie op het (verwachte) laagste punt van het perceel

Diepte	Textuur	Org	Plr	Kleur	Redox	Grind	M50	Ca	Fe	GW	M	LKL	Strat	Bijzonderheden
10	MK			brgr	o			0						Ger wortels
20	MK			brgr	o			0						Ger wortels
30	MK			brgr	o			0						Ger wortels
40	LK			gr	o			0	1					Roestvlekken, schelpfragmenten
50	LK			gr	o			0	1					Roestvlekken
60	LK			brgr	o			0	1					
70	MK	H0		dbrgr	o			0						Veraard veen in aanwezig
80	ZK			gr	or			0	2					Roestvlekken (O2)
90		V1	r	br				0						Veel riet
100		V1	r	br				0						Veel riet
110		V1	r	br				0		GW				veel riet
120		V2	r	br				0						
130		V2	r	br				0						
140		V2	hr	br				0						hout, vezelig
150		V2	r	br				0						
160	ZK			blgr				0						12 cm kleilaag, 1.55-1.65 (O1)
170		V2	r	br				0						
180		V2	r	br				0						
190		V2	r	br				0						
200		V2	r	br				0						
210		V2	r	br				0						
220		V1	r	br				0						Zwarte band
230		V1	r	br				0						1 cm kleiband
240	ZK	H0	r	brgr				0						(O4) graduele overgang
250	ZK	H0	r	brgr				0						
260	ZK	H0	r	brgr				0						
270	ZK	H1	r	gr				0						
280	ZK	H0	r	gr				0						
290		V1	r	br				0						
300		V1	r	br				0						
310		V1	r	br				0						
320	ZK	H2	r	br				0						
330	ZK	H2	r	br				0						
340	ZK	H1		gr				0						
350	ZK			gr				0						
360	ZK		r	gr				0						
370	ZK	H1		dbrgr				0						Rietfragmenten
380	ZK	H1		dbrgr				0						
390		V1	h	dbrgr				0						(O4) graduele overgang
400		V1	r	dbr				0						
410		V1	hr	dbr				0						
420		V1	r	dbr				0						
430		V1	r	dbr				0						
440		V1	r	br				0						
450		V1	r	br				0						(O4) Graduele overgang
460	ZK	H1	r	brgr				0						
470	MK	H1	r	brgr				0						
480	MK	H0	r	brgr				0						
490	MK		r	gr				0						
500	MK	H0	r	brgr				0						
510	MK	H1		brgr				0						
520	ZK	H0	r	brgr				0						
530	MK		r	gr				0						
540	MK		r	gr				0						
550	MK		r	gr				0						
560	ZK	H0	r	brgr				0						
570	ZK	H1	r	brgr				0						
580	ZK	H2	r	dbr				0						
590		V1	r	dbr				0						
600		V1	r	dbr				0						

Boring: 202102004

Diepte	Textuur	Org	Plr	Kleur	Redox	Grind	M50	Ca	Fe	GW	M	LKL	Strat	Bijzonderheden
610		V1	r	dbr				0						
620		ZV	r	dbrgr				0						
630		VZ		zw				0				+		Zwart horizont
640	FZ			gr			150-210	0						

Einde boring: 202102004

Boorpunt: 202102005 Namen: 005 Jaar: 2021 Groep: 02 Datum: 14-3-2021

Coordinaten		Hoogte	Diepte
Xco	Yco	Z [m]	[cm]
260539	586729	-2.6	640

KAARTEENHEID	Geomorfogenetische kaart:
Geologische kaart:	Grondwatertrap:
Begroeiingskaart:	Bodemkaart:

Laag punt op perceel, op basis van AHN
Slootdiepte = 50cm
Slootbodem tot maaiveld = 150cm

Diepte	Textuur	Org	Plr	Kleur	Redox	Grind	M50	Ca	Fe	GW	M	LKL	Strat	Bijzonderheden
10	MK			brgr	o			0						Ger, wortels
20	MK			brgr	o			0						Ger, wortels
30	MK			brgr	o			0						Ger, wortels
40	MK			brgr	o			0						Ger
50	MK			gr	or			0	1					
60	LK			gr	or			0	1					
70	LK			dgr	or			0						
80	MK	H0		dgr	or			0						
90		V1	r	br	or			0		GW				
100		V1	r	br				0						Sponzig
110		V2		br				0						
120		V3	h	br				0						Vezelig veen
130		V3	h	br				0						Hout (sample 5.1): bosveen
140		V2	hr	br				0						
150		V1	r	br				0						
160	ZK	H2	r	br				0						(O4)
170	ZK	H1	r	brgr				0						
180	ZK	H1	r	brgr				0						
190	MK			gr				0						
200	ZK	H1	r	brgr				0						
210	ZK	H1	r	brgr				0						
220	ZK	H1	r	brgr				0						
230		V1	r	grbr				0						
240	ZK	H2	r	brgr				0						(O4)
250		V1	r	br				0						
260		V1	r	br				0						
270		V1	r	br				0						
280		V1	r	br				0						
290		V1	r	br				0						
300	ZK	H2	r	br				0						
310	ZK	H1	r	br				0						Zaadjes
320	MK			gr				0						(O3)
330	MK	H2		brgr				0						
340	ZK	H2	r	zwbr				0				-		laklaag
350		V1	r	br				0						
360		V1	r	br				0						
370	ZK	H2	r	br				0						
380	ZK	H2	r	grbr				0						
390	ZK	H1	hr	brgr				0						
400	ZK	H0	hr	gr				0						
410	MK	H0	r	gr				0						
420	MK	H0	r	gr				0						
430	MK			gr				0						
440	MK		r	gr				0						
450	MK		hr	gr				0						
460	MK		hr	gr				0						elzenhout, foto
470	MK			gr				0						
480	MK		h	gr				0						
490	MK			gr				0						
500	MK			gr				0						
510	MK	H0	r	gr				0						
520	MK	H1	r	brgr				0						
530	MK	H0	r	brgr				0						
540	MK	H0	r	brgr				0						
550	MK	H1	r	brgr				0						
560	MK	H1	r	brgr				0						
570	MK		r	gr				0						
580	MK		r	gr				0						
590	MK	H0	r	gr				0						
600	MK	H0	r	gr				0						

Boring: 202102005

Diepte	Textuur	Org	Plr	Kleur	Redox	Grind	M50	Ca	Fe	GW	M	LKL	Strat	Bijzonderheden
610	MK	H1	r	dgr				0						
620		ZV		zw				0				+		
630		VZ		gr				0						Overgang gr-zw-zand 10cm
640	FZ			br			150-210	0						Bruin zand onderaan

Einde boring: 202102005

Boorpunt: 202102006 Namen: 006 Jaar: 2021 Groep: 02 Datum: 14-3-2021

Coordinaten		Hoogte	Diepte
Xco	Yco	Z [m]	[cm]
260260	586720	-2.35	560

KAARTEENHEID	Geomorfogenetische kaart:
Geologische kaart:	Grondwatertrap:
Begroeiingskaart:	Bodemkaart:

Noordkant perceel, in het pad gezette boring.
10m accuracy ipv 1m, andere GPS-app

Diepte	Textuur	Org	Plr	Kleur	Redox	Grind	M50	Ca	Fe	GW	M	LKL	Strat	Bijzonderheden
10	MK			brgr				0						Ger
20	MK			brgr				0						Ger
30	MK			brgr				0						Ger
40	MK			brgr				0	1					Ger
50	MK			brgr				0	1					
60	MK			gr				0	1					
70	LK			dgr				0		GW				veraard veen bijgemengd
80		V1	r	br				0						
90		V1	r	dbr				0						3 cm kleilaag (O1)
100		V1	r	br				0						
110		V2	r	br				0						
120		V2	r	br				0						Vezelig
130		V2	r	br				0						
140		V3	r	br				0						
150		V2	r	br				0						
160		V2	r	br				0						
170		V2	r	br				0						3 cm kleilaag (O1)
180	ZK	H2	r	brgr				0						
190	ZK	H2	r	brgr				0						
200		V3	h					0						Houtstuk
210		V3	h					0						Houtstuk
220		V3	h					0			M			Houtstuk, sample 6.1
230	ZK	H0	r	brgr				0						5 cm hout
240	ZK	H0	r	brgr				0						
250	ZK	H2	r	brgr				0						
260		V1	r	dbr				0						(O3)
270		V2	r	br				0						
280		V2	r	br				0						
290		V1	r	br				0						
300	ZK	H2	r	dbrgr				0				-		
310		V1	r	br				0						1 cm kleilaag
320		V1		br				0						
330	ZK	H2		gr				0						
340	ZK	H2	r	br				0						
350		V1	r	br				0						
360		V1	r	zwbr				0						
370		V1	r	grbr				0						
380		V1	r	grbr				0						
390	MK	H0	r	gr				0						(O3)
400	MK		r	gr				0						
410	MK		r	gr				0						
420	MK		r	gr				0						
430	MK		r	gr				0						
440	MK		r	gr				0						
450	MK			gr				0						
460	MK		r	gr				0						
470	MK		r	gr				0						
480	MK		r	gr				0						
490	MK		r	gr				0						
500	MK	H1	r	brgr				0						
510	MK	H1	r	brgr				0						
520	MK	H2	r	grbr				0						
530		V2	r	br				0						
540		VZ		zw				0				+		
550	FZ			gr			150-210	0						10 cm zwarte horizont=al lemig
560	FZ			gr			150-210	0						bodemhorizonten grad. overgang

Einde boring: 202102006

Boorpunt: 202102007 Namen: 007 Jaar: 2021 Groep: 02 Datum: 15-3-2021

Coordinaten		Hoogte	Diepte
Xco	Yco	Z [m]	[cm]
260229	586519	-2.58	540

KAARTEENHEID	Geomorfogenetische kaart:
Geologische kaart:	Grondwatertrap:
Begroeiingskaart:	Bodemkaart:

Eerste boring aan de noorkant van het westelijk traject (W.01)

Diepte	Textuur	Org	Plr	Kleur	Redox	Grind	M50	Ca	Fe	GW	M	LKL	Strat	Bijzonderheden
10	MK			brgr				0						wortels, ger
20	MK			brgr				0						wortels, ger
30	MK			brgr				0	1					ger
40	MK			brgr				0	1					ger
50	MK			brgr				0	1					
60	MK			brgr				0	1					
70	MK			brgr				0	1					
80	MK			brgr				0						
90		V1	r	br				0		GW				
100		V1	r	br				0						
110	MK	H2	r	brgr				0						#
120		V1	r	br				0						o1
130	MK		r	gr				0						o2
140		V2	r	br				0						vezelig
150		V2	r	br				0						
160		V2	r	dbr				0						
170		V2	r	br				0						
180		V1	r	dbr				0						#
190		V2	r	dbr				0						#
200		V2	r	br				0						1cm kleiband
210		V1	r	grbr				0						
220	ZK	H2	r	brgr				0						graduele overgang klei -> veen
230	ZK	H1	r	brgr				0						
240	ZK	H1	r	gr				0						
250	ZK	H0	r	gr				0						#
260	ZK	H0	r	gr				0						#
270	ZK	H2	r	brgr				0						graduele overgang veen -> klei
280		V2	r	br				0						
290		V2	r	br				0						
300		V1	r	br				0						
310		V1	r	br				0						#
320	ZK	H1	r	gr				0						#
330	ZK	H0		gr				0						
340	ZK	H0		gr				0						
350	ZK	H2		brgr				0						
360	ZK	H1	h	brgr				0						
370	ZK	H2		dbr				0						graduele overgang klei -> veen
380		V1	r	dbr				0						rietknopen
390		V1	r	dbr				0						#
400		V1	h	dbr				0						#, bosveen?
410		V1	r	dbr				0						
420		V1	r	dbr				0						
430	ZK	H2	r	brgr				0						graduele overgang veen-> klei
440	ZK	H2	hr	brgr				0						
450	ZK	H1	r	brgr				0						
460	ZK	H0	hr	gr				0						#
470	ZK	H2	r	brgr				0						#
480		V1	r	brgr				0						zwarte gloed, 2cm breed
490		V1	r	brgr				0						
500		V1	r	brgr				0						
510		V2	r	grbr				0						kleiband 1cm
520		V1		dbr				0						compact veen
530		ZV		zw				0				+		
540		VZ		gr				0						#

Einde boring: 202102007

Boorpunt: 202102008 Namen: 008 Jaar: 2021 Groep: 02 Datum: 15-3-2021

Coordinaten		Hoogte	Diepte
Xco	Yco	Z [m]	[cm]
260327	586316	-2.25	590

KAARTEENHEID	Geomorfogenetische kaart:
Geologische kaart:	Grondwatertrap:
Begroeiingskaart:	Bodemkaart:

boring 2 op transect west (n->z), steek op 3m zonder sediment, wel verwacht! Mogelijk nogmaals boren wanneer selectie voor extensometer

Diepte	Textuur	Org	Plr	Kleur	Redox	Grind	M50	Ca	Fe	GW	M	LKL	Strat	Bijzonderheden
10	MK			brgr										ger
20	MK			brgr										ger
30	MK			brgr										ger
40	MK			brgr					1					
50	MK			brgr					1					
60	MK			gr					1					
70	MK	H0		brgr										zwart
80	MK	H0		gr						GW				
90		V1	r	br										#
100		V1	r	br										graduele overgang klei-> veen
110		V1	r	dbr										
120		V1	r	zwbr										
130		V2	r	lbr										
140		V2	r	br										
150		V1	r	dbr										o1
160	ZK			blgr										
170	ZK			blgr										#
180		V2	r	br										#
190		V2	r	br										
200		V2	r	br										
210		V2	r	grbr										graduele overgang
220	ZK	H1	r	brgr										
230	ZK		r	gr										
240	MK		r	gr										#
250	MK		r	gr										#,mogelijk verkeerde gutssteek
260	MK		r	gr										40 cm kwijt, GM
270	MK		r	gr										
280	MK		r	gr										#
290		V2	r	br										#
300		V2	h	br										bosveen
310		V1	h	br										
320	ZK	H2		br										
330	ZK	H2		br										
340		V1	h	br										
350	ZK	H2		br										
360		V1	h	dbr										#
370		V1		dbr										#
380		V1	hr	dbr										
390		V1	hr	br										
400		V1	h	br										
410		V1	hr	br										
420		V1	r	grbr										
430	ZK	H2	r	grbr								-		zwarte gloed
440	MK	H1	hr	grbr										#
450		V1	r	br										#
460	MK	H1	r	brgr										
470	ZK	H1	r	brgr										
480	ZK	H2	r	brgr										
490	ZK	H2	r	brgr										
500	ZK	H1	r	brgr										
510	MK	H1	r	brgr										
520	ZK	H2	r	brgr										#
530	ZK	H2	r	brgr										#
540	ZK	H2	r	brgr										
550		V1	r	grbr										compact
560		V2	r	br										
570		ZV		zw								+		
580		VZ		dbrgr								-		
590	FZ			gr			150-210							#

Einde boring: 202102008

Boorpunt: 202102009 Namen: 009 Jaar: 2021 Groep: 02 Datum: 15-3-2021

Coordinaten		Hoogte	Diepte
Xco	Yco	Z [m]	[cm]
260403	586150	-2.57	530

KAARTEENHEID	Geomorfogenetische kaart:
Geologische kaart:	Grondwatertrap:
Begroeiingskaart:	Bodemkaart:

3e boring op westelijk traject.

3.35: bovenkant kleiband, 5cm (01): duidelijke gelaagdheid, zwarte + bruine banden (zie foto). Abrupte verandering afz milieu

Diepte	Textuur	Org	Plr	Kleur	Redox	Grind	M50	Ca	Fe	GW	M	LKL	Strat	Bijzonderheden
10	MK			brgr										wortels, ger
20	MK			brgr										ger
30	MK			brgr										ger
40	MK			brgr					1					ger,
50	MK			brgr					1					
60	MK			brgr					1					
70	MK			brgr					1					
80	MK	H1	r	brgr						GW				veraard veen?
90	ZK	H1	r	gr										#
100	ZK	H2	r	grbr										graduele overgang
110		V1	r	br										
120		V2	r	br										
130		V2	r	br										
140		V1	r	br										
150		V2	r	br										
160		V2	r	lbr										#
170		V1	r	br										#, 2cm kleiband
180		V1	hr	dbr										
190	ZK	H2	r	brgr										grad overgang
200	ZK	H1	r	brgr										
210	ZK	H1	r	brgr										
220	ZK	H0	r	gr										
230	ZK		r	gr										#
240	ZK	H0	r	gr										#
250	ZK	H0	r	brgr										o3
260		V1	r	br										
270		V2	r	br										
280		V2	r	dbr										
290		V2	r	dbr										
300		V2	r	dbr										
310		V1	r	dbr										# 3cm kleiband
320		V2	r	dbr										#
330		V1	r	dbr										
340		V1	r	dbr										3.35 kleiband, zie opm
350		V1	hr	dbr										
360		V1	hr	dbr										
370		V1	r	dbr										
380		V1	r	dbr										
390		V1	r	dbr										#
400		V1	r	dbr										#
410		V1	r	dbr										
420		V1	r	br										
430		V2	r	br										
440		V2	r	grbr										
450		V2	r	grbr										
460		V1	hr	grbr										
470		V1	hr	grbr										#
480	MK	H2	r	brgr										#
490	ZK	H2	hr	brgr										
500	ZK	H2	r	br										
510		VZ		zw								+		bodemhorizonten
520	FZ			gr			150-210							
530	FZ			brgr			150-210							#

Einde boring: 202102009

Boorpunt: 202102010 Namen: 010 Jaar: 2021 Groep: 02 Datum: 15-3-2021

Coordinaten		Hoogte	Diepte
Xco	Yco	Z [m]	[cm]
260157	586679	-2.16	590

KAARTEENHEID	Geomorfogenetische kaart:
Geologische kaart:	Grondwatertrap:
Begroeiingskaart:	Bodemkaart:

bereikbaar vanaf de weg!

Diepte	Textuur	Org	Plr	Kleur	Redox	Grind	M50	Ca	Fe	GW	M	LKL	Strat	Bijzonderheden
10	MK			brgr				0						wortels, ger
20	MK			brgr				0						ger
30	MK			brgr				0						ger
40	MK			brgr				0	1					ger
50	MK			brgr				0	1					
60	MK			brgr				0	1					wit kiezels
70	MK			brgr				0	1					wit kiezels
80	MK			brgr				0						
90	MK			brgr				0						
100		V1	r	grbr				0						
110		V1	r	dbr				0						
120		V1	r	dbr				0		GW				
130		V2	r	br				0						#
140		V1	r	br				0						
150		V1	r	br				0						kleiband 5mm
160		V2	r	br				0						
170		V2	r	br				0						
180	ZK	H2	r	grbr				0						
190	ZK	H2	r	brgr				0						
200	MK	H1	r	brgr				0						#
210	ZK	H2	r	grbr				0						#
220		V1	r	grbr				0						
230		V1	r	grbr				0						
240		V2	hr	br				0						
250		V2	hr	br				0						
260		V2	hr	br				0						
270		V2	hr	br				0						
280		V1	hr	br				0						#
290	ZK			gr				0						#
300	MK	H2	h	dgrbr				0						
310	MK	H2	hr	dgrbr				0						
320		V1	r	dgrbr				0						graduele overgang
330		V1	r	br				0						
340		V1	r	zw				0						
350	ZK	H2	r	brgr				0						graduele overgang
360	ZK	H2	r	brgr				0						#
370	ZK	H0	hr	gr				0						#
380	MK		r					0						
390	LK		r					0						
400	LK		r					0						
410	LK		r					0						
420	LK		plr					0						
430	LK		plr	blgr				0						#
440	MK		h	blgr				0						#
450	LK		r	blgr				0						
460	LK		r	blgr				0						
470	LK		r	blgr				0						
480	LK		r	blgr				0						
490	LK		r	blgr				0						
500	LK		r	blgr				0						
510	LK		r	blgr				0						#
520	LK		r	gr				0						#
530	LK		r	gr				0						
540	LK	H0	r	gr				0						graduele overgang
550	MK	H1	r	brgr				0						
560		V1	r	br				0						
570		ZV	r	zwbr				0				+		zandig veen
580		VZ		zw				0				+		
590	FZ		r	gr			150-210	0						#

Einde boring: 202102010

Boorpunt: 202102011 Namen: 011 Jaar: 2021 Groep: 02 Datum: 16-3-2021

Coordinaten		Hoogte	Diepte
Xco	Yco	Z [m]	[cm]
260506	585934	-2.38	580

KAARTEENHEID	Geomorfogenetische kaart:
Geologische kaart:	Grondwatertrap:
Begroeiingskaart:	Bodemkaart:

zuidelijke boring transect west.
verwachting boxtel dieper 6m , verwachting 1.5m kleidek

Diepte	Textuur	Org	Plr	Kleur	Redox	Grind	M50	Ca	Fe	GW	M	LKL	Strat	Bijzonderheden
10	MK			brgr				0						ger
20	MK			brgr				0						ger
30	MK			brgr	o			0						ger
40	LK			gr	o			0	1					
50	LK			gr	or			0	1					
60	MK			gr	or			0	2					
70	LK			gr	or			0	2					
80	MK			gr	or			0	1					
90	LK			brgr	or			0						veraard veen bijgemengd
100	LK		r	brgr	or			0		GW				
110	LK		r	gr				0						01
120	ZK	H0	hr	gr				0						
130	ZK	H0	hr	brgr				0						graduele overgang klei-> veen
140		V1	hr	grbr				0						
150		V1	r	br				0						
160		V2	r	br				0						
170		V2	hr	br				0						
180		V1	r	br				0						#
190		V2	r	br				0						#
200		V1	r	br				0						
210		V1	r	br				0						
220		V2	r	br				0						
230		V2	hr	br				0						
240		V1	r	br				0						
250		V2	hr	br				0						
260	ZK		r	gr				0						#, o1 beide kanten, 6cm klei
270		V2	r	grbr				0						#
280		V2	r	grbr				0						
290		V3	r	br				0						
300		V3	r	br				0						
310		V2	hr	br				0						
320		V1	hr	dbr				0						
330		V1	hr	dbr				0						
340		V1	r	dbr				0						#
350		V1	r	br				0						#
360		V1	hr	br				0						
370		V1	r	br				0						
380	ZK		r	gr				0						o1, beide kanten, niet humeus
390		V1	r	br				0						
400		V1	r	dbr				0						
410		V1	hr	dbr				0						
420		V1	r	dbr				0						#
430		V1	r	br				0						#
440		V1	hr	dbr				0						
450		V1	hr	dbr				0						
460		V1	hr	dbr				0						
470		V1	hr	br				0						
480		V2	r	grbr				0						
490		V2	r	grbr				0						
500		V1	r	brgr				0						#
510	ZK	H2	hr	grbr				0						#
520		V1	r	dbr				0						
530		V1	r	dbr				0						
540		V2	r	br				0						
550		V2	r	grbr				0						
560		ZV	hr	dgrbr				0						
570		VZ	h	zw				0				+		elzenhout
580	FZ			gr			150-210	0						#

Einde boring: 202102011

Boorpunt: 202102012 Namen: 012 Jaar: 2021 Groep: 02 Datum: 16-3-2021

Coordinaten		Hoogte	Diepte
Xco	Yco	Z [m]	[cm]
260843	585850	-2.1	660

KAARTEENHEID	Geomorfogenetische kaart:
Geologische kaart:	Grondwatertrap:
Begroeiingskaart:	Bodemkaart:

In het Luzerneveld, hoek, 5m vanaf sloten, samen met Esther

Diepte	Textuur	Org	Plr	Kleur	Redox	Grind	M50	Ca	Fe	GW	M	LKL	Strat	Bijzonderheden
10	MK			brgr				0						
20	MK			brgr				0						
30	MK			brgr				0						
40	MK			gr				0	1					
50	LK			gr				0	1					
60	LK			gr				0	1					
70	MK			brgr				0	2					
80	ZK			zw				0	2			+		veraard veen
90	ZK			brgr				0	1					
100	ZK	H1	plr	brgr				0						zwarte vlekken
110	ZK	H1	r	brgr				0		GW				o3
120		V2	r	br				0						
130		V2	r	br				0						
140		V2	r	br				0						
150		V2	hr	br				0						elzenhout
160		V2	r	br				0						
170		V2	r	br				0						
180		V2	r	br				0						
190		V2	hr	br				0						#
200		V2	r	br				0						#
210		V2	r	br				0						
220		V2	hr	br				0						
230		V2	hr	br				0						
240		V2	hzr	br				0						
250		V2	hzr	br				0						
260		V2	hzr	br				0						
270		V2	hr	br				0						#
280		V2	r	br				0						#
290		V2	hr	br				0						
300		V2	rz	br				0						
310		V2	hr	br				0						
320		V2	hr	br				0						
330		V2	r	br				0						
340		V2	zr	br				0						
350		V2	r	br				0						#
360		V2	r	br				0						#
370		V2	r	br				0						
380		V2	r	br				0						
390		V2	r	br				0						
400		V2	rz	br				0						
410		V2	r	br				0						#
420		V2	r	br				0						#, o3
430	MK	H0	rh	blgr				0						foto van hout!
440	MK	H0	r	blgr				0						
450	MK	H0	r	blgr				0						
460	MK	H0	r	blgr				0						
470	MK	H0	r	blgr				0						#
480	LK			blgr				0						#
490	LK		r	blgr				0						
500	LK		r	blgr				0						
510	LK		r	blgr				0						
520	LK		r	gr				0						
530	LK		r	gr				0						
540	LK		r	gr				0						
550	LK		r	gr				0						#
560	LK		r	blgr				0						#, compactere klei
570	MK		r	blgr				0						
580	MK	H0	r	blgr				0						o3 klei->veen
590		V2	hr	br				0						
600		V2	rz	br				0						nauwelijks H2S

Boring: 202102012

Diepte	Textuur	Org	Plr	Kleur	Redox	Grind	M50	Ca	Fe	GW	M	LKL	Strat	Bijzonderheden
610		V2	rh	br				0						
620		V2		br				0						amorf veen
630		ZV	plr	zw				0				+		#
640		ZV		zw				0				+		#
650	FZ			gr			150-210	0						
660	FZ			gr			150-210	0						#

Einde boring: 202102012

Boorpunt: 202102013 Namen: 013 Jaar: 2021 Groep: 02 Datum: 16-3-2021

Coordinaten		Hoogte	Diepte
Xco	Yco	Z [m]	[cm]
260850	585953	-2.43	170

KAARTEENHEID	Geomorfogenetische kaart:
Geologische kaart:	Grondwatertrap:
Begroeiingskaart:	Bodemkaart:

25m ten noorden van boring 001

Op 1.4m diepte: laminatie in klei (o1). Bovenste helft = organisch materiaal met mm kleilaagjes, onderste helft = klei met mm laagjes organisch

Diepte	Textuur	Org	Plr	Kleur	Redox	Grind	M50	Ca	Fe	GW	M	LKL	Strat	Bijzonderheden
10	MK			brgr				0						ger
20	MK			brgr				0						ger
30	MK			brgr				0						ger
40	MK			gr				0	1					ger
50	MK			gr				0	1					
60	MK	H1		dgr				0						
70	ZK	H1		gr				0	1					
80	ZK	H1	h	gr				0		GW				geel-witte vlekken,bruist niet
90	ZK	H1	r	brgr				0						
100		V1	r	grbr				0						#, o2 klei -> veen
110		V1	r	br				0						H2S-geur
120		V2	hr	br				0						
130		V2	r	br				0						
140	ZK	H2	r	gr				0						zie bovenstaand
150		V3	r	br				0						
160		V3	rz	br				0						
170		V2	r	dbr				0						#

Einde boring: 202102013

Boorpunt: 202102014 Namen: 014 Jaar: 2021 Groep: 02 Datum: 16-3-2021

Coordinaten		Hoogte	Diepte
Xco	Yco	Z [m]	[cm]
260782	586120	-2.49	260

KAARTEENHEID	Geomorfogenetische kaart:
Geologische kaart:	Grondwatertrap:
Begroeiingskaart:	Bodemkaart:

25m ten noorden van boring 002.
Potentiele veen extensometer locatie.

Diepte	Textuur	Org	Plr	Kleur	Redox	Grind	M50	Ca	Fe	GW	M	LKL	Strat	Bijzonderheden
10	MK			brgr	o			0						ger
20	MK			brgr	o			0						ger
30	MK			brgr	o			0						ger
40	MK			gr	or			0	1					ger
50	MK			gr	or			0	1					ger, wortels
60	MK			gr	or			0	1					wortels
70	ZK			grbr				0	1					MnO
80		V1		br				0						veraard
90		V2	rh	br				0						
100		V2	rh	br				0		GW				
110		V2	r	dbr				0						#, weinig H2S
120		V2	rh	dbr				0						elzenhout, broekveen
130		V3	rh	br				0						
140		V3	r	br				0						
150		V3	rz	br				0						
160		V3	rh	br				0						H2S, verticaal riet
170		V3	rz	br				0						
180		V3	r	br				0						#
190		V3	rhz	br				0						# rood elzenhout?
200		V2	r	dbr				0						1.90-1.94, kleilaag, o1
210		V3	rz	br				0						h2s
220		V3	rz	dbr				0						
230		V3	rzh	br				0						
240		V3	rz	dbr				0						
250		V3	rz	dbr				0						
260		V3	rz	dbr				0						#

Einde boring: 202102014

Boorpunt: 202102015 Namen: 015 Jaar: 2021 Groep: 02 Datum: 16-3-2021

Coordinaten		Hoogte	Diepte
Xco	Yco	Z [m]	[cm]
260930	585779	-1.93	190

KAARTEENHEID	Geomorfogenetische kaart:
Geologische kaart:	Grondwatertrap:
Begroeiingskaart:	Bodemkaart:

Oostzijde luzerneveld, klei locatie extensometer ?

Diepte	Textuur	Org	Plr	Kleur	Redox	Grind	M50	Ca	Fe	GW	M	LKL	Strat	Bijzonderheden
10	MK													ger
20	MK													ger
30	MK				or				1					ger
40	MK			brgr	or				1					ger
50	MK			brgr	or				1					ger
60	MK			gr	or				2					ger
70	MK			gr	or				2					
80	MK			gr	or				2					
90	ZK			gr	or				2					MnO
100	ZK			gr	or				1					MnO
110	ZK			gr	or				1	GW				geel-witte vlekken
120		V2	r	dgrbr										#, o3
130		V2	r	br										
140		V2	r	br										
150		V2	r	br										
160		V2	r	br										
170		V3	rh	br										H2S
180		V3	rh	br										
190	ZK	H0		brgr										#

Einde boring: 202102015

Boorpunt: 202102016 Namen: 016 Jaar: 2021 Groep: 02 Datum: 16-3-2021

Coordinaten		Hoogte	Diepte
Xco	Yco	Z [m]	[cm]
260904	585609	-1.91	250

KAARTEENHEID	Geomorfogenetische kaart:
Geologische kaart:	Grondwatertrap:
Begroeiingskaart:	Bodemkaart:

Luzernveld, zuidelijk, potentiële kleilocatie

Diepte	Textuur	Org	Plr	Kleur	Redox	Grind	M50	Ca	Fe	GW	M	LKL	Strat	Bijzonderheden
10	MK			brgr				0						ger
20	MK			brgr				0						ger, witte vlekken
30	MK			brgr				0						ger
40	MK			gr	or			0	1					ger
50	MK			gr	or			0	1					ger, schelpfr
60	MK			gr	or			0	1					
70	MK			gr	or			0	2					wortels
80	MK			gr	or			0	2					
90	MK			gr	or			0	2					
100	ZK	H2		dgrzw	or			0	1					MnO
110	MK	H2		gr	r			0		GW				
120	ZK	H0	r	gr	r			0						#
130	ZK	H0	rh	gr	r			0						
140	ZK	H0	r	gr				0						
150	ZK	H0	rh	gr				0						
160	ZK	H0	r	gr				0						#
170	ZK	H0	r	gr				0						#
180	ZK	H1	r	brgr				0						o4, graduele overgang
190	ZK	H1	r	brgr				0						
200		V3	r	br				0						
210		V2	r	dbr				0						
220		V3	r	br				0						
230		V3	r	br				0						
240		V2	rh	br				0						
250		V2	rh	br				0						#, H2S

Einde boring: 202102016

Boorpunt: 202102017 Namen: 017 Jaar: 2021 Groep: 02 Datum: 18-3-2021

Coordinaten		Hoogte	Diepte
Xco	Yco	Z [m]	[cm]
260846	585490	-1.52	640

KAARTEENHEID	Geomorfogenetische kaart:
Geologische kaart:	Grondwatertrap:
Begroeiingskaart:	Bodemkaart:

ijzerrijke grond (rodoorn? knipklei?), boxtel tussen 6m en 7m verwacht. zuidwestelijke hoek luzernveld
Potentiële kleilocatie
2.55-2.65: graduele overgang klei -> veen

Diepte	Textuur	Org	Plr	Kleur	Redox	Grind	M50	Ca	Fe	GW	M	LKL	Strat	Bijzonderheden
10	MK			brgr				0						ger,wor
20	MK			brgr				0						ger, wor
30	MK			brgr				0						ger, wor
40	LK			gr	or			0	1					
50	MK			blgr	or			0	2					wor
60	MK			gr	or			0	2					wor
70	MK			gr	or			0	2					witgele vlekken, bruist niet
80	MK	H0		zwgr	or			0	2					veraard org material
90	MK			gr	or			0	2					wor, MnO
100	MK		r	gr	or			0	1					wor
110	MK		plr	gr	or			0	2					gele strepen
120	MK		r	gr	or			0	2					gele strepen, zie foto
130	MK	H0	plr	brgr	or			0	2					
140	MK		r	gr	or			0	2					MnO
150	MK		r	blgr	or			0	1					
160	MK		r	blgr				0		GW				
170	ZK		r	gr				0						#
180	ZK		r	gr				0						
190	ZK	H0	r	gr				0						
200	ZK	H0	r	gr				0						
210	ZK	H1	r	gr				0						
220	ZK	H1	r	gr				0						
230	ZK	H1	r	gr				0						
240	ZK	H1	rz	gr				0						#
250	ZK	H1	r	gr				0						#
260	ZK	H2	rh	gr				0						o4 klei-> veen
270		V2	r	grbr				0						takjes
280		V2	rh	br				0						elzenhout, broekveen
290		V3	r	br				0						H2S
300		V3	r	br				0						
310		V3	r	br				0						
320		V3	r	br				0						#
330		V3	r	br				0						#
340		V1	r	br				0						
350		V2	rh	br				0						
360		V2	r	br				0						
370		V3	r	lgrbr				0						
380		V3	r	br				0						
390		V3	rhz	dbr				0						rietveen
400		V3	rhz	dbr				0						#, elzenhout
410		V3	r	dbr				0						#
420		V2	hr	br				0						
430		V2	hrz	br				0						
440		V2	rh	br				0						takjes
450		V3	rh	br				0						1cm kleiband (MK)
460		V2	rh	br				0						
470		V3	r	br				0						#
480		V2	rh	br				0						#, graduele overgang
490	ZK	H2	rh	brgr				0						3cm hout, elzenhout
500		V1	rh	brgr				0						
510	ZK	H2	rh	blgr				0						
520	ZK	H1	rh	gr				0						
530	ZK	H1	rh	gr				0						takjes
540	ZK	H1	r	gr				0						
550	ZK	H2	rh	grbr				0						
560		V1	rh	grbr				0						#
570	ZK	H1	rh	gr				0						#, boomstronk, foto, hard hout
580	ZK	H2	rh	gr				0						
590		V1	rh	grbr				0						
600		V1	rh	grbr				0			M01			zaadjes, sample

Boring: 202102017

Diepte	Textuur	Org	Plr	Kleur	Redox	Grind	M50	Ca	Fe	GW	M	LKL	Strat	Bijzonderheden
610		V2	rh	br				0						zaadjes
620		V3	r	dbr				0						
630		ZV	r	zw				0				+		
640		VZ		gr				0						#

Einde boring: 202102017

Boorpunt: 202102018 Namen: 018 Jaar: 2021 Groep: 02 Datum: 18-3-2021

Coordinaten		Hoogte	Diepte
Xco	Yco	Z [m]	[cm]
260759	586124	-2.5	670

KAARTEENHEID	Geomorfogenetische kaart:
Geologische kaart:	Grondwatertrap:
Begroeiingskaart:	Bodemkaart:

20m veld in t.o.v. boring 014 (westelijke richting)
Potentiële veen locatie
Drie verkennende boringen rondom om optimale veendek te localiseren (20,21,22)

Diepte	Textuur	Org	Plr	Kleur	Redox	Grind	M50	Ca	Fe	GW	M	LKL	Strat	Bijzonderheden
10	MK			brgr										ger, wor
20	MK			brgr										ger, wor
30	MK			brgr										ger, wor
40	MK	H1		zwgr										veraard veen
50		V2		zw										veraard veen
60		V2	r	brzw										veraard veen
70		V2	r	br										
80		V3	r	br						GW				
90		V3	r	br										
100		V3	r	br										#
110		V3	r	br										
120		V3	rh	br										elzenhout, bosveen, landiger
130		V3	r	br										
140		V3	r	br										
150		V3	r	br										#
160		V3	r	br										#
170		V3	r	br										
180		V3	r	br										
190		V3	rh	dbr										elzenhout
200		V3	rh	br										elzenhout
210		V3	r	br										
220		V3	rh	br										
230		V3	rh	br										#
240		V3	r	dbr										#
250		V2	rh	br										1cm kleiband, elzenhout
260		V2	rh	dbr										
270		V2	rh	dbr										
280	ZK	H2	r	blgr										V1?
290	ZK			lgr										
300		V3	hr	dbr										bosveen
310		V3	r	dbr										#, bosveen
320		V3	r	dbr										#
330		V3	hr	dbr										
340		V3	r	dbr										
350		V3	hr	dbr										
360		V3	r	dbr										
370		V3	r	br										
380		V2	r	grbr										
390	ZK	H1	r	gr				0						#
400	MK		r	gr				0						#
410	ZK		r	gr				0						
420	ZK	H0	r	gr				0						
430	ZK	H0	r	gr				0						
440	ZK		r	gr				0						gele vlekken
450	ZK		r	gr				0						verkoold hout?
460	ZK		r	gr				0						#
470	ZK		hr	gr				0						#, heel hard zwart hout
480	MK		hr	gr				0						
490	MK		r	gr				0						
500	LK		r	gr				0						
510	LK		plr	gr				0						zandiger, minder glad
520	LK			dgr				0						brokkelig
530	LK			dgr				0						"
540	LK			dgr				0						#
550	LK		plr	dgr				0						#
560	ZZL			dgr				0						brokkelig
570	ZZL		plr	dgr				0						
580	ZZL			dgr				0						
590	ZZL		plr	dgr				0						
600	LK		r	dgr				0						

Boring: 202102018

Diepte	Textuur	Org	Plr	Kleur	Redox	Grind	M50	Ca	Fe	GW	M	LKL	Strat	Bijzonderheden
610	LK		r	dgr				0						
620	LK		r	dgr				0						#
630	LK	H0	r	gr				0						#
640	LK	H0	r	gr				0						
650	ZZL		rh	gr										
660		ZV		gr										
670	FZ			gr			150-210							#

Einde boring: 202102018

Boorpunt: 202102019 Namen: 019 Jaar: 2021 Groep: 02 Datum: 18-3-2021

Coordinaten		Hoogte	Diepte
Xco	Yco	Z [m]	[cm]
260496	586892	-1.65	830

KAARTEENHEID	Geomorfogenetische kaart:
Geologische kaart:	Grondwatertrap:
Begroeiingskaart:	Bodemkaart:

Midden op de kreekrug
Samen met Hans Middelkoop
Locatie drainagebuis aangeboord.....

Diepte	Textuur	Org	Plr	Kleur	Redox	Grind	M50	Ca	Fe	GW	M	LKL	Strat	Bijzonderheden
10	MK			brgr				0	0					ger, wor
20	MK			brgr				0	0					ger, wor
30	MK			brgr				0	1					ger, wor
40	MK			brgr				0	1					
50	MK			brgr				0	1					gele vlekken, bruist nietr
60	MK			brgr				0	2					gele vlekken
70	MK	H1		brgr				0	2					
80	MK	H1	r	dgr				0	1					
90	MK	H2	r	dgr				0		GW				
100		V1	r	dgrbr				0						
110		V2	r	dgrbr				0						weinig H2S, onverwacht
120		V1	r	dgrbr				0						
130		V1						0						#,GM, overboort
140		V1						0						GM, overboort
150		V1						0						GM, overboort
160	MK	H1	r	gr				0						
170	MK	H1	r	gr				0						vlekkerig
180	MK	H1	r	gr				0						
190	MK		r	gr				0						
200	MK	H0	r	gr				0						
210	MK	H0	r	gr				0						
220	MK	H0	r	brgr				0						
230	MK	H0	r	brgr				0						#
240	ZK			gr				0						#
250	ZK			gr				0						
260	ZK			gr				0						
270	ZK			gr				0						
280	ZK			gr				0						
290	ZK		r	gr				0						#
300	ZK	H0		brgr				0						#
310	ZK			brgr				0						
320	ZK	H0		brgr				0						
330	ZK	H0		gr				0						
340	ZK			gr				0						
350	ZK			gr				0						
360	ZK			gr				0						
370	ZK			gr				0						#
380	ZK			gr				0						#
390	ZK	H0		gr				0						
400	ZK			gr				0						
410	ZK		r	gr				0						3cm, zwartgrijze band
420	ZK		r	gr				0						
430	ZK	H0		gr				0						#
440	ZK	H1		gr				0						
450	ZK			gr				0						
460	ZK			gr				0						
470	ZK			gr				0						witte puntjes
480	ZK			gr				0						
490	ZK	H0	r	gr				0						
500	ZK	H0		brgr				0						
510	ZK			gr				0						#
520	ZK			gr				0						#
530	ZK			gr				0						
540		V1	r	brgr				0						graduele overgang
550		V1	r	grbr				0						
560		V1	r	grbr				0						
570		V1	r	grbr				0						
580	ZK			gr				0						#
590	ZK			gr				0						#
600	MK			gr				0						

Boring: 202102019

Diepte	Textuur	Org	Plr	Kleur	Redox	Grind	M50	Ca	Fe	GW	M	LKL	Strat	Bijzonderheden
610	MK			gr				0						
620	MK			gr				0						
630	MK			gr				0						
640	MK			gr				0						
650	MK			gr				0						
660	MK			gr				0						#
670	MK			gr				0						#
680	MK			gr				0						
690	MK			gr				0						
700	MK		plr	gr				0						
710	MK		plr	gr				0						
720	MK			gr				0						
730	MK			gr				0						
740	MK			gr				0						
750	MK			gr				0						#
760	MK			gr				0						#
770	MK			gr				0						
780	MK			gr				0						
790	MK			gr				0						
800	MK			gr				0						
810	MK			gr				0						
820	MK			gr				0						
830	FZ			gr			150-210	0						#, o1, wrsl erosief, geen BV

Einde boring: 202102019

Boorpunt: 202103001 Namen: A01 Jaar: 2021 Groep: 03 Datum: 17-3-2021

Coordinaten		Hoogte	Diepte
Xco	Yco	Z [m]	[cm]
253069	591403	0	460

KAARTEENHEID	Geomorfogenetische kaart:
Geologische kaart:	Grondwatertrap:
Begroeiingskaart:	Bodemkaart:

Appingedam, B07F0664 (1970), perceel boer Weeke
4.36-4.50: Zandig veen
4.50-4.55: Venig zand

Diepte	Textuur	Org	Plr	Kleur	Redox	Grind	M50	Ca	Fe	GW	M	LKL	Strat	Bijzonderheden
10	MK			brgr	o			0						wor, ger
20	MK			brgr	o			0						wor, ger
30	MK			brgr	o			0						wor, ger
40	MK			brgr	o			0						wor, ger, dakpan
50	LK			brgr	o			0						ger
60	LK			brgr	o			0						ger
70	LK			brgr	or			0	2					veraard veen
80	MK			brgr	or			0	2					
90	MK	H0		brgr	or			0	1					veraard veen
100	MK	H2		brgr	or			0	1	GW				veraard veen
110		V2	r	br				0						#, zwarte gloed, H2S
120		V2	rz	br				0						
130		V2	rz	br				0						
140		V2	r	br				0						
150		V2	rh	br				0						elzenhout, bosveen
160		V2	rh	br				0						
170		V2	rh	br				0						#
180		V2	rh	br				0						# landiger veen
190		V2	rh	br				0						
200		V3	r	br				0						H2S
210		V3	r	br				0						
220		V2	r	grbr				0						graduele overgang
230	MK	H2	r	brgr				0						
240		V1	r	brgr				0						#
250		V1	r	grbr				0						#
260		V1	r	grbr				0						
270		V2	r	grbr				0						
280	ZK	H2	r	brgr				0						
290		V1	r	brgr				0						
300		V1	r	grbr				0						#
310		V2	rh	grbr				0						#, 3.18-3.21 kleiband
320		V1	r	grbr				0						H2S
330	MK	H2	r	brgr				0						
340	MK	H2	r	brgr				0						
350	MK	H2	r	brgr				0						
360		V1	r	grbr				0						graduele overgang
370		V2	r	br				0						
380		V1	r	grbr				0						#
390		V1	r	brgr				0						#
400		V2	r	grbr				0						
410		V1	r	brgr				0						
420		V2	rh	grbr				0						elzenhout
430		V3	r	br				0						H2S
440		ZV	r	br				0						
450		VZ	rh	dgrbr				0				-		bodem slecht ontwikkeld
460	FZ			gr			150-210	0						#, einde boring 4.57

Einde boring: 202103001

Boorpunt: 202103002 Namen: A02 Jaar: 2021 Groep: 03 Datum: 17-3-2021

Coordinaten		Hoogte	Diepte
Xco	Yco	Z [m]	[cm]
253016	591284	0	430

KAARTEENHEID	Geomorfogenetische kaart:
Geologische kaart:	Grondwatertrap:
Begroeiingskaart:	Bodemkaart:

Appingedam, Perceel boer Hofman, ijzerrijke bovengrond, 1970 (B07F0663)
1.90-1.95: H1
1.95-2.00: H2

Diepte	Textuur	Org	Plr	Kleur	Redox	Grind	M50	Ca	Fe	GW	M	LKL	Strat	Bijzonderheden
10	MK		plr	brgr										ger
20	MK		plr	brgr										ger
30	MK		plr	brgr	or				1					
40	LK			gr	or				2					
50	MK			gr	or				2					
60	MK			brgr	or				2					veraard veen 3cm
70	MK			gr	or				2					
80	LK			gr	or				1					
90	MK			gr	or				2					
100	MK			gr	or				1					
110	LK			gr	or				1	GW				
120	LK		r	gr	or				1					#
130	LK			gr	or				1					
140	LK			gr	or				1					
150	LK		r	blgr	r									
160	LK		r	blgr										
170	LK		r	blgr										
180	MK		r	blgr										#
190	ZK	H1	r	gr										#
200	ZK	H2	r	brgr										
210		V3	hr	br										
220		V3	hr	br										compact veen
230		V3	r	br										
240		V3	r	br										
250		V3	r	br										#
260		V3	hr	br										#, 5mm kleiband
270		V3	hr	br										landiger veen
280		V3	hr	br										
290		V3	hr	zw										
300		V3	r	lbr										rietveen
310		V3	r	lbr										
320		V2	r	lbr										#
330		V1	r	brgr										#
340		V2	r	grbr										H2S
350		V2	r	br										
360		V2	r	br										
370		V2	hr	br										
380		V2	r	br										
390		ZV	hr	brgr										#
400		ZV	hr	br										#
410		ZV		brgr										
420		VZ		brgr										
430	FZ			gr			150-210							

Einde boring: 202103002

Boorpunt: 202103003 Namen: A03 Jaar: 2021 Groep: 03 Datum: 17-3-2021

Coordinaten		Hoogte	Diepte
Xco	Yco	Z [m]	[cm]
253207	590848	0	250

KAARTEENHEID	Geomorfogenetische kaart:
Geologische kaart:	Grondwatertrap:
Begroeiingskaart:	Bodemkaart:

Perceel boer Weeke, midden Appingedam veldwerkgebied, westkant vroegere meer. 1970 (B07F0559)
2.30-2.35: veen (v2,R)
2.35-2.38: zandig veen

Diepte	Textuur	Org	Plr	Kleur	Redox	Grind	M50	Ca	Fe	GW	M	LKL	Strat	Bijzonderheden
10	MK			brgr										ger
20	MK			brgr										ger
30	MK			brgr										ger
40	MK			brgr					1					ger
50	LK			brgr					1					
60	MK			gr					2					
70		V2	r	dbr										veraard kleiig veen
80		V3	r	dbr										veraard veen
90		V3	r	dbr						GW				veraard veen
100		V3	r	dbr										veraard veen
110		V3	plr	lbr										#
120		V3	r	lbr										felrode takjes
130		V3	rh	lbr										1.26-1.30 kleiband
140		V3	rh	br										
150		V3	r	br										
160		V3	r	br										
170		V3	r	br										#
180		V3	r	br										#
190		V3	r	br										
200		V2	r	br										
210		V2	r	br										2.00-2.01 kleiband
220		V2	r	br										
230		V2	r	dbr										
240		ZV		dbr										
250		VZ		gr										#

Einde boring: 202103003

Boorpunt: 202103004 Namen: A04 Jaar: 2021 Groep: 03 Datum: 17-3-2021

Coordinaten		Hoogte	Diepte
Xco	Yco	Z [m]	[cm]
253276	590309	0	250

KAARTEENHEID	Geomorfogenetische kaart:
Geologische kaart:	Grondwatertrap:
Begroeiingskaart:	Bodemkaart:

Perceel boer Weeke, langs de weg, zuidkant, 1970(B07F0556)
2.20-2.28: zandig veen
2.28-2.55: venig zand

Diepte	Textuur	Org	Plr	Kleur	Redox	Grind	M50	Ca	Fe	GW	M	LKL	Strat	Bijzonderheden
10	MK			brgr										ger
20	MK			brgr										ger
30	MK			brgr										ger
40	MK			brgr										ger
50		V2	r	dbr										veraard veen
60		V2	r	dbr										veraard veen
70		V2	r	dbr						GW				veraard veen
80		V3	r	dbr										veraard veen
90		V3	hr	br										#
100		V3	r	br										2cm kleiband
110		V3	hr	br										takjes, elzenhout
120		V3	r	br										
130		V3	r	br										
140		V3	r	br										
150		V3	r	dbr										
160		V3	r	dbr										
170		V3	r	br										#, H2S
180		V3	r	br										#
190		V3	hr	br										1.88-1.92 kleiband
200		V3	hr	br										veel hout vrij plots
210		V3	hr	br										
220		ZV		zwbr										
230		ZV		dbr										
240		VZ		brgr										#
250		VZ		brgr										#

Einde boring: 202103004

Boorpunt: 202103005 Namen: A05 Jaar: 2021 Groep: 03 Datum: 17-3-2021

Coordinaten		Hoogte	Diepte
Xco	Yco	Z [m]	[cm]
254121	590796	0	410

KAARTEENHEID	Geomorfogenetische kaart:
Geologische kaart:	Grondwatertrap:
Begroeiingskaart:	Bodemkaart:

Perceel boer Breedijk, 1970 (B07F0563)
3.75:3.90: zandig veen
3.90:4.00: venig zand

Diepte	Textuur	Org	Plr	Kleur	Redox	Grind	M50	Ca	Fe	GW	M	LKL	Strat	Bijzonderheden
10	MK			brgr										ger
20	MK			brgr										ger
30	MK			brgr										ger
40	MK			brgr										ger
50	MK			gr					2					
60	MK			brgr					2					
70	MK			brgr					1					
80		V1		dbr										veraard veen
90		V1	r	dbr						GW				veraard veen
100		V1	r	brgr										#
110	ZK		r	gr										o2
120		V2	r	brgr										
130		V3	r	grbr										
140		V3	r	zwbr								-		
150		V3	r	br										
160		V3	r	br										
170		V3	rh	br										#
180		V3	rh	br										#, 1.76-1.78 kleiband
190		V2	plr	br										1.82-1.83 kleiband
200		V3	rh	br										
210		V3	rh	br										broekveen
220		V2	rh	br										
230		V2	r	br										
240		V3	r	br										
250		V2	r	br										#
260	ZK	H2	r	brgr										#
270		V2	rh	br										
280		V3	rh	br										
290		V2	rh	br										
300		V2	h	br										
310		V3	r	br										
320		V3	r	br										
330		V3	r	br										#
340		V3	r	br										#
350		V1	r	br										
360		V2	r	br										3cm kleiband (ZK)
370		V3	rh	br										
380		V3		br										
390		ZV		br										
400		ZV		brgr										
410	FZ			gr			150-210							

Einde boring: 202103005

Boorpunt: 202103006 Namen: A06 Jaar: 2021 Groep: 03 Datum: 17-3-2021

Coordinaten		Hoogte	Diepte
Xco	Yco	Z [m]	[cm]
254076	590490	0	310

KAARTEENHEID	Geomorfogenetische kaart:
Geologische kaart:	Grondwatertrap:
Begroeiingskaart:	Bodemkaart:

Perceel boer Breedijk, 1970 (B07F0562)
2.70-2.75: V3
2.75-3.00: zandig veen

Diepte	Textuur	Org	Plr	Kleur	Redox	Grind	M50	Ca	Fe	GW	M	LKL	Strat	Bijzonderheden
10	MK			brgr										
20	MK			brgr										
30	MK		plr	brgr										
40	MK			brgr	or				1					
50	MK			brgr	or				1					
60	MK			grbr					2					
70		V2	r	br										
80		V2	r	br						GW				
90		V3	h	br										#
100		V3	r	br										H2S
110		V3	hr	br										
120		V3	hr	br										
130		V3	hr	br										
140		V3	hr	br										
150	ZK			br										1.40-1.45 kleiband (o1)
160		V3	hr	br										#
170		V3	hr	br										#
180		V3	hr	br										
190		V3	hr	br										
200		V3	r	br										
210		V3	r	br										
220		V3	r	br										
230		V3	rz	br										
240		V2	r	br										#
250		V3	hr	br										#
260		V3	r	br										
270		V3	r	br										
280		V3	r	dbr										
290		ZV	r	dbr										#
300		ZV		dbr										#
310		VZ		gr										tot 3.05

Einde boring: 202103006

Boorpunt: 202103007 Namen: A07 Jaar: 2021 Groep: 03 Datum: 17-3-2021

Coordinaten		Hoogte	Diepte
Xco	Yco	Z [m]	[cm]
253740	591440	0	440

KAARTEENHEID	Geomorfogenetische kaart:
Geologische kaart:	Grondwatertrap:
Begroeiingskaart:	Bodemkaart:

Perceel boer Weeke, noordkant, 1970 (B07F0662)
4.20-4.32: V3
4.32-4.36: zandig veen

Diepte	Textuur	Org	Plr	Kleur	Redox	Grind	M50	Ca	Fe	GW	M	LKL	Strat	Bijzonderheden
10	MK			brgr										ger
20	MK			brgr										ger
30	MK			brgr										ger
40	MK			brgr										ger
50	MK			brgr	or				1					ger
60	MK	H0		brgr	or				1					
70	MK	H0		gr	or				2					
80	LK		plr	gr	or				1	GW				
90	MK	H1	r	brgr										#
100		V2	r	br										
110		V2	r	br										
120		V3	rz	br										takjes
130		V3	rzh	br										landiger veen
140		V3	rh	br										#
150		V3	h	br										#
160		V3	h	br										vezelig, bosveen
170		V3	hr	br										H2S
180		V3	hr	br										elzenhout
190		V3	h	lbr										
200		V3	h	br										1.95 1cm kleiband 01
210		V3	h	br										
220		V3	hr	br										#
230		V3	r	br										#
240		V3	r	grbr										
250		V2	r	grbr										
260		V2	r	grbr										
270		V2	r	grbr										
280		V2	r	grbr										GM
290		V2	r	grbr										GM
300		V2	r	grbr										#. GM
310		V1	r	br										#
320		V1	r	br										
330	MK	H2	r	brgr										
340	MK	H1	r	gr										
350	MK	H1	r	gr										
360	MK	H2	r	gr										
370	MK	H2	r	gr										#
380		V1	r	grbr										#
390		V1	r	grbr										
400		V3	r	grbr										
410		V3	r	br										
420		V3	rh	br										
430		V3	rh	br										
440		ZV												4.36 FZ

Einde boring: 202103007

ALGEMENE GEGEVENS BORING
NITG-nummer: B07F0664
X-coordinaat (m): 253070
Y-coordinaat (m): 591407
Coordinatensysteem: RD2000
Plaatsnaam: Onbekend
Provincie: Groningen
Kaartblad: 07F
Bepaling locatie: Onbekend
Maaiveldhoogte (meter t.o.v. NAP): -1.49
Bepaling maaiveldhoogte: Onbekend
Boormethode: Onbekend
Einddiepte (meter beneden maaiveld): 4.50
Datum boring: 08-09-1970
Eigenaar: Onbekend
Uitvoerder: Vrije Universiteit Amsterdam

ALGEMENE GEGEVENS LITHOLOGIE
Beschrijver lagen: Onbekend
Organisatie beschrijver: Vrije Universiteit Amsterdam
Beschrijvingsmethode: Onbekend
Nat/Droog beschreven: Onbekend
Datum laagbeschrijving: Onbekend
Kwaliteitcode beschrijving lithologie: E

LITHOLOGIE LAGEN
Bovenkant laag (m beneden maaiveld) Onderkant laag (m beneden maaiveld) Kleur Hoofdgrondsoort Sublaag Zand mediaan M63 Zandmediaanklasse Bijmenging klei Lutum % Bijmenging silt Silt% Bijmenging zand Zand % Bijmenging grind Grind % Bijmenging humus Organische stof % Kalkgehalte

0.00	0.40	onbekend	klei	---	---	---	---	20	---	---	---	---	---	---	---	---	---
0.40	0.45	onbekend	klei	---	---	---	---	30	sterk siltig	---	---	---	---	---	---	---	---
0.45	0.60	onbekend	klei	---	---	---	---	---	---	---	---	---	---	---	---	matig humeus	---	---
0.60	1.28	onbekend	klei	---	---	---	---	40	matig siltig	---	---	---	---	---	---	---	kalkrijk
1.28	2.70	onbekend	veen	---	---	---	---	---	---	---	---	---	---	---	---	---	---
2.70	4.12	onbekend	veen	---	---	---	kleiig	---	---	---	---	---	---	---	---	---	---
4.12	4.32	onbekend	veen	---	---	---	---	---	---	---	---	---	---	---	---	---	---
4.32	4.50	onbekend	zand	---	---	---	---	---	---	---	---	---	---	---	---	---	---

ALGEMENE GEGEVENS BORING
NITG-nummer: B07F0663
X-coordinaat (m): 253016
Y-coordinaat (m): 591284
Coordinatensysteem: RD2000
Plaatsnaam: Onbekend
Provincie: Groningen
Kaartblad: 07F
Bepaling locatie: Onbekend
Maaiveldhoogte (meter t.o.v. NAP): -1.24
Bepaling maaiveldhoogte: Onbekend
Boormethode: Onbekend
Einddiepte (meter beneden maaiveld): 4.50
Datum boring: 08-09-1970
Eigenaar: Onbekend
Uitvoerder: Vrije Universiteit Amsterdam

ALGEMENE GEGEVENS LITHOLOGIE
Beschrijver lagen: Onbekend
Organisatie beschrijver: Vrije Universiteit Amsterdam
Beschrijvingsmethode: Onbekend
Nat/Droog beschreven: Onbekend
Datum laagbeschrijving: Onbekend
Kwaliteitcode beschrijving lithologie: E

LITHOLOGIE LAGEN
Bovenkant laag (m beneden maaiveld) Onderkant laag (m beneden maaiveld) Kleur Hoofdgrondsoort Sublaag Zand mediaan M63 Zandmediaanklasse Bijmenging klei Lutum % Bijmenging silt Silt% Bijmenging zand Zand % Bijmenging grind Grind % Bijmenging humus Organische stof % Kalkgehalte

0.00	0.50	onbekend	klei	---	---	---	---	30	sterk siltig	---	---	---	---	---	---	---	---
0.50	0.55	onbekend	klei	---	---	---	---	35	matig siltig	---	---	---	---	---	---	---	---
0.55	0.83	onbekend	klei	---	---	---	---	35	matig siltig	---	---	---	---	---	matig humeus	---	---
0.83	2.05	grijs	klei	---	---	---	---	45	matig siltig	---	---	---	---	---	---	---	kalkrijk
2.05	4.18	onbekend	veen	---	---	---	kleiig	---	---	---	---	---	---	---	---	---	---
4.18	4.50	onbekend	zand	---	---	---	---	---	---	---	---	---	---	---	---	---	---

ALGEMENE GEGEVENS BORING
NITG-nummer: B07F0559
X-coordinaat (m): 253207
Y-coordinaat (m): 590848
Coordinatensysteem: RD2000
Plaatsnaam: Onbekend
Provincie: Groningen
Kaartblad: 07F
Bepaling locatie: Onbekend
Maaiveldhoogte (meter t.o.v. NAP): -1.74
Bepaling maaiveldhoogte: Onbekend
Boormethode: Onbekend
Einddiepte (meter beneden maaiveld): 3.00
Datum boring: 07-09-1970
Eigenaar: Onbekend
Uitvoerder: Vrije Universiteit Amsterdam

ALGEMENE GEGEVENS LITHOLOGIE
Beschrijver lagen: Onbekend
Organisatie beschrijver: Vrije Universiteit Amsterdam
Beschrijvingsmethode: Onbekend
Nat/Droog beschreven: Onbekend
Datum laagbeschrijving: Onbekend
Kwaliteitcode beschrijving lithologie: E

LITHOLOGIE LAGEN
Bovenkant laag (m beneden maaiveld) Onderkant laag (m beneden maaiveld) Kleur Hoofdgrondsoort Sublaag Zand mediaan M63 Zandmediaanklasse Bijmenging klei Lutum % Bijmenging silt Silt% Bijmenging zand Zand % Bijmenging grind Grind % Bijmenging humus Organische stof % Kalkgehalte

0.00	0.15	onbekend	klei	---	---	---	---	20	---	---	---	---	---	---	--- kalkarm
0.15	0.60	onbekend	klei	---	---	---	---	---	---	---	---	---	---	---	--- matig humeus --- ---
0.60	1.50	onbekend	veen	---	---	---	---	---	---	---	---	---	---	---	--- --- --- --- ---
1.50	2.68	onbekend	veen	---	---	---	---	---	---	---	---	zandig	---	---	--- --- --- --- ---
2.68	3.00	onbekend	zand	---	---	---	---	---	---	---	---	---	---	---	--- --- --- --- ---

ALGEMENE GEGEVENS BORING
NITG-nummer: B07F0556
X-coordinaat (m): 253276
Y-coordinaat (m): 590309
Coordinatensysteem: RD2000
Plaatsnaam: Onbekend
Provincie: Groningen
Kaartblad: 07F
Bepaling locatie: Onbekend
Maaiveldhoogte (meter t.o.v. NAP): -1.32
Bepaling maaiveldhoogte: Onbekend
Boormethode: Onbekend
Einddiepte (meter beneden maaiveld): 2.90
Datum boring: 07-09-1970
Eigenaar: Onbekend
Uitvoerder: Vrije Universiteit Amsterdam

ALGEMENE GEGEVENS LITHOLOGIE
Beschrijver lagen: Onbekend
Organisatie beschrijver: Vrije Universiteit Amsterdam
Beschrijvingsmethode: Onbekend
Nat/Droog beschreven: Onbekend
Datum laagbeschrijving: Onbekend
Kwaliteitcode beschrijving lithologie: E

LITHOLOGIE LAGEN
Bovenkant laag (m beneden maaiveld) Onderkant laag (m beneden maaiveld) Kleur Hoofdgrondsoort Sublaag Zand mediaan M63 Zandmediaanklasse Bijmenging klei Lutum % Bijmenging silt Silt% Bijmenging zand Zand % Bijmenging grind Grind % Bijmenging humus Organische stof % Kalkgehalte

0.00	0.25	onbekend	klei	---	---	---	---	25	sterk siltig	---	---	---	---	---	---	---	kalkarm
0.25	0.35	bruin-grijs	klei	---	---	---	kleiig	20	---	---	---	---	---	---	---	matig humeus	--- kalkarm
0.35	1.40	bruin	veen	---	---	---	---	---	---	---	---	---	---	---	---	---	kalkarm
1.40	1.44	grijs-blauw	klei	---	---	---	---	35	matig siltig	---	---	---	---	---	---	---	---
1.44	2.33	onbekend	veen	---	---	---	---	---	---	---	---	---	---	---	---	---	---
2.33	2.49	blauw-grijs	klei	---	---	---	---	25	sterk siltig	---	---	---	---	---	---	---	kalkarm
2.49	2.70	onbekend	veen	---	---	---	---	---	---	---	---	---	---	---	---	---	kalkarm
2.70	2.90	onbekend	zand	---	---	---	---	---	---	---	---	---	---	---	---	---	---

ALGEMENE GEGEVENS BORING
NITG-nummer: B07F0563
X-coordinaat (m): 254121
Y-coordinaat (m): 590796
Coordinatensysteem: RD2000
Plaatsnaam: Onbekend
Provincie: Groningen
Kaartblad: 07F
Bepaling locatie: Onbekend
Maaiveldhoogte (meter t.o.v. NAP): -1.40
Bepaling maaiveldhoogte: Onbekend
Boormethode: Onbekend
Einddiepte (meter beneden maaiveld): 4.30
Datum boring: 07-09-1970
Eigenaar: Onbekend
Uitvoerder: Vrije Universiteit Amsterdam

ALGEMENE GEGEVENS LITHOLOGIE
Beschrijver lagen: Onbekend
Organisatie beschrijver: Vrije Universiteit Amsterdam
Beschrijvingsmethode: Onbekend
Nat/Droog beschreven: Onbekend
Datum laagbeschrijving: Onbekend
Kwaliteitcode beschrijving lithologie: E

LITHOLOGIE LAGEN
Bovenkant laag (m beneden maaiveld) Onderkant laag (m beneden maaiveld) Kleur Hoofdgrondsoort Sublaag Zand mediaan M63 Zandmediaanklasse Bijmenging klei Lutum % Bijmenging silt Silt% Bijmenging zand Zand % Bijmenging grind Grind % Bijmenging humus Organische stof % Kalkgehalte

0.00	0.45	onbekend	klei	---	---	---	---	25	sterk siltig	---	---	---	---	---	---	---	kalkarm
0.45	0.70	onbekend	klei	---	---	---	---	30	sterk siltig	---	---	---	---	---	humeus	---	kalkarm
0.70	0.95	onbekend	veen	---	---	---	kleiig	---	---	---	---	---	---	---	---	---	kalkarm
0.95	4.10	onbekend	veen	---	---	---	kleiig	---	---	---	---	---	---	---	---	---	kalkarm
4.10	4.30	onbekend	zand	---	---	---	---	---	---	---	---	---	---	---	---	---	---

ALGEMENE GEGEVENS BORING
NITG-nummer: B07F0662
X-coordinaat (m): 253740
Y-coordinaat (m): 591440
Coordinatensysteem: RD2000
Plaatsnaam: Onbekend
Provincie: Groningen
Kaartblad: 07F
Bepaling locatie: Onbekend
Maaiveldhoogte (meter t.o.v. NAP): -1.20
Bepaling maaiveldhoogte: Onbekend
Boormethode: Onbekend
Einddiepte (meter beneden maaiveld): 4.60
Datum boring: 05-09-1970
Eigenaar: Onbekend
Uitvoerder: Vrije Universiteit Amsterdam

ALGEMENE GEGEVENS LITHOLOGIE
Beschrijver lagen: Onbekend
Organisatie beschrijver: Vrije Universiteit Amsterdam
Beschrijvingsmethode: Onbekend
Nat/Droog beschreven: Onbekend
Datum laagbeschrijving: Onbekend
Kwaliteitcode beschrijving lithologie: E

LITHOLOGIE LAGEN
Bovenkant laag (m beneden maaiveld) Onderkant laag (m beneden maaiveld) Kleur Hoofdgrondsoort Sublaag Zand mediaan M63 Zandmediaanklasse Bijmenging klei Lutum % Bijmenging silt Silt% Bijmenging zand Zand % Bijmenging grind Grind % Bijmenging humus Organische stof % Kalkgehalte

0.00	0.20	bruin	klei	---	---	---	---	35	matig siltig	---	---	---	---	---	---	---	kalkloos
0.20	0.99	onbekend	veen	---	---	---	kleiig	---	---	---	---	---	---	---	---	---	kalkloos
0.99	3.87	blauw-grijs	klei	---	---	---	kleiig	---	---	---	---	---	---	---	humeus	---	---
3.87	4.40	onbekend	veen	---	---	---	---	---	---	---	---	---	---	---	---	---	---
4.40	4.60	onbekend	zand	---	---	---	---	---	siltig	---	---	---	---	---	---	---	---

ALGEMENE GEGEVENS BORING
NITG-nummer: B07F0562
X-coordinaat (m): 254076
Y-coordinaat (m): 590490
Coordinatensysteem: RD2000
Plaatsnaam: Onbekend
Provincie: Groningen
Kaartblad: 07F
Bepaling locatie: Onbekend
Maaiveldhoogte (meter t.o.v. NAP): -1.30
Bepaling maaiveldhoogte: Onbekend
Boormethode: Onbekend
Einddiepte (meter beneden maaiveld): 3.00
Datum boring: 07-09-1970
Eigenaar: Onbekend
Uitvoerder: Vrije Universiteit Amsterdam

ALGEMENE GEGEVENS LITHOLOGIE
Beschrijver lagen: Onbekend
Organisatie beschrijver: Vrije Universiteit Amsterdam
Beschrijvingsmethode: Onbekend
Nat/Droog beschreven: Onbekend
Datum laagbeschrijving: Onbekend
Kwaliteitcode beschrijving lithologie: E

LITHOLOGIE LAGEN
Bovenkant laag (m beneden maaiveld) Onderkant laag (m beneden maaiveld) Kleur Hoofdgrondsoort Sublaag Zand mediaan M63 Zandmediaanklasse Bijmenging klei Lutum % Bijmenging silt Silt% Bijmenging zand Zand % Bijmenging grind Grind % Bijmenging humus Organische stof % Kalkgehalte

0.00	0.20	onbekend	klei	---	---	---	---	25	sterk siltig	---	---	---	---	---	---	---	kalkarm
0.20	0.55	zwart	klei	---	---	---	---	20	---	---	---	---	---	---	---	humeus	---	---
0.55	1.18	onbekend	veen	---	---	---	---	---	---	---	---	---	---	---	---	---	---	---
1.18	1.20	grijs-blauw	klei	---	---	---	---	35	matig siltig	---	---	---	---	---	---	---	kalkarm
1.20	2.80	onbekend	veen	---	---	---	---	---	---	---	---	---	---	---	---	---	---	---
2.80	3.00	onbekend	zand	---	---	---	---	---	---	---	---	---	---	---	---	---	---	---

Lithological profiles Nieuwolda water authority Hunze & Aa

Boring: 4061

GWS in cm -mv: 105
GHG in cm -mv: 70
GLG in cm -mv: 130

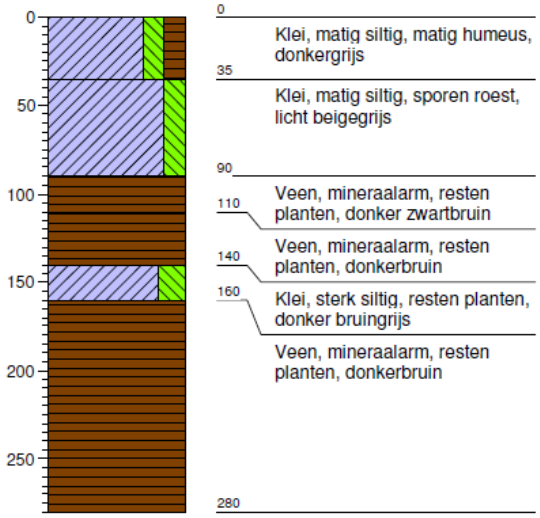

Boring: 3883

GWS in cm -mv: 50
GHG in cm -mv: 30
GLG in cm -mv: 95

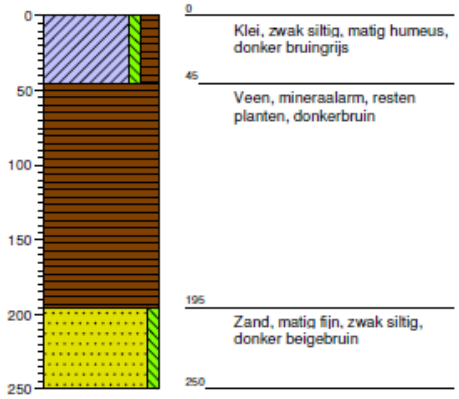

Boring: 3884

GWS in cm -mv: 60
GHG in cm -mv: 35
GLG in cm -mv: 95

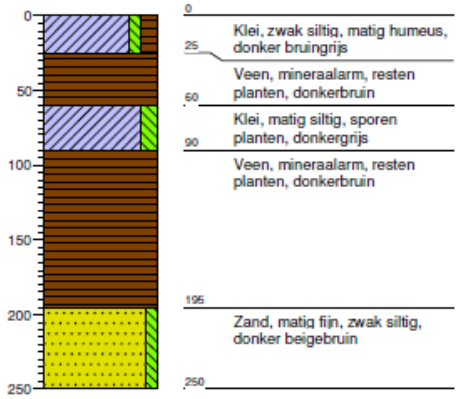

Boring: 3985

GWS in cm -mv: 110
GHG in cm -mv: 80
GLG in cm -mv: 140

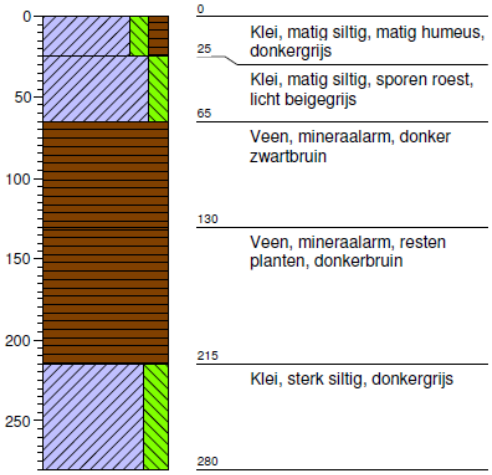

Boring: 3986

GWS in cm -mv: 90
GHG in cm -mv: 70
GLG in cm -mv: 120

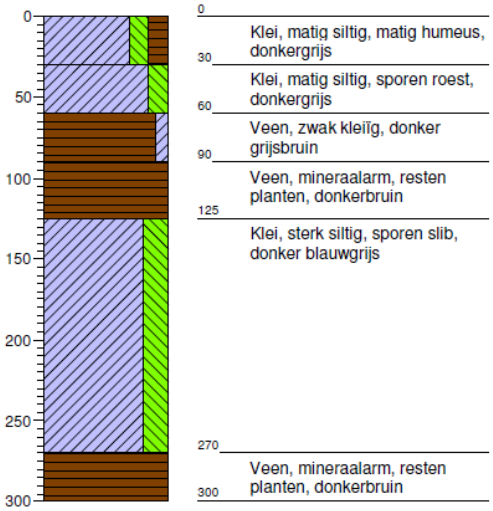

Boring: 3914

GWS in cm -mv: 120
GHG in cm -mv: 100
GLG in cm -mv: 180

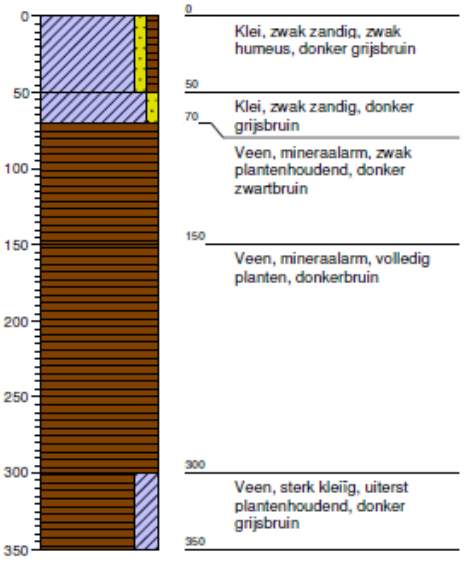

Boring: 3915

GWS in cm -mv: 110
GHG in cm -mv: 70
GLG in cm -mv: 145

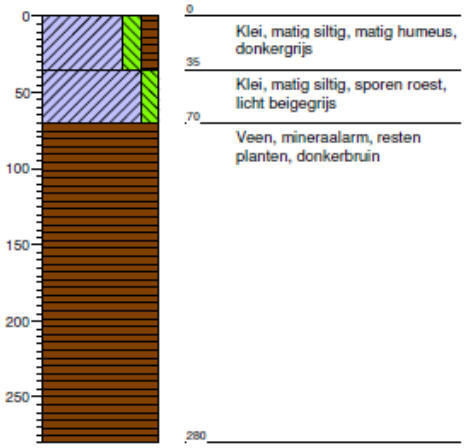

Boring: 3916

GWS in cm -mv: 95
GHG in cm -mv: 50
GLG in cm -mv: 130

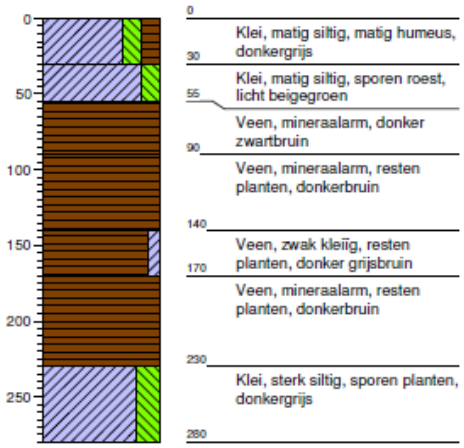

Boring: 3917

GWS in cm -mv: 90
GHG in cm -mv: 55
GLG in cm -mv: 130

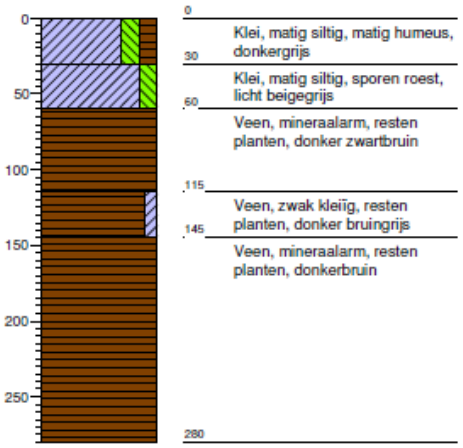

Boring: 3838

GWS in cm -mv: 80
GHG in cm -mv: 40
GLG in cm -mv: 110

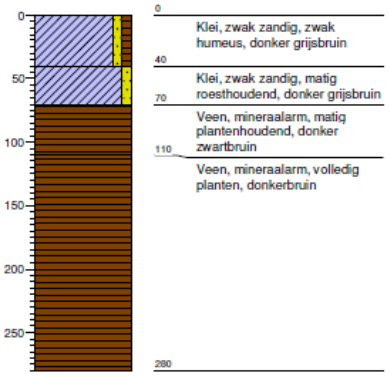

Boring: 3839

GWS in cm -mv: 100
GHG in cm -mv: 70
GLG in cm -mv: 130

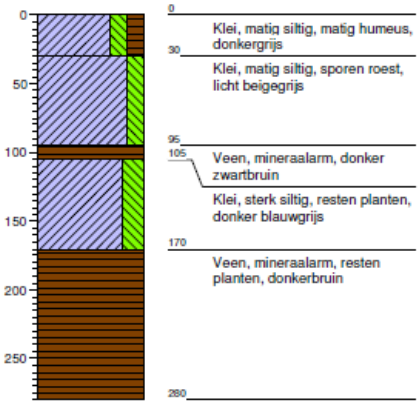

Boring: 3859

GWS in cm -mv: 70
GHG in cm -mv: 50
GLG in cm -mv: 150

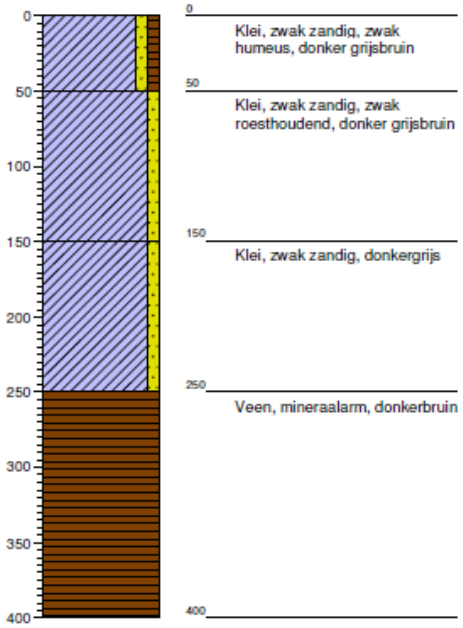

Boring: 3770

GWS in cm -mv: 80
GHG in cm -mv: 50
GLG in cm -mv: 100

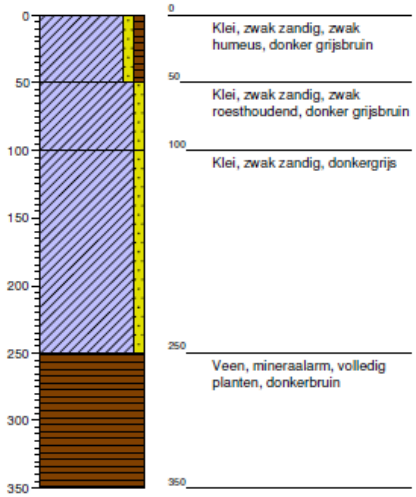

Boring: 3768

GWS in cm -mv: 100
GHG in cm -mv: 60
GLG in cm -mv: 120

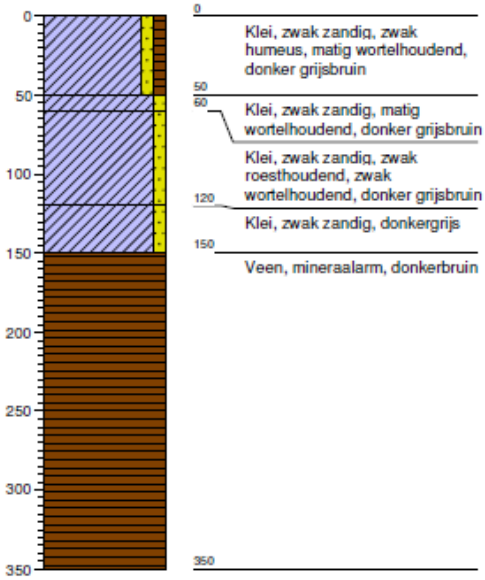

Boring: 3769

GWS in cm -mv: 120
GHG in cm -mv: 100
GLG in cm -mv: 150

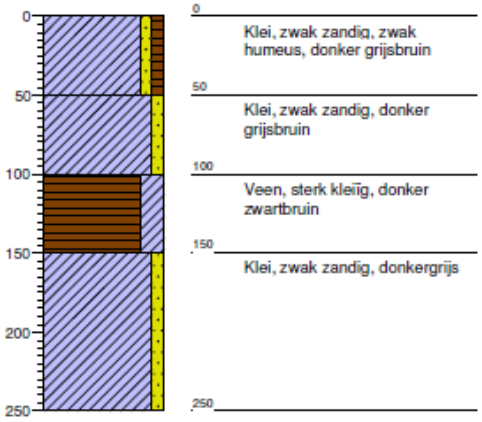

Boring: 3717

GWS in cm -mv: 120
GHG in cm -mv: 70
GLG in cm -mv: 150

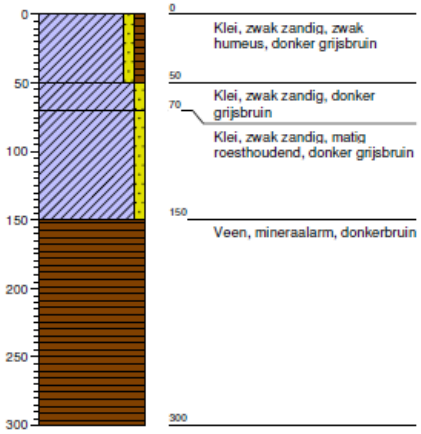

Boring: 3718

GWS in cm -mv: 130
GHG in cm -mv: 80
GLG in cm -mv: 180

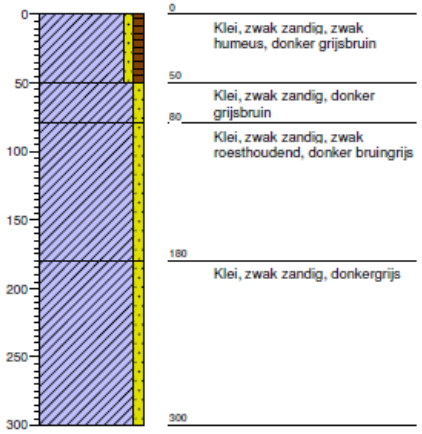

Boring: 3666

GWS in cm -mv: 150
GHG in cm -mv: 100
GLG in cm -mv: 180

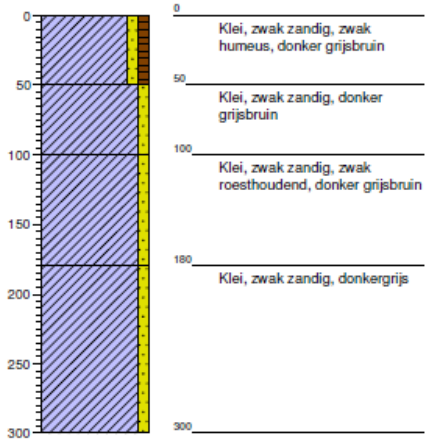

Boring: 3667

GWS in cm -mv: 80
GHG in cm -mv: 70
GLG in cm -mv: 140

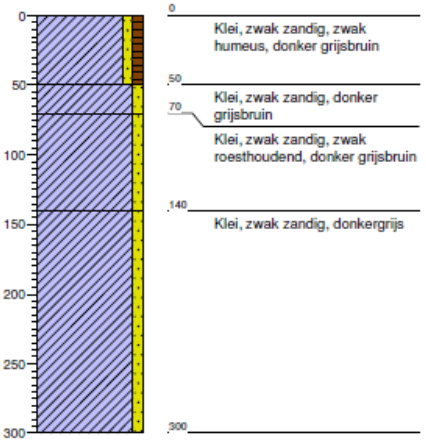

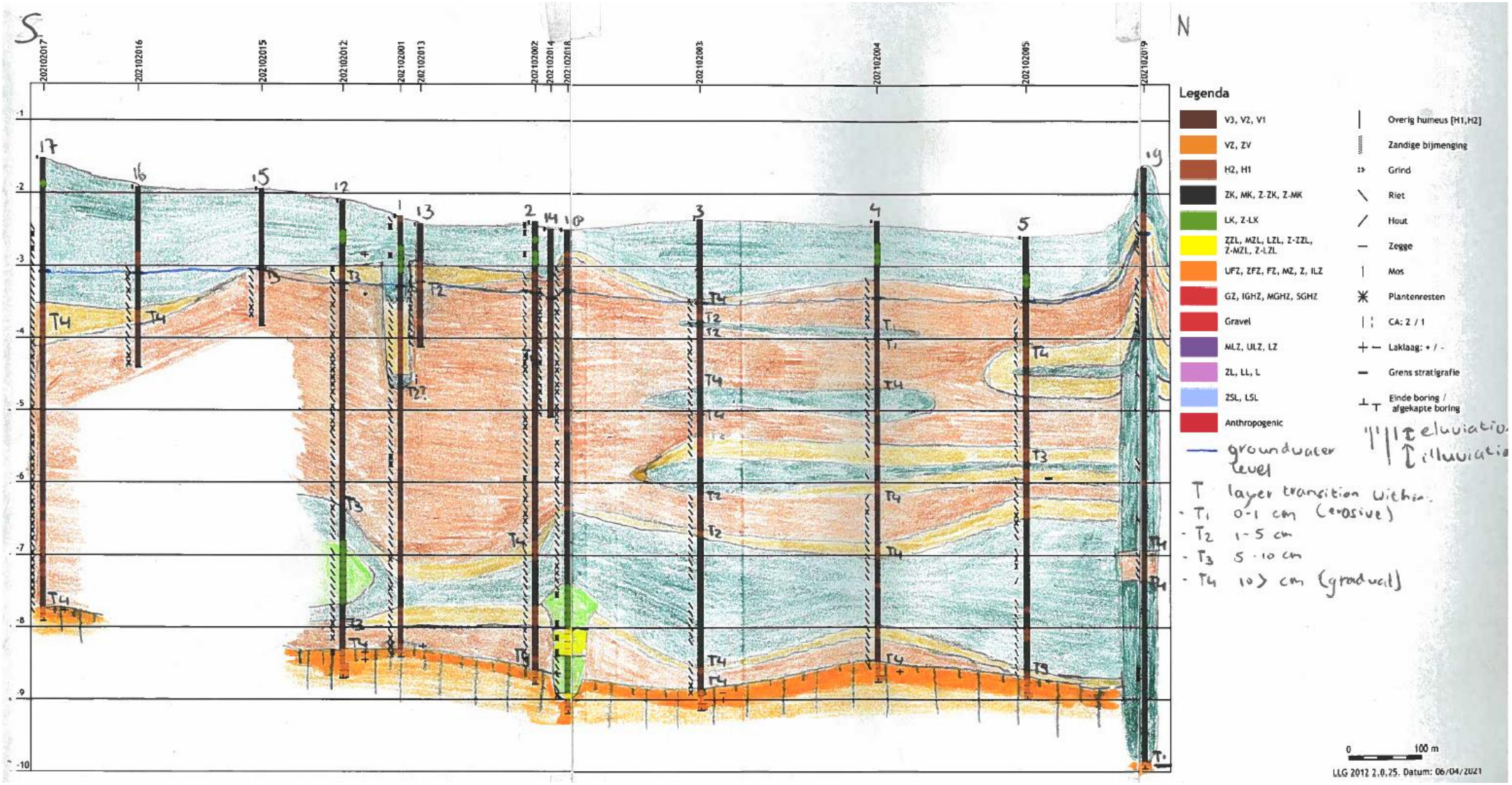
S
N
202102017
202102016
202102015
202102012
202102001
202102013
202102002
202102014
202102018
202102003
202102004
202102005
202102019
-1
-2
-3
-4
-5
-6
-7
-8
-9
-10
Legenda
V3, V2, V1
VZ, ZV
H2, H1
ZK, MK, Z-ZK, Z-MK
LK, Z-LK
ZZL, MZL, LZL, Z-ZZL, Z-MZL, Z-LZL
UFZ, ZFZ, FZ, MZ, Z, ILZ
GZ, IGHZ, MGHZ, SGHZ
Gravel
MLZ, ULZ, LZ
ZL, LL, L
ZSL, LSL
Anthropogenic
groundwater level
Overig humeus [H1,H2]
Zandige bijmenging
Grind
Riet
Hout
Zegge
Mos
Plantenresten
CA: Z / I
Laklaag: + / -
Grens stratigrafie
Einde boring / afgekapte boring
eluviation
illuviation
T layer transition within:
- T1 0-1 cm (erosive)
- T2 1-5 cm
- T3 5-10 cm
- T4 10> cm (gradual)
0
100 m
LLG 2012 2.0.25. Datum: 06/04/2021

Lithological cross-section transect West, Nieuwolda, province Groningen, the Netherlands

Luuk Reudink, 12-04-2021

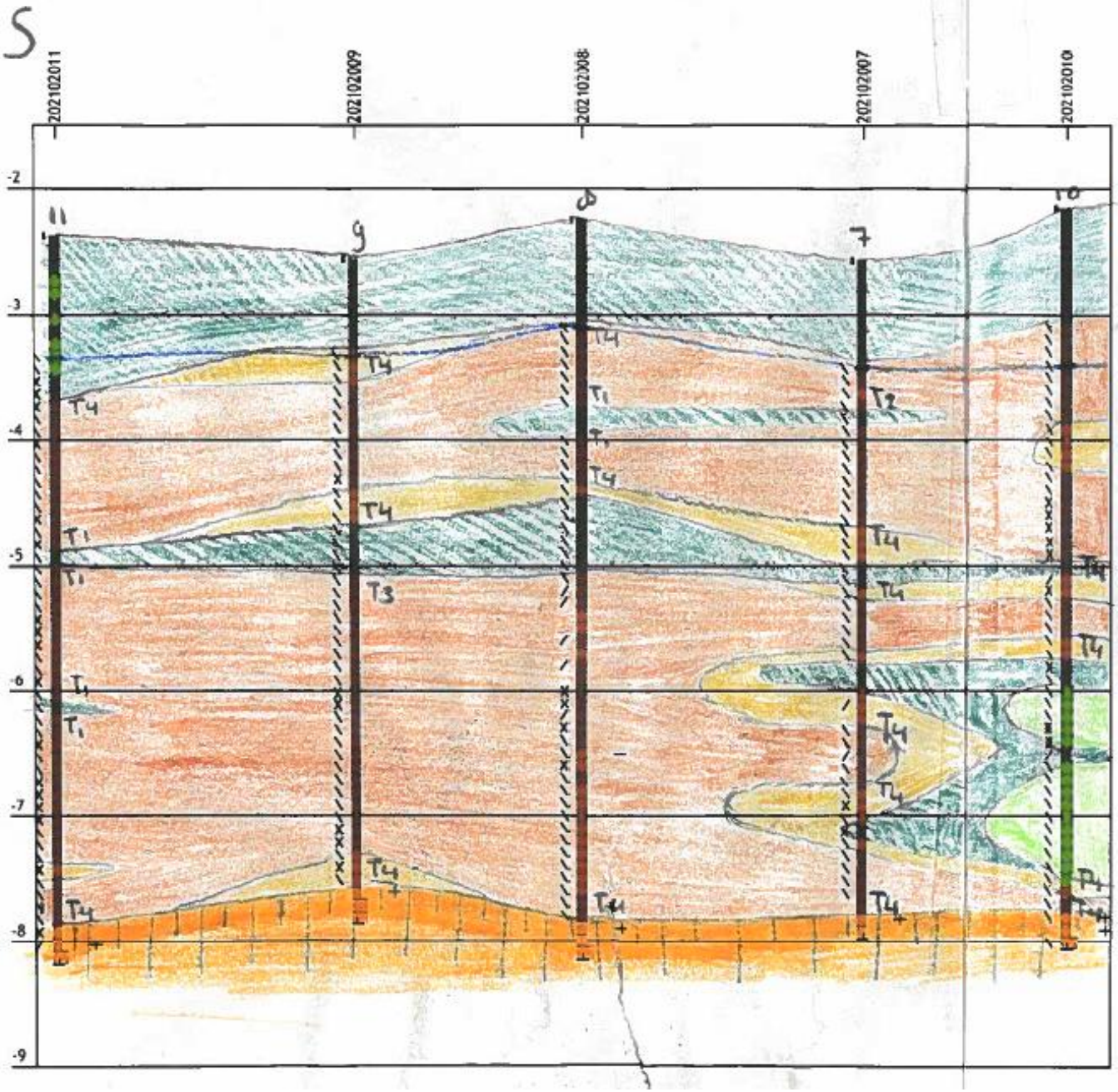

Legenda

- V3, V2, V1
- VZ, ZV
- H2, H1
- ZK, MK, Z-ZK, Z-MK
- LK, Z-LK
- ZZL, MZL, LZL, Z-ZZL, Z-MZL, Z-LZL
- UFZ, ZFZ, FZ, MZ, Z, ILZ
- GZ, IGHZ, MGHZ, SGHZ
- Gravel
- MLZ, ULZ, LZ
- ZL, LL, L
- ZSL, LSL
- Anthropogenic
- groundwater level

- Overig humeus [H1,H2]
- Zandige bijmenging
- Grind
- Riet
- Hout
- Zegge
- Mos
- Plantenresten
- CA: 2 / 1
- Laklaag: + / -
- Grens stratigrafie
- Einde boring / afgekapte boring

eluviation
illuviation

T layer transition within:

- T1 0 - 1 cm (erosive)
- T2 1 - 5 cm
- T3 5 - 10 cm
- T4 10 > cm (gradual)

0 100 m

LLG 2012 2.0.25, Datum: 06/04/2021

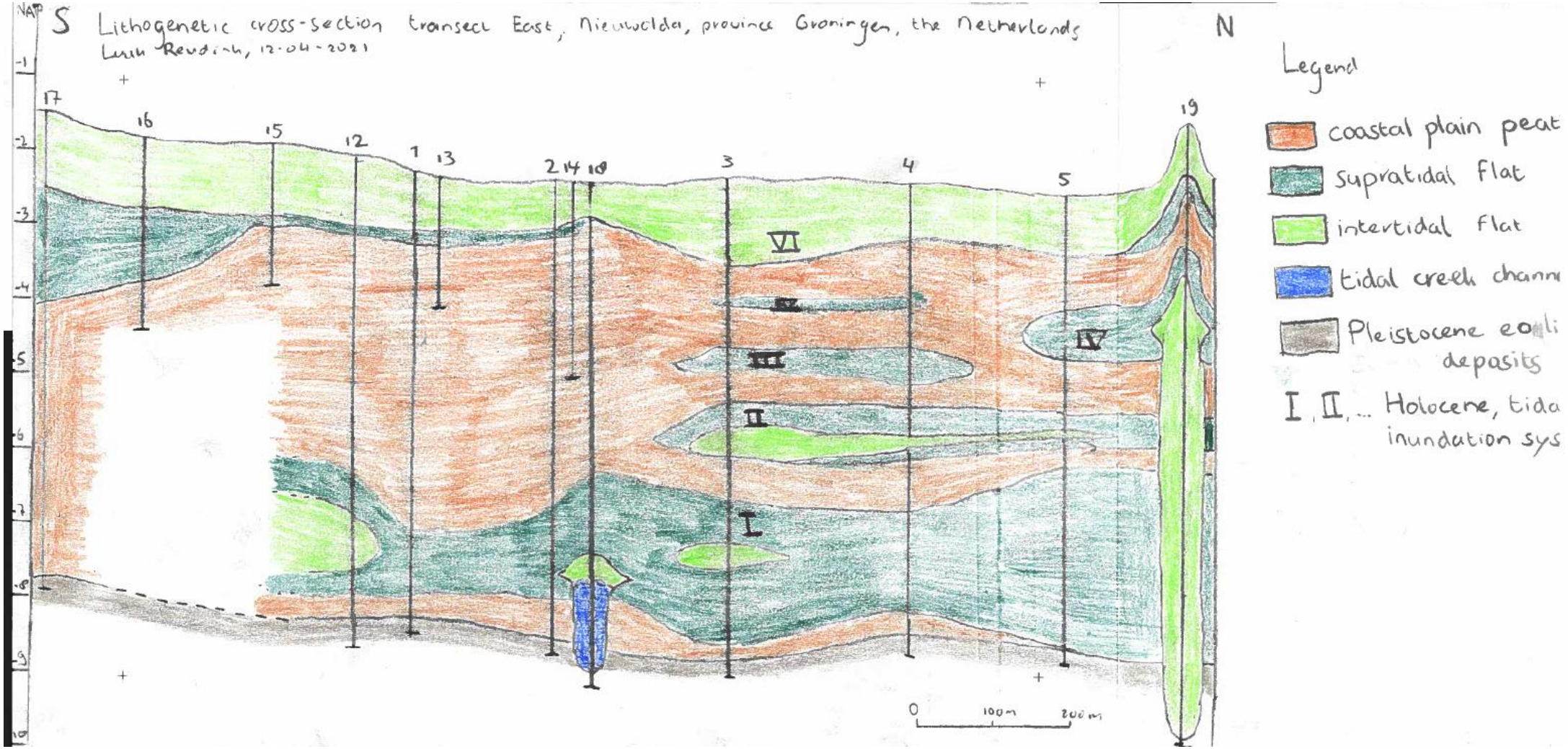
S
N
Lithogenetic cross-section transect East, Nieuwolda, province Groningen, the Netherlands
Luuk Reudink, 12-04-2021
NAP
-1
-2
-3
-4
-5
-6
-7
-8
-9
-10
17
16
15
12
7
13
2
14
18
3
4
5
19
VI
V
IV
III
II
I
0
100m
200m
Legend
coastal plain peat
supratidal flat
intertidal flat
tidal creek channe
Pleistocene eo li
depasits
I, II, ... Holocene, tida
inundation sys

Lithogenetic cross-section transect Wirdum, Nieuwolda, province Groningen, the Netherlands
Luuk Reudink, 12-04-2021

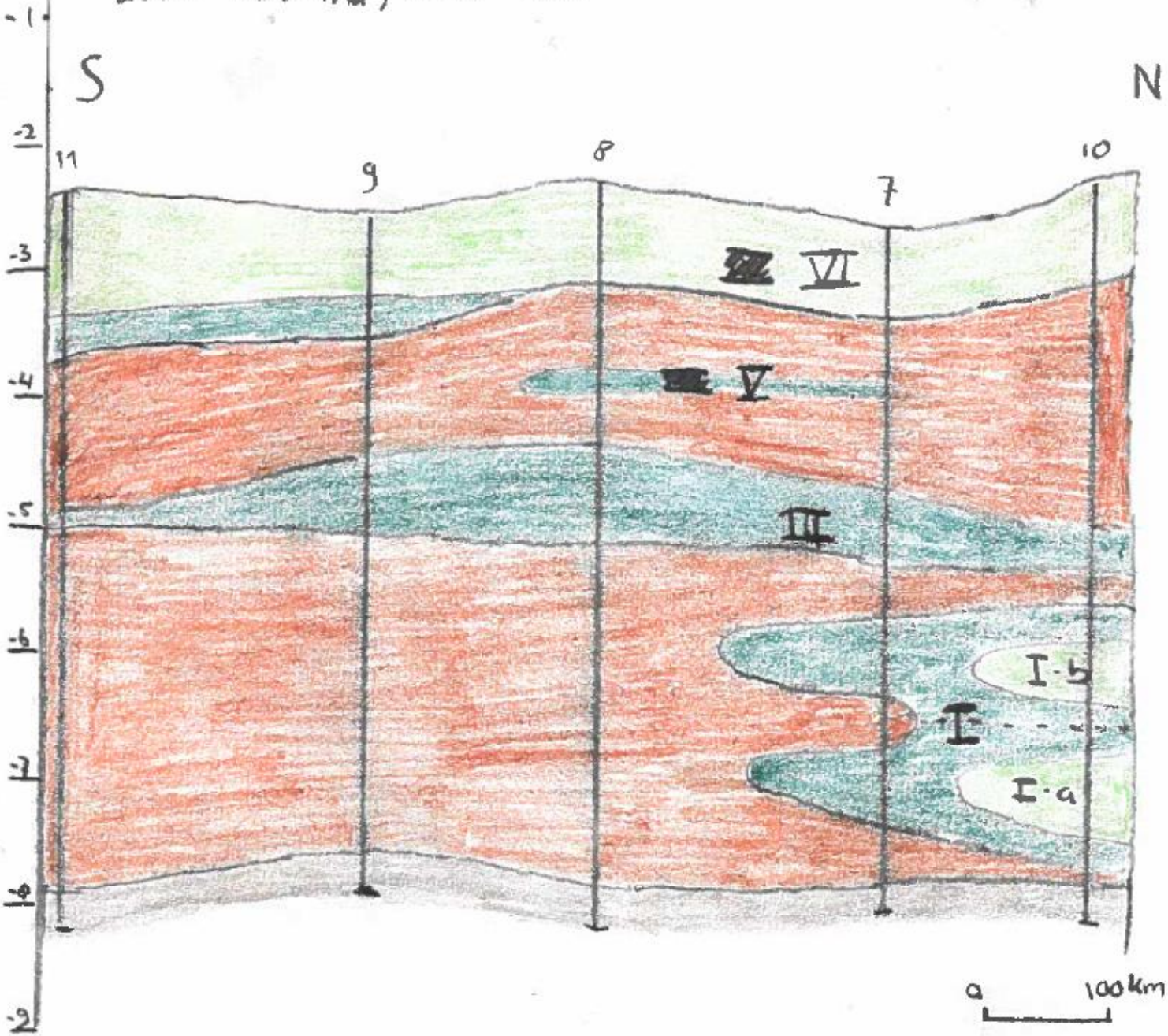

Legend

- coastal plain peatland
- supratidal flat
- intertidal flat
- Pleistocene eolian deposits
- I, II ... Holocene, tidal inundation system
- a, b phase

Bo	Number	WCr	WCs	Alpha	N	M	Lambda	Ks,fit	Kexm	B_den	Organis	Diepte mo	Diepte	GHG	GLG	Longitude	Monsterda	Latitude	Moerig-mineraal
O10	**10005**	0.0000	0.3950	0.0097	1.1899	0.1596	14.0078	1.1000	390.3	1570	2.0%	45	55	70	150	144560.00	06/06/2012	452490.00	matig humusarm
O10	**10006**	0.0000	0.3966	0.0280	1.1329	0.1173	7.4752	42.6000	1119	1655	1.5%	45	55	70	150	144560.00	06/06/2012	452490.00	zeer humusarm
O10	**10011**	0.0419	0.4800	0.0512	1.2553	0.2034	3.9706	658.7000	1249.5	1431	2.7%	40	50	160	260	208683.00	13/06/2012	468149.00	matig humusarm
O10	**10018**	0.0000	0.5920	0.0035	1.2608	0.2069	5.3276	0.3000	60	1223	2.3%	50	60	90	140	132749.00	13/06/2012	535189.00	matig humusarm
O10	**10026**	0.0000	0.4315	0.0129	1.1108	0.0998	-1.0486	1.7000	180.5	1522	2.8%	40	50	70	170	176290.00	15/05/2012	439670.00	matig humusarm
O11	**10015**	0.0000	0.4300	0.0516	1.0874	0.0804	4.6964	77.5000	1096.7	1514	0.4%	30	40	60	160	200220.00	16/05/2012	433880.00	uiterst humusarm
O11	**10016**	0.0000	0.4400	0.0146	1.1316	0.1163	-2.9127	3.8000	1726.9	1481	3.1%	30	40	60	160	200220.00	16/05/2012	433880.00	matig humusarm
O11	**10017**	0.0000	0.5860	0.0094	1.1904	0.1599	0.5400	1.7000	154.9	1095	3.7%	50	60	90	140	132749.00	13/06/2012	535189.00	matig humeus
O11	**10019**	0.0000	0.4611	0.0022	1.2580	0.2051	11.0895	0.0030	265.9	1487	2.8%	35	45	50	120	69226.00	26/06/2012	396699.00	matig humusarm
O11	**10020**	0.0000	0.4547	0.0214	1.1365	0.1201	13.4926	10.5000	719.4	1442	2.2%	35	45	50	120	69226.00	26/06/2012	396699.00	matig humusarm
O11	**10025**	0.0000	0.4151	0.0031	1.1645	0.1413	4.5850	0.1000	2138.3	1603	1.6%	40	50	70	170	176290.00	16/05/2012	439670.00	zeer humusarm
O11	**10113**	0.1950	0.4018	0.0167	1.1952	0.1633	-2.8668	0.3222	17.3	1597	1.6%	50	60	60	160	155197.28	04/05/2016	434992.54	zeer humusarm
O11	**10114**	0.2437	0.3950	0.0153	1.5796	0.3669	-2.0000	0.0860	86.1	1585	1.6%	50	60	60	160	155197.28	04/05/2016	434992.54	zeer humusarm
O11	**10119**	0.0000	0.4992	0.0709	1.0739	0.0688	0.0001	185.6515	654	1459	2.3%	43	53	60	110	126689.98	25/05/2016	413679.50	matig humusarm
O12	**10013**	0.0000	0.5553	0.0455	1.0909	0.0833	11.7509	58.3000	1438.3	1320	2.4%	60	70	60	160	125225.00	13/06/2012	527770.00	matig humusarm
O12	**10014**	0.0000	0.5100	0.0157	1.1043	0.0945	22.0982	8.8000	1143	1377	1.1%	60	70	60	160	125225.00	13/06/2012	527770.00	uiterst humusarm
O12	**10127**	0.0000	0.6377	0.0028	1.1429	0.1250	-1.9999	0.9616	391.3	926	9.7%	140	155	15	120	144669.00	24/02/2004	429099.00	zeer humeus
O12	**10128**	0.0000	0.7034	0.0057	1.1346	0.1187	0.0001	2.0000	202.9	777	10.7%	140	155	15	120	144669.00	24/02/2004	429099.00	zeer humeus
O13	**10125**	0.0000	0.5769	0.0137	1.0727	0.0677	-10.0000	0.8871	0.5	1201	4.9%	60	75	15	120	144669.00	24/02/2004	429099.00	matig humeus
O13	**10126**	0.0000	0.5657	0.0172	1.0588	0.0555	0.0001	3.0191	2.3	1182	4.4%	60	75	15	120	144669.00	24/02/2004	429099.00	matig humeus
O13	**10132**	0.1048	0.5569	0.0066	1.0850	0.0783	-20.0000	0.1077	2.2	1209	2.6%	65	75	30	130	144697.00	12/03/2004	429164.00	matig humusarm
O16	**10167**	0.0000	0.9300	0.0055	1.3563	0.2627	1.9427	0.8403	66.6	150	97.2%	50	60	90	230	265508.15	07/06/2018	518499.30	veen
O16	**10168**	0.0000	0.9150	0.0089	1.3261	0.2459	0.7093	1.6007	6.4	143	94.9%	50	60	90	230	265508.15	07/06/2018	518499.30	veen
O16	**10173**	0.0000	0.9180	0.0055	1.3145	0.2393	7.5588	1.2060	9.1	159	93.4%	30	40	15	60	188657.96	08/06/2018	543572.97	veen
O16	**10174**	0.0000	0.9110	0.0040	1.3018	0.2319	11.8021	1.0144	3.3	166	93.2%	30	40	15	60	188657.96	08/06/2018	543572.97	veen
O17	**10097**	0.0000	0.7900	0.0143	1.1073	0.0969	24.2857	63.8000	204.5	641	39.5%	35	45	30	90	122550.00	28/05/2014	458880.00	zeer zware klei
O17	**10098**	0.0000	0.7800	0.0260	1.0874	0.0804	13.2412	42.8000	12.9	519	31.5%	35	45	30	90	122550.00	28/05/2014	458880.00	zeer zware klei
O17	**10135**	0.0000	0.7818	0.0048	1.3056	0.2341	0.0001	30.1853	89.2	410	73.5%	180	190	100	200	129843.52	27/03/2017	399406.89	veen
O17	**10140**	0.0000	0.7582	0.0017	1.4455	0.3082	0.0001	4.5973	1789.9	433	62.7%	130	140	150	250	129777.60	27/03/2017	399192.52	veen

xture	Texture group	ORES	OSAT	ALFA	NPAR	M	LEXP	KSFIT	Kexp	B_den	ganische st	Depth TOP	Depth Bot	GHG	GLG	Longitude	Date	Latitude
O10	**zware zavel**	0.000	0.454	0.0135	1.1736	0.1459	6.44	11.43	437.45	1492.5	2.15%	45.0	55.0	75.0	152.5			
O11	**lichte klei**	0.063	0.451	0.0118	1.2366	0.1819	3.13	2.36	729.83	1470.0	0.0237	41.4	51.4	62.9	147.1			
O12	**matig zware klei**	0.000	0.639	0.0074	1.1167	0.1038	-4.00	1.28	198.23	968.0	0.0843	113.3	128.3	15.0	120.0			
O13	**zeer zware klei**	0.035	0.567	0.0125	1.0721	0.0672	-10.00	1.34	1.67	1197.3	0.0397	61.7	75.0	20.0	123.3			
O16	**oligotroof veen**	0.000	0.919	0.0060	1.3247	0.2449	5.50	1.17	6.27	154.5	94.68%	40.0	50.0	52.5	145.0			
O17	**mesotroof en eutroof veen**	0.000	0.770	0.0033	1.3756	0.2711	0.00	17.39	89.2000	421.5	68.10%	155.0	165.0	125.0	225.0			

*** CONTENTS ***
* Filename: Nieuwolda1.swp
* Contents: Main input data
* Author: Luuk Reudink
* Date: april 2021
* Reseacrh: MSc-Thesis
* Subject: Shallow subsidence Groningen, Nieuwolda.
* Description: Modelling accurate, daily GW-levels as input for empirical subsidence model

* Location: Monitoring well in Nieuwolda
* Goal: mimic the measured groundwater level between 2016 and 2019 as best as possible

* Structure
* - General section
* - Meteorology section
* - Crop section
* - Soil water section
* - Lateral drainage section
* - Bottom boundary section
* - Heat flow section
* - Solute transport section

*** GENERAL SECTION ***
 PROJECT = 'Nieuwolda' ! Project description [A80]
 PATHWORK = ' ' !! Path to work folder [A80]
 PATHATM = ' ' !! Path to folder with weather files [A80]
 PATHCROP = ' ' !! Path to folder with crop files [A80]
 PATHDRAIN = ' ' !! Path to folder with drainage files [A80]
 SWSCRE = 1 !! Switch, display progression of simulation run to screen:
 SWERROR = 1 !! Switch for printing errors to screen [Y=1, N=0]
 TSTART = 01-jan-2016 ! Start date of simulation run, give day-month-year [dd-mmm-yyyy]
 TEND = 31-dec-2019 ! End date of simulation run, give day-month-year [dd-mmm-yyyy]
 NPRINTDAY = 1 !! Number of output times during a day [1..1000, I]
 SWMONTH = 0 ! Switch, output each month [Y=1, N=0]
 PERIOD = 1 !! Fixed output interval, ignore = 0, [0..366, I]
 SWRES = 0 !! Switch, reset output interval counter each year [Y=1, N=0]
 SWODAT = 0 !! Switch, extra output dates are given in table below [Y=1, N=0]
 SWYRVAR = 0 !! 0 = each year output at the same date
 DATEFIX = 31 12 !! Specify day and month for output of yearly balances [dd mm]
 OUTFIL = 'Result' ! Generic file name of output files [A16]
 SWHEADER = 1 !! Print header at the start of each balance period [Y=1, N=0]

* Output/Results
 SWVAP = 0 ! Switch, output soil profiles of moisture, solute and temperature [Y=1, N=0]
 SWBLC = 1 ! Switch, output file with detailed yearly water balance [Y=1, N=0]
 SWATE = 0 ! Switch, output file with soil temperature profiles [Y=1, N=0]
 SWBMA = 0 ! Switch, output file with water fluxes, only for macropore flow [Y=1, N=0]
 SWDRF = 0 ! Switch, output of drainage fluxes, only for extended drainage [Y=1, N=0]
 SWSWB = 0 ! Switch, output surface water reservoir, only for extended drainage [Y=1, N=0]
 SWAFO = 0 ! Switch, output file with formatted hydrological data
 SWAUN = 0 ! Switch, output file with unformatted hydrological data

* Calculation input
 CRITDEVMASBAL = 0.00001 ! Critical Deviation in water balance during PERIOD [0.0..1.0 cm, R]

```
 DZNEW        = 50.0   150.0   450.0    105.0                  !  thickness of compartments [1.0d-6...5.0d2, cm, R]

*** METEOROLOGY SECTION ***
 METFIL       = 'Eelde'      !  File name of meteorological data without extension .YYY, [A200]
 SWETR        = 0           !! 0 = Use basic weather data and apply Penman-Monteith equation
 LAT          = 53.0        !  Latitude of meteo station [-90..90 degrees, R, North = +]
 ALT          = 3.23        !  Altitude of meteo station [-400..3000 m, R]
 ALTW         = 10.0        !  Height of wind speed measurement above soil surface (10 m is default) [0..99 m, R]
 ANGSTROMA    = 0.25        !! Fraction of extraterrestrial radiation reaching the earth on overcast days [0..1 -, R]

 ANGSTROMB    = 0.50        !! Additional fraction of extraterrestrial radiation reaching the earth on clear days [0..
1 -, R]
 SWDIVIDE     = 1           !! 1 = Distribution E and T based on direct application of Penman-Monteith
 SWETSINE     = 0           !!
 SWRAIN       = 0           !!
 SWMETDETAIL  = 0           !! 0 = time interval is equal to one day

*** CROP SECTION ***
 SWCROP       = 1           ! 1 = cultivated soil
 SWIRFIX      = 0           ! 0 = no irrigation applications are prescribed
 SWIRGFIL     = 0           ! 0 = irrigation data are specified below

* Table Croptype
     INITCRP    CROPSTART      CROPEND      CROPNAME   CROPFIL     CROPTYPE
       1      01-jan-2015    31-dec-2019   'Grass'    'GrassS_mowing_grazing'      1
* -------------------------------------------------------------------------------------

* Table Irrigation
        IRDATE   IRDEPTH     IRCONC   IRTYPE
 05-jan-2012       5.0     1000.0
 1
* -------------------------------------------------------------------------------------

*** SOIL WATER SECTION ***
 SWINCO       = 2        !  2 = pressure head of each compartment is in hydrostatic equilibrium with initial groundwa
ter level
 GWLI         = -50.0    !  Initial groundwater level [-10000..1000 cm, R]
 SWPONDMX     = 0        !  0 = Ponding threshold for runoff is constant
 PONDMX       = 0.5      !  In case of ponding, minimum thickness for runoff [0..1000 cm, R]
 RSRO         = 0.5      !! Drainage resistance for surface runoff [0.001..1.0 d, R]
 RSROEXP      = 1.0      !! Exponent in drainage equation of surface runoff [0.01..10.0 -, R]
 SWRUNON      = 0        !! 0 = No input of runon data
 CFEVAPPOND   = 1.25     !! When ETref is used, evaporation coefficient in case of ponding  [0..3 -, R]
 SWCFBS       = 0        !! 0 = soil factor is not used
 CFBS         = 0.5      !! Soil factor CFBC in Epot = CFBS * ETref [0..1.5 -, R]
 RSOIL        = 30.0     !! Soil resistance of wet soil [0..1000.0 s/m, R]
 SWREDU       = 1        !! 0 = reduction to maximum Darcy flux
 COFRED       = 0.35     !! Soil evaporation coefficient of Black [0..1 cm/d1/2, R],
 RSIGNI       = 0.5      !! Minimum rainfall to reset method of Black [0..1 cm/d, R]
 SWSOPHY      = 0        !! 0 = Analytical functions with input of Mualem - van Genuchten parameters
 SWHYST       = 0        !  0 = no hysteresis
 RDS          = 200.0    !! Maximum rooting depth allowed by the soil profile [1..5000 cm, R]
 SWMACRO      = 0        !  0 = no macropore flow
 SWSNOW       = 0        !  Switch, calculate snow accumulation and melt [Y=1, N=0]
```

```
 SWFROST      = 0       !  Switch, in case of frost reduce soil water flow [Y=1, N=0]

* Calculate Soilhydraulic equations  !To improve the modelling speed
 DTMIN        = 1.0d-7  !! Minimum timestep [1.d-7..0.1 d, R]
 DTMAX        = 0.2     !! Maximum timestep [dtmin..1 d, R]
 GWLCONV      = 100.0   !! Maximum difference of groundwater level between time steps [1.d-5..1000 cm, R]
 CRITDEVH1CP  = 1.0d-2  !! Maximum relative difference in pressure heads per compartment [1.0d-10..1.d3 -, R]

 CRITDEVH2CP  = 1.0d-1  !! Maximum absolute difference in pressure heads per compartment [1.0d-10..1.d3 cm,
R]
 CRITDEVPONDDT = 1.0d-4  !! Maximum water balance error of ponding layer [1.0d-6..0.1 cm, R]
 MAXIT        = 30      !! Maximum number of iteration cycles [5..100 -, I]
 MAXBACKTR    = 3       !! Maximum number of back track cycles within an iteration cycle [1..10 -,I]
 SWKMEAN      = 1       !! 1 = unweighted  arithmic mean
 SWKIMPL      = 0       !! 0 = no update

* Table Vertical discretization
   ISUBLAY   ISOILLAY  HSUBLAY  HCOMP  NCOMP
     1         3       50.0     1.0     50
     2         2      150.0     3.0     50
     3         1      450.0     10.0    45
     4         4      105.0     5.0     21

* end of table

* Table soil hydraulic properties
 ISOILLAY1      ORES       OSAT       ALFA       NPAR       KSATFIT       LEXP       KSATEXM      ALFA
W    H_ENPR    BDENS
     1         0.06       0.45       0.0118     1.2366     2.36       3.13       72.83      0.05       0.0       1470.0     ! licht
e klei
     2         0.00       0.64       0.0074     1.1167     1.28       -4.00      19.23      0.05       0.0       968.0      ! mati
g zware klei
     3         0.03       0.57       0.0125     1.0721     1.34       -10.00     1.67       0.05       0.0       1197.3     ! zee
r zware klei
     4         0.00       0.77       0.0033     1.3756     17.39      0.00       89.20      0.05       0.0       421.5      ! eutr
oof veen

* end table

*** LATERAL DRAINAGE SECTION ***
 SWDRA       = 1            ! 0 = No simulation of drainage
 DRFIL       = 'Nieuwolda'   ! File name with drainage input data without extension .DRA [A16]
! This file is used as appendix in MSc-Thesis and the drainage file has been added to the regular swp.file

DRAMET   = 3                          ! 3 = use drainage and/or infiltration resistance, multi-level if needed
SWDIVD   = 1                          ! Calculate vertical distribution of drainage flux in groundwater [Y=1, N=0]
COFANI   = 1.0   1.0    1.0   1.0          ! one value for every discretized layer
SWDISLAY = 0                            ! switch to adjust discharge layer [0..2 -, I]
NRLEVS   = 2                          ! Number of drainage levels [1..5 -, I]
SWINTFL  = 1                          ! Switch for interflow [0..1 -, I]
SWTOPNRSRF = 0
COFINTFLB = 0.05                        ! Coefficient for interflow relation  [0.01..10.0 d, R]
EXPINTFLB = 1.0                         ! Exponent for interflow relation  [0.1..1.0 -, R]
*--------------------------------Drainage level 1---------------------------------------
```

```
DRARES1  = 8000.0                ! Drainage resistance [10..1d5 d, R]
INFRES1  = 6000.0                ! Infiltration resistance [0..1d5 d, R]
SWALLO1  = 1                     ! 1 = Drainage and infiltration are both allowed
L1       = 60.0                  ! Drain spacing [1..1000 m, R]
ZBOTDR1  = -600.0                ! Level of drainage medium bottom, [-1000..0 cm, R]
SWDTYP1  = 2                     ! Type of drainage medium:

     DATOWL1   LEVEL1    ! (maximum MAOWL records)
  01-jan-2016   -156.0
  31-dec-2019   -156.0
* End of table

*---------------------------------Drainage level 2-------------------------------------

DRARES2  = 10.0                  ! Drainage resistance [10..1d5 d, R]
INFRES2  = 1000.0                ! Infiltration resistance [0..1d5 d, R]
SWALLO2  =   1                   ! 1 = Drainage and infiltration are both allowed
L2       = 1.0                   ! Drain spacing [1..1000 m, R]
ZBOTDR2  = -30.0                 ! Level of drainage medium bottom, [-1000..0 cm, R]
SWDTYP2  = 2                     ! Type of drainage medium:

     DATOWL2   LEVEL2    ! (maximum MAOWL records)
  01-jan-2016    -30.0
  31-dec-2019    -30.0

* End of table

*** BOTTOM BOUNDARY SECTION ***
SWBBCFILE      = 1                ! Switch for file with bottom boundary data:
BBCFIL         = 'Nieuwolda_2015_2019'   ! File name without extension .bbc [A16]

SWBOTB         = 3            ! Switch for bottom boundary [1..8,-,I]
SWBOTB3RESVERT  = 1           ! 0 = Include vertical hydraulic resistance
SWBOTB3IMPL     = 0           ! 0 = explicit solution (choose always when SHAPE < 1.0)
SHAPE          = 0.5          ! Shape factor to derive average groundwater level [0..1 -, R]
HDRAIN         = -156.0       ! Mean drain base to correct for average groundwater level [-1d4..0 cm, R]
RIMLAY         = 9000.0       ! Vertical resistance of aquitard [0..1d5 d, R]
SW3            = 2            ! 2 = table

*** HEAT FLOW SECTION ***
  SWHEA      = 0            ! Switch for simulation of heat transport [Y=1, N=0]

*** SOLUTE SECTION ***
  SWSOLU     = 0            ! Switch for simulation of solute transport, [Y=1, N=0]
```

```
% 1D EMPIRICAL SHALLOW SUBSIDENCE MODEL
% Luuk Reudink
% 21-01-2020

% --- Part of a MSc-Thesis on the disentanglement of shallow subsidence
% mechanisms as oxidation, compression and shrinkage in northern Netherlands

clear
close all

%% ---INITIALIZATION---
%% Vertical discretization
% Initial
Subsurface         = xlsread('Parameter_Peat_location.xlsx');  % LOAD SUBSURFACE CHARACTERISTICS

L_th_ini           = Subsurface(:,1);                  % initial layer thickness             (m)
L_th_final         = Subsurface(:,11);                 % final layer thickness               (m)
nr_L               = length(L_th_ini);                 % number of layers
Tot_th_ini         = sum(L_th_ini);                    % total thickness of the profile      (m)
L_depth_bot_ini    = cumsum(L_th_ini)*-1;              % initial depth bottom for every layer  (m)
L_depth_top_ini    = L_depth_bot_ini + L_th_ini;       % initial depth top for every layer     (m)

%% Parameters
clay_fr        = Subsurface(:,5);  % clay fraction in peat          (-)
rho_w          = 1000;             % density of water               (kg/m3)
rho_gr         = Subsurface(:,8);  % Density of the sediments       (kg/m3)
g              = 9.81;             % gravitational acceleration     (m/s2)
n              = Subsurface(:,7);  % porosity                       (-)
% fitting parameters
v_ox           = Subsurface(:,3);  % oxidation rate                 (m/day)
shr_factor     = Subsurface(:,4);  % factor shaping shrinkage       (-)
v_shr          = Subsurface(:,6);  % shrinkage rate                 (m/day)
Cp             = Subsurface(:,9);  % Primary compression parameter  (-)
Cs             = Subsurface(:,10); % Secondary compression parameter (-)

%% LOAD GROUNDWATER LEVELS
Data       = readtable('GW_Peat_location_drains.txt');          % load all SWAP hydrology output   (-)
Data       = table2array(Data(:,17));           % Only consider GW-levels          (cm)
GW_temp    = Data(0== sum(isnan(Data), 2), :);  % Remove NaN values                (cm)
GW_m       = GW_temp/100;                       % convert GW from cm to meters     (m)
GW         = min(GW_m,0);                       % exclude ponding                  (m)
GW_cm      = GW*100;
GW_pos     = GW*-1;                             % convert to positive in downward direction (m)
GW_mean    = mean(GW);
GW_lin     = repmat(GW_mean,length(GW),1);
GW_lin_cm  = GW_lin*100;
%% TIME DOMAIN
time           = 1:length(GW);          % total model period (dependent on number of GW-measurements)
Layer          = 1:nr_L;                % total number of layers
%% INITIALIZE VECTORS                   % initialise (temporary) output, most often for every layer (L) and every
 time step (t)
GW_delta       =zeros(length(GW),1);       % change in groundwaterlevel between two timesteps
          (m)                                                    (m)
L_thickness    =zeros(length(GW),nr_L);    % thickness                                                    (m)
```

```
L_thickness_cm  =zeros(length(GW),nr_L);
L_sat           =zeros(length(GW),nr_L);    % saturated thickness                                    (m)
L_unsat         =zeros(length(GW),nr_L);    % unsaturated thickness                                  (m)
L_ox            =zeros(length(GW),nr_L);    % thickness prone to decomposition
(m)
L_shr           =zeros(length(GW),nr_L);    % thickness prone to shrinkage                           (
m)
decr_shr        =zeros(length(GW),nr_L);    % deformation by shrinkage                               (
m/day)
decr_ox         =zeros(length(GW),nr_L);    % deformation by oxidation                               (
m/day)
decr_pri_com    =zeros(length(GW),nr_L);    % deformation by only primary compression
          (m/day)
decr_sec_com    =zeros(length(GW),nr_L);    % deformation by only secundary compression
           (m/day)
decr_com        =zeros(length(GW),nr_L);    % deformation by compression
 (m/day)
decr_ox_time    =zeros(length(GW),1);       % total deformation by oxidation per timestep
      (m)
decr_shr_time   =zeros(length(GW),1);       % total deformation by shrinkage per timestep
      (m)
decr_com_time   =zeros(length(GW),1);       % total deformation by compression per timestep
          (m)
decr_total_time =zeros(length(GW),1);       % total deformation per timestep
(m)
L_thickness_tot =zeros(length(GW),1);       % Total thickness subsurface                             (
m)                          (m)
S_eff_ver_sat   =zeros(length(GW),nr_L);    % vertical effective stress within each layer when saturated
            (kg m^-1 s^-2)
S_eff_ver_unsat =zeros(length(GW),nr_L);    % vertical effective stress within each layer when unsaturated
               (kg m^-1 s^-2)
Cum_stress_wet  =zeros(length(GW),nr_L);    % cummulative effective stress (overburden included) each layer whe
n saturated                (kg m^-1 s^-2)
Cum_stress_dry  =zeros(length(GW),nr_L);    % cummulative effective stress (overburden included) each layer whe
n unsaturated              (kg m^-1 s^-2)
sigma           =zeros(length(GW),nr_L);    % cummulative effective stress (overburden included) each layer both satu
rated as unsaturated   (kg m^-1 s^-2)
delta_sigma     =zeros(length(GW),nr_L);    % change in stress between timesteps
   (kg m^-1 s^-2)
L_depth_top     =zeros(length(GW),nr_L);    % bottom depth of every later, measured from the surface
             (m)
L_depth_bot     =zeros(length(GW),nr_L);    % top depth of every layer, measured from the surface
           (m)
sat_rel         =zeros(length(GW),nr_L);    % relative saturated content                             (-)
unsat_rel       =zeros(length(GW),nr_L);    % relative unsaturated content                           (-)

mean_sat        =zeros(nr_L,1);             % averaged saturation state per layer                    (-)
sigma_incr      =zeros(length(GW),nr_L);    % change in stress relative to former timestep
      (kg m^-1 s^-2)
L_sat_com       =zeros(length(GW),nr_L);    % thicknes saturated for compression calculations
L_unsat_com     =zeros(length(GW),nr_L);    % thickness unsaturated for compression calculations
%% --- CALCULATION ---                      % Caculations in a loop at everytimestep (t) and every layer (
L)
for t=2:length(GW)                          % IMPORTANT: loop for every timestep (t) in a timeseries, determi
```

```
ned by the number of groundwaterlevels
   for L=1:nr_L                                % IMPORTANT: loop for every discretized layer (L) in a subsurface/s
oil profile
      % Initialiase parameters at t=0 as starting position
      L_thickness(1,L)    = L_th_ini(L,1);          % initial thickness          (m)
      decr_ox(1,L)        = 0;                      % initial oxidation reduction      (m)
      decr_shr(1,L)       = 0;                      % initial shrinkage reduction      (m)
      decr_com(1,L)       = 0;                      % initial compression reduction    (m)
      % Calculate new thickness
      L_thickness (t,L)  = L_thickness(t-1,L)-decr_ox(t-1,L)-decr_shr(t-1,L)-decr_com(t-1,L);    % New thickness af
ter shallow deformation      (m)
      L_thickness_cm (t,L) = L_thickness(t,L)*100;
      L_depth_bot (t,L)  = sum(L_thickness(t,:))*-1;                    % Depth bottom each layer below s
urface        (m)
      L_depth_top (t,L)  = L_depth_bot(t,L)+L_thickness(t,L);           % Depth top each layer below
surface          (m)
      % calculate saturation state fluctuating GW-level
      if GW(t)>L_depth_top(t,L)                   % GW-level above top of the layer
         L_sat(t,L)      =L_thickness(t,L);       % layer = fully saturated     (m)
      elseif GW(t)    == 0                        % GW-level at surface
         L_sat(t,L)  =L_thickness(t,L);
      elseif L_depth_bot(t,L) <GW(t)&& GW(t)< L_depth_top(t,L)          % GW-level between top a
nd bottom of the layer
         L_sat (t,L) = L_thickness(t,L)+(GW(t)-L_depth_top(t,L));       % layer = partly saturated
          (m)
      else                                        % GW-level below bottom of the layer

         L_sat (t,L) =0;                          % layer = unsaturated          (m)
      end
      L_unsat (t,L)   = L_thickness (t,L)-L_sat(t,L);                   % layerthickness of the unsaturated p
art       (m)
      sat_rel (t,L)   = L_sat (t,L)/L_thickness (t,L);                  % relative thickness saturated
  (-)
      unsat_rel (t,L) = L_unsat (t,L)/L_thickness (t,L);                % relative thickness unsaturated
       (-)
      % Caluclate stauration state constant GW-level (compression)
      if GW_lin(t)>=L_depth_top(t,L)              % GW-level above top of the layer
         L_sat_com(t,L)      =L_thickness(t,L);   % layer = fully saturated     (m)
      elseif L_depth_bot(t,L) <GW_lin(t)&& GW_lin(t)< L_depth_top(t,L)  % GW-level between to
p and bottom of the layer
         L_sat_com (t,L) = L_thickness(t,L)+(GW_lin(t)-L_depth_top(t,L));   % layer = partly saturated
               (m)
      else                                        % GW-level below bottom of the layer

         L_sat_com (t,L) =0;                      % layer = unsaturated          (m)
      end
      L_unsat_com(t,L)   = L_thickness (t,L)-L_sat_com(t,L);
      % Calculate stress
      S_eff_ver_sat (t,L)     = (1-n(L))*(rho_gr(L)-rho_w)*g*L_sat_com(t,L);  % vertical effective stress  when satur
ated                    (kg m^-1 s^-2)
      S_eff_ver_unsat(t,L)    = (1-n(L))*rho_gr(L)*g*L_unsat_com(t,L);       % vertical effective stress  when unsatu
rated                   (kg m^-1 s^-2)
      Cum_stress_wet(t,L)     = sum(S_eff_ver_sat (t,:));           % cummulative effective stress (overburden inc
luded) when saturated     (kg m^-1 s^-2)
```

```
    Cum_stress_dry(t,L)     = sum(S_eff_ver_unsat (t,:));              % cummulative effective stress (overburden in
cluded) when unsaturated   (kg m^-1 s^-2)
    sigma(t,L)              = Cum_stress_wet(t,L)+ Cum_stress_dry(t,L);     % total cummulative stress
                (kg m^-1 s^-2)
    delta_sigma(t,L)        = sigma(t,L)-sigma(t-1,L);                % absolute difference in stress between two times
teps                (kg m^-1 s^-2)
    delta_sigma(2,L)        = 0;
    delta_sigma(3,L)        = 0;
    sigma_incr(t,L)         = (sigma(t,L)+delta_sigma(t,L))/sigma(t,L);     % change/increase in stress with former ti
mesteps             (kg m^-1 s^-2)
    % Calculate contribution compression
    decr_pri_com  (t,L)     = 1/Cp(L)*log(sigma_incr(t,L));                 % deformation by primary compression
                (m)
    decr_pri_com  (t,nr_L)  = 0;                                    % no primary compression in Boxtel Formation
    decr_sec_com  (t,L)     = 1/Cs(L)*log(1+time(1,t)/1)*log(sigma_incr(t,L));      % deformation by secondary co
mpression                   (m)
    decr_sec_com  (t,nr_L)     = 0;                                 % no secondary compression in Boxtel Formation

    % decr_com      (t,L)     = decr_pri_com(t,L)+decr_sec_com(t,L);          % total deformation by compressio
n
    % Calculate contribution oxidation & shrinkage
    if L_thickness (t,L)== L_sat (t,L)                                  % whenever layer is fully saturated...
       L_ox (t,L)      = 0;                                             % ... no oxidation
       L_shr(t,L)      = 0;                                             % ....no shrinkage
    else
       L_ox(t,L)       = L_thickness(t,L)-L_sat(t,L)- clay_fr(L,1)*(L_th_ini(L,1)-L_sat(t,L));     % layer thickness pr
one to oxidation           (m)
       L_shr(t,L)      = L_thickness(t,L)-L_sat(t,L)- shr_factor(L,1) *(L_th_ini(L,1)-L_sat(t,L)); % layer thickness p
rone to shrinkage          (m)
    end
    decr_ox(t,L)    = L_ox(t,L)*(1-exp(-v_ox(L)));                      % decrease by oxidation
      (m)
%       decr_shr(t,L)   = L_shr(t,L)*(1-exp(-v_shr(L)));                % decrease by shrinkage
        (m)
  end % end loop for every layer (L)
  GW_delta(t)       = GW(t)-GW(t-1);                                    % change in GW-level between two timesteps
(m)
  L_thickness_tot(t)  = sum(L_thickness(t,:));                          % total thickness                 (m)
  decr_ox_time(t)     = sum(decr_ox(t,:));                              % total deformation by oxidation every timestep     (
m)
  decr_shr_time(t)    = sum(decr_shr(t,:));                             % total deformation by shrinkage every timestep
(m)
  decr_com_time(t)    = sum(decr_com(t,:));                             % total deformation by compression every timest
ep   (m)
  decr_total_time (t) = decr_ox_time(t)+ decr_shr_time(t)+decr_com_time(t);  % total deformation every timestep
end     % end loop for every timestep (t)
decr_ox_total_layer= sum(decr_ox);                          % sum of deformation by oxidation for every layer
decr_ox_total =sum(decr_ox_total_layer(:));                 % total deformation by oxidation
decr_shr_total_layer = sum(decr_shr);                       % sum of deformation by shrinkage for every layer
decr_shr_total =sum(decr_shr_total_layer(:));               % total deformation by shrinkage
decr_com_total_layer = sum(decr_com);                       % sum of deformation by compression for every layer
decr_com_total =sum(decr_com_total_layer(1,1:6));           % total deformation by compression
L_thickness_tot_cm = L_thickness_tot*100;
L_thickness_tot_final_cm = L_thickness_tot_cm(length(GW));
```

```
% loop to calculate relative saturation state through time
for i=1:nr_L
   mean_sat(i) = mean(sat_rel(:,i));                    % average saturation state per layer
end

%% --- VISUALIZATION ---
Variables =[GW_cm decr_ox_time*100 L_thickness_tot_cm];
figure (1)
capt_title={'Groundwater level','Deformation by oxidation per timestep','Total Holocene sediment thickness'};
capt_y_axis={'Depth [cm]','Deformation[cm]','Thickness [cm]'};
for p=1:3
   Variable = Variables(:,p);
   subplot(3,1,p);plot(time(3:length(GW)),Variable(3:length(GW)),'b')
   xticks([0 365 730 1095 1461])
   xticklabels({'2016','2017','2018','2019','2020'})
   xlim([0 1461])
   title_fig = capt_title(p);
   title(title_fig);
   y_axis_fig= capt_y_axis(p);
   ylabel(y_axis_fig);
   set(gca,'Fontsize',15)
   hold on
   subplot(3,1,1);plot(time(3:length(GW)),L_depth_top(3:length(GW),2)*100,'--k')
   subplot(3,1,1);legend('groundwater level','upper boundary peat layer')
   subplot(3,1,2);ylabel({'Deformation[cm]';' '})
end

figure
plot(L_depth_top(3:length(GW),:))
```

MANUAL SWAP/FORTRAN

This manual will provide necessary, practical explanations when consulting the model. For any questions please contact l.reudink@uu.nl or luuk266@hotmail.com .

Last updated: 20 June 2021 by Luuk Reudink

1. INTRODUCTION

This manual is built to provide hands-on guidance and assistance when modelling in SWAP (Soil-Water-Atmosphere-Plant). SWAP is an ecohydrological, process-based, one-dimensional model developed by Wageningen University & Research that simulates the transport of water, solutes and heat in variably saturated soils. SWAP does not contain a modelling environment but is executed as a batch file in a command prompt. The code is written in Fortran language. Kroes et al. (2017) provide additional theoretical information on incorporated soil and subsurface processes.

2. GFORTRAN INSTALLATION

There are some options downloading Fortran, but I recommend to use GFortran or GNU Fortran. Watch the following videos that will guide you through the installation.

Fortran install guide Windows or Installing MinGW with gFortran

3. GFORTRAN PROGRAMMING LANGUAGE

Fortran is a programming language and not a model. The code for the SWAP-model is therefore written in a textfile using the Fortran programming language. There are various options for textfiles to use (Notepad). I used Notepad ++ because it is clearly structured. Notepad ++ can be downloaded from:

Notepad++ download

Some basic advice for modelling with Fortran:

- The SWAP-model will give an error when there is a ''tab'' in the code. So do not use a tab to create structure in the code but rather multiple spaces .
- Both *of ! can be used to provide explanation as written language in the code.
- A file can be saved in multiple extensions dependent on the format required for the swap input. Instead of a regular .txt file you can save any the document in any three letter format, for example swap.qqq

4. SWAP MODEL DOMAIN, STRUCTURE AND PROCESSES

Vertically, the SWAP-model reaches from the vegetation cover to several meters below the groundwater level. Meteorological data and potential irrigation serve as input at the surface, whereas the user can select various forms of hydraulic heads or fluxes at the lower boundary. The flow of water in the saturated zone uses Darcy's Law and the concept of hydraulic head. The extraction of soil moisture by the roots of vegetation can be implemented. In the unsaturated zone, the flow of water is calculated with use of the Richards equation, which incorporates the dependency of the hydraulic conductivity on the variable volumetric moisture content through time. In the horizontal direction, the model simulates lateral drainage in the saturated zone with the use of analytical drainage formulas.

5. SWAP INSTALLATION

The SWAP-model can be downloaded form the Internet site:

https://www.swap.alterra.nl/DownloadRecent/swap4.0.1/Swap4.0.1.htm

Carefully read the instructions on the website.

Note: later you will have to link the command prompt to the location where you saved SWAP on your computer. Therefore, I recommend to save SWAP directly on the C/ disk to prevent unnecessary long addressing.

6. SWAP MODEL INPUT

6.1 MAIN INPUT FILE

Comprises:

- Meteorology
- Vegetation
- Soil-water and soil-hydraulic properties
- Bottom boundary
- Lateral drainage

6.2 METEOROLOGY FILE

1. Go to the website of KNMI to find historical climate data.

https://www.knmi.nl/nederland-nu/klimatologie

Choose *'Metingen en waarnemingen'*

Choose *'Dagwaarden van weerstations'*

Choose the correct time interval and the correct weather station

Download the data!

2. The data has been downloaded as a text-file. Open the data in Excell
3. This steps includes the 'clean up' of the entire meteorlogy file. The KNMI uses different abbrevations, decimals etc then the SWAP model requires. These should be adapted manually. Table below shows the important meteorology parameters between weather station data (KNMI) and SWAP input.

SWAP input parameters	Description	Unit in SWAP	Number notation SWAP	Corresponding KNMI colum	Unit KNMI
Station	Station number	-	'number'	Copy the station	-
DD	Day	-	integer	YYYYMMDD	-
MM	Month	-	integer	YYYYMMDD	-
YYYY	Year	-	integer	YYYYMMDD	-
RAD	Global radiation	kJ/m2	1 decimal	Q	J/cm2
Tmin	Minimum temperature	Celsius	1 decimal	TN	0.1 degrees Celsius

Tmax	Maximum temperature	Celsius	1 decimal	TX	0.1 degrees Celsius
HUM	Humidity	kPa	2 decimals	TG	0.1 degrees Celsius
				UG	%
WIND	Windspeed	m/s	1 decimal	FG	0.1 m/s
RAIN	Daily precipitation	mm	1 decimal	RH	0.1 mm
ETref	Referention evaporation	mm	1 decimal	EV24	0.1 mm
WET	Duration precipitation per day	days	4 decimals	DR	0.1 hour

STATION: Copy the number of the station into a column. Place the number in between apostrophes otherwise SWAP will not run!

DD/MM/YYYY: By loading the textfile into Excell, you should address the entire data column to the correct date settings. By doing so, you can use the Excell calculations =YEAR(.) =MONTH(.) =DAY(.) to separate the date into year, data and month, which is required in the SWAP model. These are integer numbers.

RAD: Convert KNMI radiation 'Q' (J/cm2) into RAD (kJ/m2) → multiply Q by 10

Tmin: Convert TN (0.1 degrees Celsius) into Tmin (degrees Celsius) → divide TN by 10

Tmax: Convert TX (0.1 degrees Celsius) into Tmax (degrees Celsius) → divide TX by 10

HUM:

SVP (kPa) = 0,611 *EXP((17,27*TempGem)/(TempGem+237,3))

VPD (kPa) = HUM (kPa) = (UG/100)*SVP

WIND: Convert FG (0.1 m/s) into WIND (m/s) → divide FG by 10

RAIN: Convert RH (0.1 mm) into RAIN (mm) → divide RH by 10. Note, the SWAP model will give an error for negative rainvalues. Convert manually all the negative values into zero.

ETref: Convert EV24 (0.1 mm) into ETref (mm) → divide EV24 by 10

WET: Convert DR (0.1 hour) into WET (days) → divide DR by 240

Make sure the values contain a dot (English language of Excell) instead of a komma otherwise SWAP will not work

Make sure all the parameter values have the correct length of decimals

Paste into different excell-worksheet with use of 'Paste Values & Source formatting'

4) When the input for SWAP in Excell is ready, export to a formatted textfile which is space delimited. (I investigated to see if it is possible to export multiple worksheets in one Excell file into different formatted textfiles. This is only possible for a simple .txt file. However, this .txt file is not space delimited and therefore the SWAP model has difficulties reading. Thus, every individual year you would want to model must be exported).

5) Save the space delimited textfile as f90-file and give it the same name as the SWAP main input file. The extension must be the the last three digits of the year from which the meteorology data is stored.

Hupsel.002 (save as 'All files'', only then a yyy extension will be recognized and properly saved)

6) The meteorlogy file is now ready. Do this for all the years that you want to model.

7) Place the meteorology file in the same folder as the SWAP main input file.

6.3 CROP GROWTH FILE

In the Swap download, several crop input files are attached. These files do not need to be adjusted but can be used for every study

1. Make sure how the land of the investigated area is cultivated.
2. Pick the right crop input file from the SWAP download
3. Place the crop input file in the same folder as the main input file

6.4 DRAINAGE FILE

For drainage there are multiple decisions need to be made.

1) Firstly, consider whether to implement drainage. In a natural situation it might be that drainage is not required to accurately model the subsurface architecture. However, in the Netherlands the water management is extensive and most areas are artificially drained. Drainage might be of importance, depending on the type of study, location etc.

2) For further info I refer to the SWAP manual where the drainage section is extensively described.

7. SWAP MODEL RUN

1. Start by connecting the command prompt to the SWAP-model. Type the correct path where SWAP is installed at your computer.

path %PATH%;C:\SWAP\bin

2. Go to the correct map where your swap input files are stored.

cd OneDrive\Documenten\Aardwetenschappen\Jaar 7_Master Thesis\SWAP\Cases\Nieuwolda_BUIZEN\Clay

3. Run the model by typing swap.exe followed by the name of the SWAP main input file.

Swap.exe Hupsel.swp

4. The SWAP will now run on your screen. Probably it will generate some errors the first times. Solve those errors by correcting info/data in the SWAP input files. The TTutil manual can provide further assistance to obtain more information on the obtained error

8. SWAP MODEL OUTPUT

Modelled output is stored in a textfile. The model computes a water balance regarding the exchange of water between atmosphere, vegetation, open water and soil-, groundwater in the subsurface.

9. DATA ANALYSIS (MATLAB / PYTHON / EXCELL)

To investigate the model results the data can be incorporated into a program to before data statics such as Microsoft Excell, Python or Matlab.

MANUAL EMPIRICAL SHALLOW SUBSIDENCE MODEL

This empirical shallow subsidence model was developed by Luuk Reudink in 2021 as a part of a MSc-thesis on shallow subsidence. The model is built to incorporate groundwater levels dynamics in the computation of shallow subsidence. This manual will provide necessary explanation when consulting the model. Any improvement made with this model should be added to this manual to keep it updated. For any questions please contact l.reudink@uu.nl or luuk266@hotmail.com .

Last updated: 20 June 2021 by Luuk Reudink

1. GENERAL MODEL PERFORMANCE

MODELLING ENVIRONMENT

Matlab was chosen as modelling environment as this program is taught in the Earth Surface & Water master at UU. The script can be adapted to *Python*. When more computational power is required the model could be converted into a *Fortran* script.

MODEL DOMAIN

The vertical model domain reaches from the surface level down to the first appearance of an incompressible layer (Figure 1). Deep subsidence does not affect shallow subsidence because the surface level is set as zero and marks the upper limit of the model domain. In fact, groundwater levels are modelled with respect to the surface level, creating a differential saturation state through time.

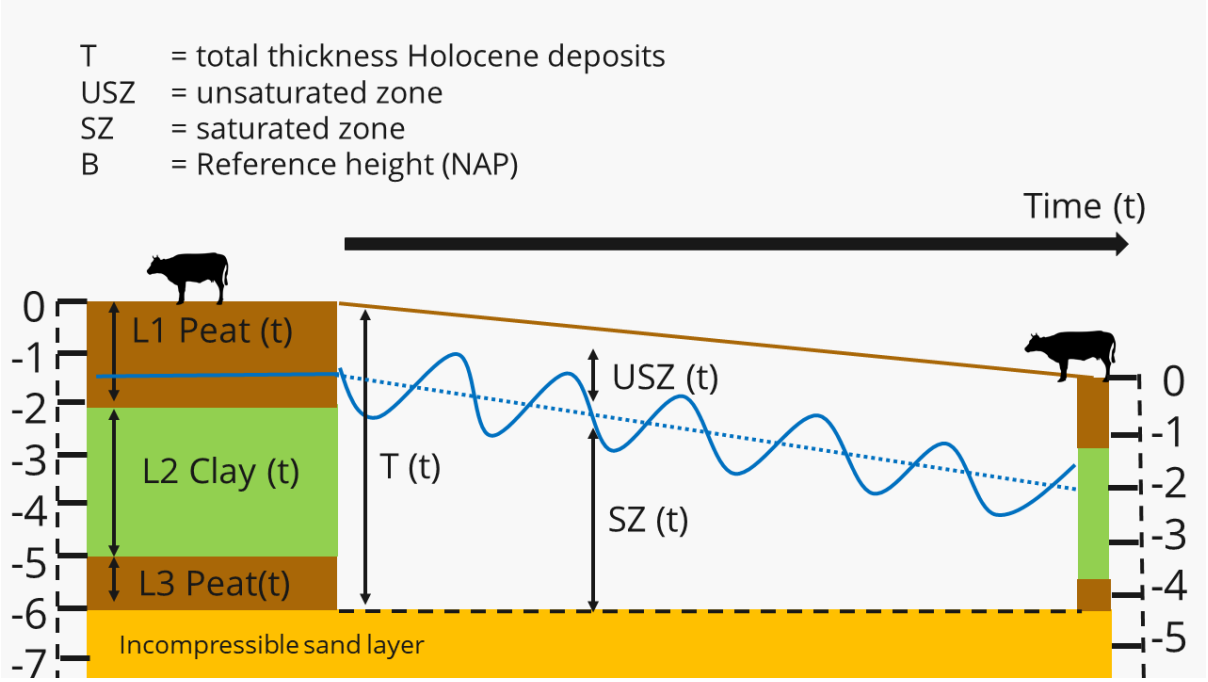

FIGURE 1: SCHEMATIZATION OF THE SUBSIDENCE MODEL PERFORMANCE. THE SURFACE IS MODELLED STATIC TO ACCURATELY MIMIC THE SATURATION STATE OF THE SUBSURFACE THROUGH TIME AND TO EXCLUDE INFLUENCES OF DEEP SUBSIDENCE FROM GAS EXTRACTION.

BASIC MODEL STRUCTURE

A lithological profile of the desired location is discretized into layers containing specific parameters. The groundwater levels that were produced using SWAP are incorporated and used to compute the saturation state of every layer at one moment in time. Next the model computes the decrease in layer thickness caused by compression and oxidation for every layer, starting at the top and continuing in downward direction. After

calculating the deformation of all layers at one moment in time, the model computes the new thickness of all these layers. These new thicknesses are then used to calculate the deformation at the next timestep. To summarize, the model operates with a double loop. In the first loop subsidence is computed for every discretized layer, in the second loop the deformation is calculated at every moment in time (Figure 2).

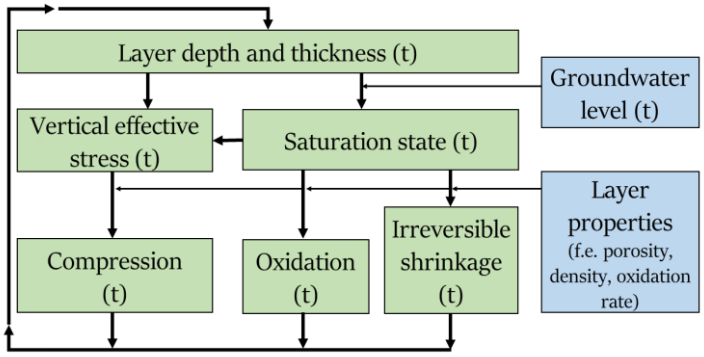

FIGURE 2: FLOW CHART OF THE SUBSIDENCE MODEL METHODOLOGY WITH A LOOP COMPUTING THE SUBSIDENCE IN EVERY LAYER AT ANY MOMENT IN TIME.

2. MODEL INPUT

The model concepts are based on the model from the study by Fokker et al. (2019). For example, equations regarding the computation of stress and strain, compression and oxidation are similar. This model however computes layer deformation based on a differential subsurface saturation state from dynamic groundwater levels.

VERTICAL DISCRETIZATION

The vertical discretization is obtained by loading an Excell file using the function ''xlsread('*name of the file'*). A lithological profile can be obtained using DINOloket/literature or from a fieldwork.

SUBSURFACE PARAMETERIZATION

Lithological parameters are assigned to every discretized layer in the subsurface profile (Table 1). Assigning different parameter values for each layer enables the differentiation between layers with the same texture group but a different subsidence history. Required parameters per layer are:

- Thickness
- Oxidation rate (whenever organic matter is present in the lithology).
- Porosity
- Matrix density
- Primary compression rate
- Secondary compression rate
- Shrinkage rate (optional)
- Shrinkage factor (optional)

	Texture	**h_initial**	**V_ox**	**res_clay**	**n**	**rho_gr**	**Prim Com**	**Sec Com**
Unit	-	*m*	*cm m-1 a-1*	-	-	*kg m-3*	*m a-1*	*m a-1*
L1	Clay	0.4	0	0	0.75	1400	9497	42369
L2	Peat	2.3	0.88	0	0.85	1100	2557	23741
L3	Clay	0.2	0	0	0.75	1400	9497	42369
L4	Peat	0.9	0.88	0	0.85	1100	2557	23741
L5	Clay	1.1	0	0	0.75	1400	9497	42369

L6	Loam	1.6	0	0	0.75	1470	9497	42369

Table 1: Sediment characteristics per discretized layer in the subsidence model.

LOADING GROUNDWATER MEASUREMENTS

Groundwater levels are incorporated by loading a text file containing the modelled groundwater levels from the SWAP-model. The model requires groundwater levels with respect to the surface level (note not NAP). Groundwater levels are negative in downward direction. Positive groundwater levels (ponding) are converted to zero, still indicating full saturation of the subsurface. The saturation state is determined by an if-statement indicating whether the layer is either fully saturated, partly saturated, or unsaturated. Layers that were entirely located above the groundwater level were assumed to be completely dry and therefore disposed of water.

INITIALIZING VECTORS

In the subsidence computations several vectors are required. The output of these vectors might be of interest as well, f.e. to detect possible errors. Therefore, the vectors used in the computations have to be initialized, such that the model saves the temporary output. The initialization is based on the number of timesteps (rows) and number of layers (columns). The initialization does not need to be changed as it automatically copies the length of the total duration and the number of layers.

3. COMPUTATIONS

One iterative cycle contains the following steps for one layer (L) at one moment in time (t) :

1. Calculate new thickness from the deformation of the former timestep
2. Calculate saturation state
3. Calculate mechanical stresses
4. Calculate compression
5. Calculate oxidation

STRESS AND STRAIN

The effective stress σ'_{eff} [kg m^-1 s-2] is computed following Terzaghi's Law (see 3.1) by the difference between the total vertical stress $\sigma_{tot,v}$ [kg m^-1 s-2] and the hydrostatic pressure μ [kg m^-1 s-2]. The effective stress is separately computed for the unsaturated (dry) and saturated (wet) part of every layer, using the gravitational constant g [m s-2], the layer thickness h [m], the layer porosity n [-], the density of the grains ρ_{gr} [kg m-3] and the density of water ρ_w [kg m-3]. The contribution of the exerted effective stress by the saturated and unsaturated part within every layer is added and gives the effective stress for every layer. Finally, the total effective stress that a certain layer experiences is the contribution of the total exerted effective stress of all the overlain layers combined.

$$\sigma_{tot,v(wet)} = \Big((1-n) * \rho_{gr} + \rho_w\Big) * g * h \quad (1)$$

$$\sigma_{tot,v\,(dry)} = (1-n) * \rho_{gr} * g * h \quad (2)$$

$$\mu = \rho_w * h \quad (3)$$

$$\sigma'_{eff(dry)} = (1-n) * \rho_{gr} * g * h \quad (4)$$

$$\sigma'_{eff(wet)} = (1-n) * (\rho_{gr} - \rho_w) * g * h \quad (5)$$

$$\sigma'_{eff} = \sigma'_{eff(wet)} + \sigma'_{eff(dry)} \quad (6)$$

$$\sigma'_{tot,eff} = \sum_L \sigma'_{eff} \quad (7)$$

COMPRESSION

The model computes compression using the 1D-Koppejan model (Koppejan 1948), differentiating between primary and secondary compression. Δh_{pr} [m] and Δh_s [m] are respectively the decrease because of primary and secondary compression. C_p [m day-1] and C_s [m day-1]] are respectively the primary and secondary compression parameters. t = timestep [days], and $\Delta\sigma$ is the difference in total, vertical effective stress between the former and the current timestep. Note that $\Delta\sigma$ will be positive for a decreasing groundwater level, and negative for an increasing groundwater level. This stsudy assumed that all the obtained effective stresses were smaller than the preconsolidation stress, based on the fact that there is no average decrease in the measured groundwater level observed. Based on this assumption, the model only accounts for reversible compression.

$$\Delta h_{com} = \Delta h_{pr} + \Delta h_s = \left(\left(\frac{1}{C_p} + \frac{1}{C_s} * \log\left(\frac{1+t}{1}\right)\right) * \ln\left(\frac{\sigma' + \Delta\sigma'}{\sigma'}\right)\right) * h_L \quad (8)$$

PEAT OXIDATION

The model first computes which part of the peat can truly be decomposed. The model considers aerobic peat decomposition such that peat oxidation only occurs under unsaturated conditions. Second, the relative clastic admixture α in peat is excluded from the computation of peat oxidation because only organic matter in peat can be decomposed.

$$\Delta h_{ox,p} = h_p - h_{p,wet} - \alpha * h_{p(t=0)} \quad (9)$$

Next, the actual decrease in thickness due to peat oxidation is approached by an exponential decay function. The exponential decay constant is the oxidation rate v_{ox} [m day-1].

$$\frac{dh_{ox,p}}{dt} = -v_{ox} * t \quad (10)$$

Finally, equation 12 and 13 are combined to compute the decrease in thickness Δh_{ox}due to peat oxidation at any timestep for every layer.

$$\Delta h_{ox} = \left(h_p - h_{p,wet} - \alpha * h_{p,(t=0)}\right) * \left(1 - e^{-v_{ox} * \Delta t}\right) \quad (11)$$